The deglacial development of the Oxygen Minimum Zone in the Bering Sea: A study based on high-resolution laminated sediment records

Dissertation zur Erlangung des akademischen Grades
eines Doktors der Naturwissenschaften
am Fachbereich Geowissenschaften
der Universität Bremen

vorgelegt von
Hartmut Kühn

Bremerhaven, September 2015

Gutachter:
Prof. Dr. Ralf Tiedemann
Prof. Dr. Gerhard Bohrmann

N a m e : ..... Datum .....

Anschrift : .....

E r k l ä r u n g

Hiermit versichere ich, dass ich

1. die Arbeit ohne unerlaubte fremde Hilfe angefertigt habe,

2. keine anderen als die von mir angegebenen Quellen und Hilfsmittel benutzt habe und

3. die den benutzten Werken wörtlich oder inhaltlich entnommenen Stellen als solche kenntlich gemacht habe.

_____, den .....

(Unterschrift)

This PhD thesis has been conducted within the Marine Geology department of the Alfred-Wegener-Institut Helmholtz-Zentrum für Polar- und Meeresforschung (AWI), between August 2010 and September 2015. The study was embedded within the MARUM project OC3 “Glacial to Holocene atmosphere-ocean interactions between high and low latitudes”. The studied sediment cores were retrieved in 2009 within the Innovative NOrth Pacific EXperiment cruise SO202-INOPEX.

Abstract

In the past decades several paleoceanographic studies found evidence for millennial scale climate variability during the late Pleistocene. While these climate fluctuations are well studied in the North Atlantic, the paleoceanographic history in the North Pacific is less well known. The last glacial termination is of special interest, as it represents the most recent transition from glacial to deglacial conditions. In the North Pacific these changes led to a strengthening of the mid-depth oxygen minimum zone (OMZ) to anoxic bottom water conditions and the deposition of laminated sediments. The main objective of this thesis was to gain new insights into the deglacial mid-depth OMZ dynamics in the Bering Sea, using a suite of mid-depth, partly laminated sediment cores that were collected during R/V Sonne cruise SO202-INOPEX.

It will be shown that during the Bølling–Allerød (BA) and early Holocene the Bering Sea OMZ strengthened to anoxic values of <0.1 ml/l, which led to the formation of laminations, and expanded vertically to water depths of >2100 m. Based on a correlation of ^{14}C-dated, laminated sediment cores it is revealed that throughout the Bering Sea and the Gulf of Alaska the onset of deglacial anoxia at 14.6 ka and 11.7 ka was a synchronous event, while the disappearance of laminations was a diachronous process. A decadal-scale correlation of two ^{14}C dated, layer counted sediment cores with seasonal resolution from the northeastern Bering Sea slope to the NGRIP δ^{18}O record revealed, that (1) the formation of laminations was tightly coupled to warm phases of the B/A and the early Holocene, which implies an atmospheric teleconnection between the North Atlantic and Bering Sea, and (2) the presence of annually laminated sediments (varves). The established age model was partly independent from radiocarbon ages and allowed the calculation of surface reservoir ages, which are 770 yr, 910yr and 875 yr for the Holocene, Younger Dryas and B/A respectively. The anoxia were driven on millennial scales by basin-wide remineralization of organic matter in intermediate waters, in combination with decadal-scale export productivity increases during times of warm temperatures. Based on a stacked sea surface temperature (SST) record, SSTs of about 6 °C persisted during times of lamina formations, while SSTs showed values of about 5 °C during times were laminations were not widespread. Other factors that enhanced the export productivity during the B/A and Holocene were increased stratification, a change towards seasonal sea ice, and an input of nutrients and organic carbon from the Alaska hinterlands, which started at 16.6 ka in the Bering Sea. Spectral analyses of X-ray-fluorescense-based Cl values of single laminae, which were used as a indicator for biosiliceous productivity, revealed a sharp spectral peak of 18.8 yr and a broader peak of 30 – 60 yr in the B/A and early Holocene. The first peak was related to the 18.6 yr nodal tidal cycle and the latter peak to the Pacific Decadal Oscillation. They influenced primary productivity through nutrient delivery to the surface via tidal mixing, SST variations and stratification. Both processes act in the modern subarctic

Pacific, which suggests that productivity variations in the subarctic Pacific are consistently influenced by a combination of external and internal forcing mechanisms since the last deglacial.

Kurzfassung

In den vergangenen Jahrzehnten haben zahlreiche paläozeanographische Studien Beweise für eine spät-Pleistozäne Klimavariabilität auf tausendjährigen Zeitskalen gefunden. Während diese Klimaschwankungen im Nordatlantik gut untersucht sind, ist die paläozeanographische Entwicklung im Nordpazifik weniger genau bekannt. Die letzte glaziale Termination ist von besonderem Interesse, da sie den jüngsten Übergang von glazialen zu interglazialen Bedingungen darstellt. In den mittleren Meerestiefen des Nordpazifik führten diese Änderungen zu einer Verstärkung der Sauerstoffminimumzonen hin zu anoxischen Bodenwasserverhältnissen und der Ablagerung von laminierten Sedimenten. Das primäre Ziel dieser Doktorarbeit war es, mit einer Reihe von teilweise laminierten Sedimentkernen aus mittleren Meerestiefen, welche während der Ausfahrt SO202-INOPEX mit dem Forschungsschiff Sonne geborgen wurden, neue Erkenntnisse über die Dynamik der deglazialen Sauerstoffminimumzone in der Beringsee zu erlangen.

Er wird gezeigt, daß sich während des Bølling–Allerøds (B/A) und des frühen Holozäns die Sauerstoffminimumzone im Beringmeer auf anoxische Verhältnisse von <0.1 ml/l verstärkt hat, was zur Bildung von laminierten Sedimenten führte, und sich vertikal auf Wassertiefen von >2100 m ausgedehnt hat. Basierend auf einer Korrelation von ^{14}C-datierten, laminierten Sedimentkernen zwischen der Beringsee und dem Golf von Alaska wird offenbar, daß das Einsetzten deglazialer Anoxia bei ca. 14.600 Jahren und ca. 11.700 Jahren ein synchrones Ereignis war, während das Verschwinden der Laminae ein diachroner Vorgang war. Eine Korrelation von zwei ^{14}C datierten Sedimentkernen mit Lagenzählungen und jahreszeitlicher Auflösung aus dem nordöstlichen Beringmeer zum NGRIP δ^{18}O Signal zeigte, daß (1) die Bildung der Laminationen sehr eng an die warmen Phasen des B/A und frühen Holozäns gekoppelt war, was eine atmosphärische Telekonnektion zwischen dem Beringmeer und dem Nordatlantik voraussetzt, und (2) das Vorhandensein von jährlich laminierten Sedimenten (Varven). Das erstellte Altersmodell ist teilweise unabhängig von Radiokarbondatierungen und erlaubt es die Oberflächen-Reservoir-Alter zu berechnen, welche 770 Jahre für das Holozän, 910 Jahre für die Jüngere Dryas und 875 Jahre für das B/A sind. Die Anoxia wurden auf tausendjährigen Zeitskalen durch beckenweite Remineralisation von organischem Material im Zwischenwasser angetrieben, in Kombination mit einem Anstieg der Exportproduktion auf dekadischen Zeitskalen in wärmeren Zeiten. Basierend auf einem kompilierten Oberflächenwassertemperatursignal herrschten Oberflächenwassertemperaturen von ca 6 °C in Zeiten der Laminabildung und 5 °C wenn Laminae nicht weitverbreitet waren. Andere Faktoren, welche die Exportproduktion verstärkten waren erhöhte Stratifizierung, eine Änderung hin zu saisonalem Meereis und ein Eintrag von Nährstoffen und organischem Material aus dem Hinterland von Alaska, welcher im Beringmeer vor ca. 16.600 Jahren begann. Eine Spektralanalyse von Röntgenfluoreszenz-basierten Cl-Werten einzelner Laminae, welche als Indikator für die silikatische Bioproduktivität genommen

wurden, ergab einen scharf begrenzten Spektralgipfel bei 18,8 Jahren und einen breiteren Spektralgipfel bei 30 – 60 Jahren. Der erste Spektralgipfel steht im Zusammenhang mit dem 18,6-jahre Tidenzyklus und der letztere mit der Pazifischen Dekadischen Oszillation. Diese beeinflußten die Primärproduktion durch Nährstoffeintrag an die Oberfläche bei tidaler Durchmischung, Oberflächenwassertemperaturänderungen und Stratifizierung. Beide Prozesse agieren auch im heutigen subarktischen Pazifik, was darauf hindeutet, daß Produktivitätsänderungen im subarktischen Pazifik seit dem letzten Deglazial durchweg von internen und externen Steurerungsmechanismen beeinflußt werden.

Acknowledgements

First, I would like to thank my supervisor Prof. Ralf Tiedemann who gave me the opportunity to do my Ph.D at the Alfred-Wegener-Institut. I would also like to thank Dr. Rainer Gersonde for his supervision, support and patience during my work and the excellent sediment cores retrieved during the Innovative NOrth Pacific EXperiment (INOPEX) cruise. Extra thanks go to Dr. Lars Max, Dr. Oliver Esper and especially Dr. Lester Lembke-Jene for their scientific support, which resulted in a lot of fruitful discussions and all their help with everything else. Further I thank Prof. Gerhard Bohrmann for the review my thesis.

I am thankful to Dr. Frank Lamy for his scientific advice and Prof. Helge Arz, Rainer Bahlo and Sascha Plewe for their help during my time at the Leibniz Institut für Ostseeforschung. Dr. Jens Hefter, Susanne Wiebe, Ute Bock, Ruth Cordelair and Rita Fröhlkin are thanked for technical support here at the AWI.

A big thank you goes to my roommates Nadine and Verena for coffee, laughs, discussions and everything else that was or was not science-related. More thanks go to my Ph.D colleagues Edith, Jian, Johannes, Marc and Thomas for all their moral support in hard times. Back in Kiel I thank Prof. Michael Sarnthein, who never lost interested in my work and a was big help in the earliest days of my scientific career.

Finally, I want to thank my family for all their help, love and opportunities they provided me over all theses years.

Table of contents

1. Introduction

1.1 Motivation of this thesis

During the Pleistocene global climate underwent a succession of glacial and interglacial climate changes. Superimposed on these orbital-scale variations, millennial-scale warm interstadial and cold stadial phases occurred that are particularly well studied over the last glacial cycle. Global reference records of these changes were established in Greenland and Antarctic ice cores (EPICA community members, 2004; NGRIP members, 2004). While these global climatic and corresponding greenhouse gas changes are evidently recorded in polar ice cores, these archives do not provide a complete picture of Earth's climate variability with its multitude of hemispheric and regional changes and forcing factors, due to their polar locations. Thus, to understand paleoclimatic development and the underlying processes, high-resolution paleoclimate records from key locations are needed, both in the terrestrial and marine realm.

Over the last decades, millennial-scale variations in multiple surface and deep ocean properties were uncovered in a number of marine sediment cores, e.g. from the North Pacific (e.g. Kennett and Ingram, 1995) and the North Atlantic (e.g. Bond et al., 1993; Sarnthein et al., 2000). While in the Atlantic the timing of these variations is clearly related to the Meridional Overturning Circulation (MOC; McManus et al., 2004), in the North Pacific the timings of glacial and deglacial climate oscillations are rather less well constrained. This is mainly due to the lack of sediment records with millennial- to decadal scale resolution and sufficiently accurate age control. The last glacial termination, in particular, is of considerate interest to the paleoclimate community as it constitutes the last time interval with fundamental reorganizations in the global climate system, including changing temperatures (Clark et al., 2012), ice volumes and rising sea levels (Carlson and Clark, 2012), rapid collapses and resumptions of the MOC (McManus et al., 2004), and a glacial-interglacial atmospheric CO_2 rise of about 80 ppmv (Monnin et al., 2001). The latter is thought to be principally due to changes in the global ocean's carbon cycle, with major contributions by the high latitude, subpolar regions in the Southern Ocean and North Pacific through changes in the strength and efficiency of the "biological carbon pump" (Sigman et al., 2010).

Specifically, deglacial millennial-scale variations in the MOC are accompanied by rapid, concomitant variations in North Pacific physical (Okazaki et al., 2010, Max et al., 2014, Praetorius and Mix, 2014) and biogeochemical changes (Galbraith et al., 2007; Kohfeld and Chase 2011; Lam et al., 2013) that are thought to play a significant role in the ocean-atmosphere carbon exchange, overturning and Northern Hemisphere climate forcing and teleconnections.

One important aspect of the last deglacial transition was the deglacial strengthening of ocean mid-depth Oxygen Minimum Zones (OMZs), as evidenced by the formation of laminated sediments in the North Pacific (Fig. 1.1; e.g. Jaccard and Galbraith, 2012; Jaccard et al., 2014). With oxygen concentrations of <0.1 ml/l such areas represent ocean "dead zones" that have severe impacts on ocean ecosystems (e.g. Behl and Kennett, 1996; Hofmann et al., 2011; Moffitt et al., 2015). As with ongoing global warming studies forecast a decrease of the world oceans oxygen content, with strong implications for human economy (e.g. Schmittner et al., 2008; Hofmann et al., 2011), a better understanding of the timing and involved processes of OMZ strengthening is important. Here the Bering Sea is of special interest as it located near the terminus of the global conveyor belt and represents today one of the most productive marginal seas in the world (Springer et al., 1996). Furthermore, this area is already effected by the global warming, which leads to a shift of the biological communities from artic conditions towards one that is characteristic for subarctic conditions (Grebmeier et al., 2006).

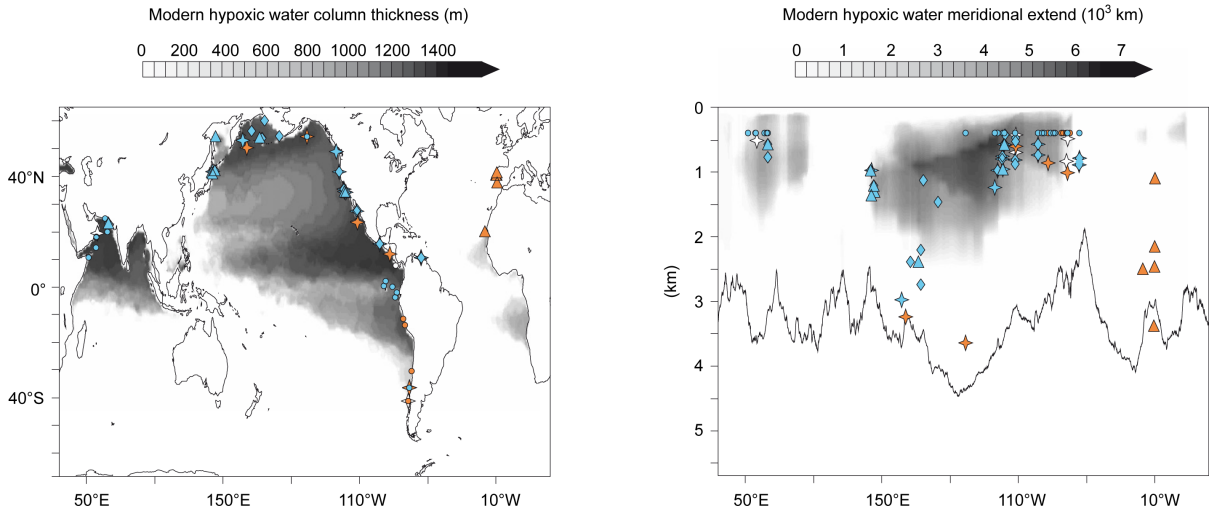

Figure 1.1: Qualitative changes in oxygenation proxies between Heinrich Stadial 1 and Bølling–Allerød (17.5 – 15 ka). Diamonds mark laminations, triangles indicate benthic foraminifera assemblages, stars show redox sensitive trace metal element concentrations, circles show bulk sedimentary $\delta^{15}N$. Blue colors indicate relative decrease in oxygenation, orange shows an increase and white colors indicates no clear oxygenation change. Shadings in upper panel indicate meridional extend and modern vertical thickness of hypoxic waters (Jaccard and Galbraith, 2012 modified).

This thesis was embedded within the MARUM project OC3 "Glacial to Holocene atmosphere-ocean interactions between high and low latitudes", which aimed on investigating the past ocean-atmosphere teleconnections in the Pacific during the Holocene and the timing of Pacific climate variability during the last glacial and Termination I. The sediment cores used in this thesis were retrieved in 2009 within the Innovative NOrth Pacific EXperiment project (SO202-INOPEX; Gersonde, 2012). The goal of this

project was to reconstruct the paleoceanographic and paleoclimatic history of different time slices from the subarctic North Pacific and Bering Sea.

1.2 Aim of the study and structure of the thesis

I use a suite of several, partly laminated, mid-depth Bering Sea records to gain new insights into the development of the deglacial OMZ. The main objectives of this thesis are to:

- analyze the timing, patterns and dynamics of the subarctic Pacific deglacial OMZ intensification into anoxic conditions;
- discern the underlying processes and forcing factors for the occurrence of widespread North Pacific anoxia in the context of deglacial climate dynamics;
- improve the understanding of deglacial North Pacific climate variability and its hemispheric coupling to the North Atlantic region on millennial- to interdecadal time scales;
- identify potential forcing mechanisms for regional sub-centennial oscillations in paleoceanographic proxydata by time series analyses;
- establish a deglacial layer-counted, partly ^{14}C-independent, age model for a Bering Sea marine reference record with sub-centennial-scale resolution.

In the following part of *Section 1.2* gives the specific research questions of this thesis. *Section 1.3* provides an overview on modern Bering Sea oceanography, followed by the paleoceanography of the deglacial Bering Sea in *Section 1.4*. *Chapter 2* gives a brief overview of the materials and methods. The detailed results of this work are presented as three separate manuscripts in *Chapters 3 to 5*. These manuscripts are either published or will be submitted to scientific journals.

The chapters three to five that present the results and are ordered in the following manner:

Chapter 3 **"Laminated sediments in the Bering Sea reveal atmospheric teleconnections to Greenland climate on millennial to decadal timescales during the last deglaciation"** (published in "Climate of the Past") presents results from two deglacial, high-resolution sediment records recovered on the NE Bering Sea slope. Based on a combination of layer counts, X-ray-fluorescense (XRF) measurements, diatom counts, geochemical analyses and AMS ^{14}C dating of benthic and planktic foraminifera the results address the following questions:

- Do the laminations in the northeastern Bering Sea represent varves?
- Is it possible to establish a radiocarbon-independent age model to calculate surface reservoir ages?

- How are changes in biogenic productivity related to deglacial mid-depth and upper ocean characteristics on different time scales?
- Are Bering Sea intermediate water ventilation and nutrient concentration changes a dominant factor in deglacial anoxia development?
- What are the different temporal scales (millennial-decadal) of teleconnection patterns between Bering Sea and Greenland climate?

Chapter 4 **"Tidal forcing and ocean-atmosphere dynamics drive productivity variations in the deglacial Bering Sea"** (to be submitted to "Geophysical Research Letters") uses the sediment record introduced in the previous chapter and applies additional ultra-high resolution micro-XRF scanning to the varved sediment section. The resulting subannually-resolved time series of biological productivity were subjected to spectral analyses for cyclic variations to address the following topics:

- Are primary productivity variations recorded in laminated sediment sections during the Bølling–Allerød (B/A) and early Holocene from the northern Bering Sea of a cyclic nature?
- How do these cyclic variations influence the development of single laminae?
- To which modern processes are recorded cyclic variations likely connected?
- What are potential forcing factors (external vs. internal) for dominant cyclic changes?

Chapter 5 **"Timing and forcing mechanisms of anoxia in the Bering Sea during the last deglaciation"** (to be submitted to "Journal of Quaternary Science") puts the results based on the NE Bering Sea slope record into a broader spatial and temporal perspective by providing a compilation of all laminated sediment core sections recovered during the INOPEX cruise. Based on AMS ^{14}C dating, XRF scanning and selected geochemical analyses these cores are placed into the basin-wide context of deglacial OMZ intensification, their lateral and vertical dynamics and their causal relationship with forcing factors. Specifically, the following topics are addressed:

- What was the timing of anoxia occurrence in the Bering Sea during the deglaciation, can laminated sections be thus used as precise stratigraphic markers?
- How did the deglacial OMZ intensify and extend laterally and vertically in the Bering Sea in a basin-wide context?
- What were the most probable causes for the Bering Sea OMZ intensification?
- Was the Bering Sea OMZ intensification similar to other North Pacific regions in characteristics and causal relationship?
- Can the age model of the Bering Sea reference core be extended towards ages older than the B/A?

After the main results the final *Chapter 6* provides the conclusions of this thesis and presents an outlook for potential future work on the material presented here.

1.3 Bering Sea modern oceanographic situation

Located near the terminus of the global MOC, the semi-enclosed Bering Sea is the third largest marginal sea in the world with a surface area of $2.3*10^6$ km^2 (Hood, 1983). In the northern and western areas the Bering Sea is bordered by Sibiria and Alaska. The large continental shelf is a characteristic feature with less than 200 m water depth in the northeastern Bering Sea, compared to the relatively narrow shelf in the northwestern parts. The central part of the Bering Sea is dominated by the deep Aleutian Basin (3500 m water depth, Stabeno et al., 1999). Two bathymetric heights (<2000 m water depth) are the Shirshov Ridge in the north and the Bowers Ridge in the south (Fig. 1.2). The Anadyr, Kuskokwin and Yukon River are the major rivers entering the Bering Sea, the latter having the largest discharge with $5*10^3 m^3 s^{-1}$ annual mean flow (Hood, 1983). The Bering Sea is connected to the North Pacific through several passages between the Aleutian Islands. Of these passages, the Kamchatka Strait is the deepest with 4400 m water depth (Fig. 1.2).

The surface circulation is fed by the westward flowing Alaskan Stream, which enters through the passages between the Aleutian Islands. Inside the Bering Sea, the surface circulation constitutes mainly a counterclockwise gyre, formed by the Bering Slope Current (BSC) and Aleutian North Slope Current (ANSC) in the east the East Kamchatka Current (EKC) in the west (Stabeno et al., 1999). The BSC feeds the northward-flowing Anadyr Current (AC), and in part the EKC (Rella et al., 2012). Surface waters leave the Bering Sea through the shallow (50 m water depth) Bering Strait into the Arctic Ocean, and with the EKC into the North Pacific, mainly through the Kamchatka Strait (Fig. 1.2; Stabeno et al., 1999). Exchange of deep waters below 1 km occurs through the deep Near Strait and Kamchatka Strait (Fig. 1.2; Roden, 1995).

Primary production is high and dominated by siliceous plankton, mainly diatoms (Takahashi et al., 2002). It reaches values of up to 175 – 275 $gCm^{-2}yr^{-1}$ and areas of high productivity are located along the shelf edges. This gave this region the name “Green Belt” (Springer et al., 1996). The nutrients are delivered to the euphotic zone via tidal mixing, eddy-induced mixing processes and melting of sea ice (Springer et al., 1996; Rella et al., 2012). Sea ice formation starts about November and forms mainly in polynias in the northern parts. Maximum sea ice extension occurs between March to April and reaches the shelf break, minimum sea ice extension occurs in July to September (Fig. 1.2; Niebauer, 1980). These strong seasonal differences, that influence also sea surface temperatures (SSTs), result from an interplay between the Aleutian Low and Sibirian High (Niebauer, 1980). Cyclic climate

patterns that are reported to be most dominant in the Bering Sea are the Pacific Decadal Oscillation (PDO) and Arctic Oscillation (AO; Stabeno, 2001; Zhang et al., 2010).

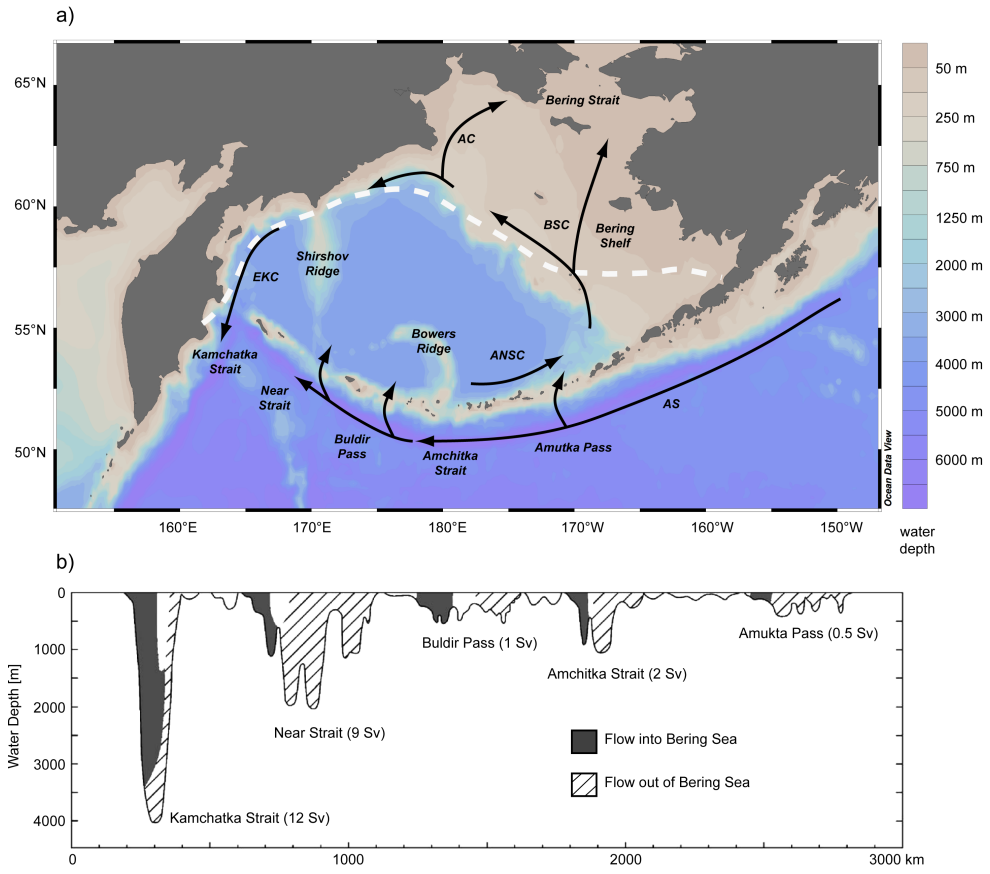

Figure 1.2: Overview of the surface circulation in the Bering Sea and the exchange of surface and deep waters with the North Pacific. (a) Bathymetric map of the Bering Sea showing the surface circulation (black arrows) and the position of sediment cores recovered during the INOPEX cruise. Cores marked in red contain lamination from the last deglaciation. Modern maximum sea ice extension is shown by the dashed white line (Reynolds et al., 2002). AS: Alaska Stream; ANSC: Aleutian North Slope Current; BSC: Bering Slope Current; AC: Anadyr Current; EKC: East Kamchatka Current. Map drawn with the Ocean Data View software (Schlitzer et al., 2002). (b) Cross section of the passes between the Aleutian Islands with the inflow and outflow of waters given in Sverdrup (Sv; Stabeno et al., 1999 modified).

Despite the high primary productivity that is observed in the Bering Sea today, bottom water oxygen contents don't reach values of 0.1 ml/l or lower and thus no laminated sediments are formed. However, an OMZ exists which is centered at 900 m water depth (Roden et al., 1995; Cook et al., 2005). Lowest oxygen contents found today reach 0.4 ml/l (Fig. 1.3; Garcia et al., 2010). Above 900 m water depth the oxygen profile shows an oxygenated surface layer, a sharp oxycline between 150 – 500 m and a gradual oxygenation increase below the core of the modern OMZ (Roden, 1995). Like the sea ice, the strength of the OMZ also has a strong seasonality with oxygen concentration ranging

between 0.4 – 0.7 ml/l, with lowest concentrations occurring between January to April (Fig. 1.3; Garcia et al., 2010).

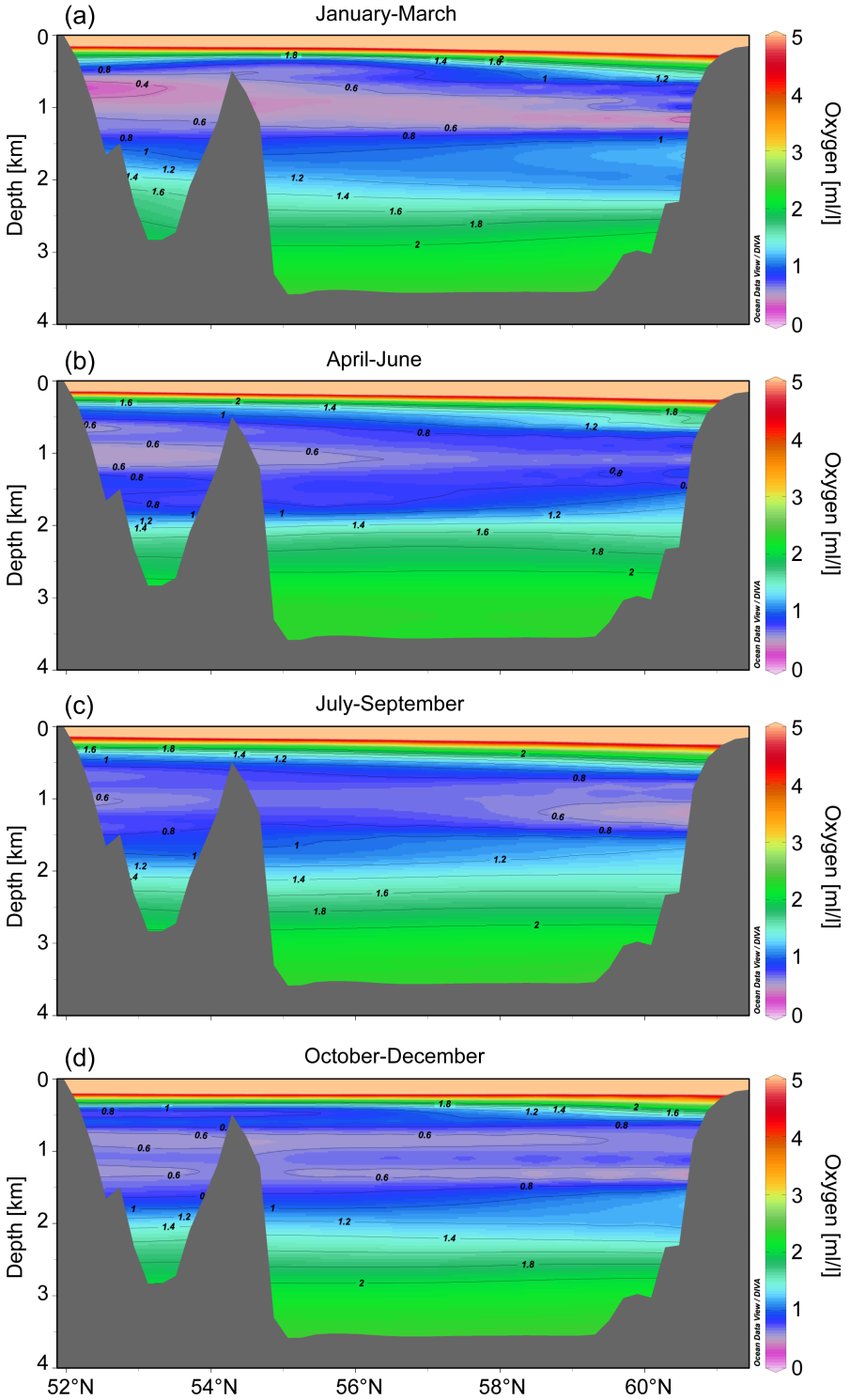

Figure 1.3: North-south transect through the Bering Sea showing the oxygen concentration in (a) January–March, (b) April–June, (c) July–September and (d) October–December. Areas of low oxygen contents are shown in pink color. Data is based on the World Ocean Atlas 2010 (Garcia et al., 2010).

1.4 Bering Sea paleoceanography

Since the last glacial the Bering Sea underwent a succession of fundamental paleoceanographic changes. During glacial times the primary productivity was low due to enhanced sea ice cover with shorter and colder summers and decreased nutrient supply to the surface as the stratification increased (e.g. Nakatsuka et al., 2005; Takahashi, 2005; Itaki et al., 2012). Based on diatom assemblages it was also suggested that perennial sea ice existed at the eastern Umnak Plateau (Caissie et al., 2010). The combination of low primary productivity and high sea ice cover led to a better ventilation of deeper Bering Sea water masses (e.g. Cook et al., 2005; Caissie et al., 2010) and a possible contribution of the Bering Sea to the formation of North Pacific Intermediate Water (NPIW; Ohkushi et al., 2003; Tanaka and Takahashi, 2005). The glacial bathymetry was also different, as the global sea level was about 120 m lower compared to today (Lambeck et al., 2014). This left the large eastern shelf areal exposed and the Bering Sea was a more isolated basin with the Bering Strait and shallower Aleutian passes being closed (Manley, 2002; Stabeno et al., 2002; Tanaka and Takahashi, 2005). The glacial vegetation of the exposed shelf areas was most likely dominated by birch–graminoid tundra (Elias et al., 1996).

During the warmer B/A and early Holocene the primary productivity increased in the Bering Sea and resulted in higher contents of total organic carbon (TOC), biogenic opal and pronounced carbonate peaks in marine sediment cores (Fig. 1.4; e.g. Okazaki et al., 2005; Kim et al., 2011; Riethdorf et al., 2013). Such $CaCO_3$ peaks are a common in the North Pacific, Okhotsk and Bering Sea and were assigned to the B/A and early Holocene (e.g. Keigwin et al., 1992; Keigwin, 1998; Gorbarenko et al., 2005). The high productivity is related to an increase in SSTs, with a shift towards seasonal sea ice (Caissie et al., 2010; Max et al., 2012) and increased thermal stratification (Riethdorf et al., 2013a). Nutrient supply was also enhanced and delivered by higher input of freshwater and the Alaska Stream (Khim et al., 2010). Higher SSTs in the Bering Sea during the B/A and early Holocene point towards an in-phase relationship between the North Atlantic and North Pacific ocean-climate systems, in line with other North Pacific proxy and model data (e.g. Mikolajewicz et al 1997; Praetorius and Mix, 2014). However, there is an ongoing discussion of this phase relationship, as other studies from the North Pacific argued for an out-of-phase scenario (e.g. Saenko et al., 2004; Gebhardt et al., 2008).

To date, most of these studies dealing with in- or out-of-phase relationships between different ocean basins and timing of North Pacific climate events, were severely limited by large uncertainties in the radiocarbon-based age control for deglacial sediment sections in the North Pacific (Sarnthein et al., 2007; Lund et al., 2011) that can comprise several hundreds or even thousand years. For the Bering Sea most studies assumed a constant planktic reservoir age of 700 yr (e.g. Cook et al., 2005; Itaki et

al., 2009). This age can only be seen as a first approximation, as it was shown that planktic reservoir ages varied during the glacial termination in the North Pacific (e.g. Sarnthein et a., 2007; Sarnthein et al., 2015).

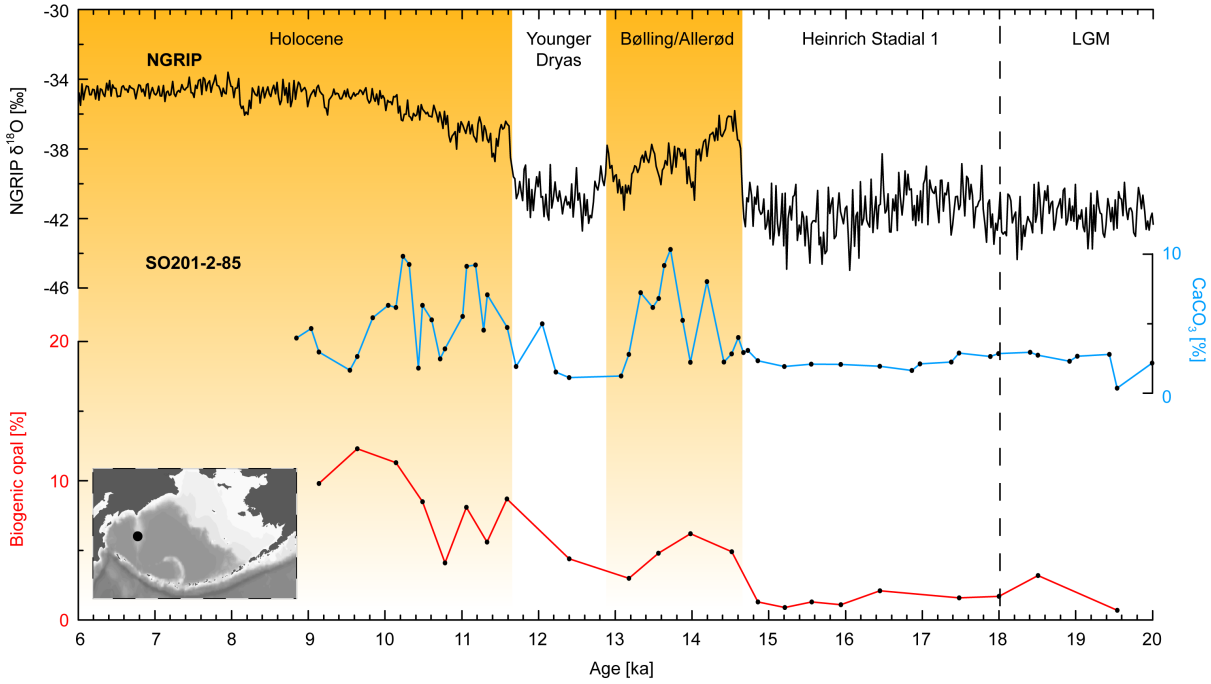

Fig. 1.4: Comparison of the NGRIP stable isotope record (black plot in upper panel; Rasmussen et al., 2006) and productivity records of core SO201-2-85 (968 m water depth; Riethdorf et al., 2013) from the Shirshov Ridge. NGRIP data is plotted on the GICC05 timescale. Carbonate concentrations are given in blue and biogenic opal in red color. The warm Bølling–Allerød and Holocene are marked with orange boxes. The dashed line depicts the boundary between Heinrich Stadial 1 and the Last Glacial Maximum (LGM). The location of the sediment core is depicted in the small map by a black circle.

The B/A and early Holocene were also times where the OMZ in the north Pacific and Bering Sea intensified (e.g. Behl and Kennett, 1996; Cook et al., 2005; Jaccard and Galbraith, 2012). The oxygen depletion reached values of <0.1 ml/l and, as a consequence, laminated sediments formed, because no bioturbating benthic macrofauna could thrive any longer (e.g. Behl and Kennett, 1996, Watanabe et al., 2007). In the North Pacific, sediments with laminations during the B/A and early Holocene are found in the Gulf of California (e.g. Zheng et al., 2000), the Santa Barbara Basin (e.g. Behl and Kennett, 1996), at the continental margins off Japan (e.g. Ikehara et al., 2006), at the Alaska Margin (e.g. Davies et al., 2011) and the Bering Sea (e.g. Cook et al., 2005). However, the exact timing of OMZ strengthening and the involved factors are discussed controversially. Suggested mechanisms include increased export productivity (e.g. Mix et al., 1999) but other studies did not provide evidence for higher export productivity and argued instead for ventilation changes of intermediate waters (e.g.

Kennett and Ingram, 1995), or suggested a combination of both factors (e.g. Shibehara et al., 2007). In many cases, it remained unclear if the laminations represent varves. For the deglacial Bering Sea previous studies argue for both, annual laminated sediments (Cook et al., 2005) or see no evidence for annual deposition (Caissie et al., 2010).

So far, only few detailed layer counts have been carried out on laminated sediment sections in the Bering Sea. Such layer counts, however, can give information on the climatic and oceanograpphic development with unprecedented temporal resolution and age control during times of OMZ strengthening and can also be used to establish radiocarbon independent ages models and calculate surface reservoir ages.

2. Material and Methods

2.1 Sediment cores

During expedition SO202-INOPEX fifteen sediment cores were recovered in the Bering Sea. They cover a depth transect from 1066 m to 3821 m (Fig. 2.1; Tab. 2.1; Gersonde, 2012). Two different coring gears were deployed to retrieve the sediment cores: A piston corer and a kasten corer. The first device was used to gain rather long cores with more than 23 m length and a core diameter of 10.5 cm. The latter device consist of 30 cm long rectangular sides and was used to recover large volume cores with up to 9.5 m length. It was deployed at three positions to complement the piston cores (Fig. 2.1). A prominent feature of ten sediment cores, from water depths of 1066 m to 2109 m, is the appearance of two or more laminated sediment sections. The thickness of these intervals vary between 14 cm in piston core SO202-12-3 (2109 m water depth) to 465 cm in piston core SO202-18-3 (1111 m water depth). The single lamina vary in their individual thickness on sub-millimeter to millimeter scale and represent an alternation between diatom-rich and rather terrigenous laminae. Their preservation is also different between the cores. The best preserved laminae were found in cores SO202-18-3 and SO202-18-6, while the poorest preservation occurred in the deep cores SO202-12-1/-3 and SO202-21-1. This was also reflected in the layer counts, which revealed 1990 laminae couplets in core SO202-18-3 in contrast to 12 laminae couplets in SO202-12-3 (Tab. 2.1). Therefore, this thesis focuses on cores SO202-18-3 and SO202-18-6. They were used as reference sites to establish the age model (*Chapters 3* and *5*) and for spectral analysis (*Chapter 4*).

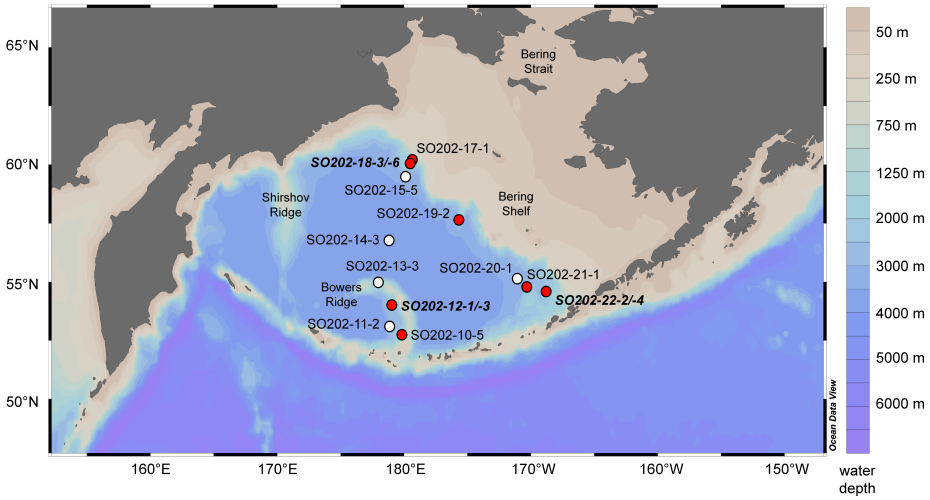

Figure 2.1: Location of sediment cores retrieved during expedition SO202 INOPEX in the Bering Sea. Cores without laminations are shown with white circles and cores containing laminated sections are marked with red circles. Core locations in bold-italic letters give locations where a piston core and a neighbouring kasten core were recovered. Map generated with Ocean Data View (Schlitzer, 2002).

Table 2.1: Locations of sediment cores from the Bering Sea retrieved during R/V *Sonne* cruise SO202-INOPEX.

Sediment Core	Latitude	Longitude	Depth (mbsl)	Laminated	Coring device	Counted laminae
SO202-10-5*	52°44.57'N	179°50.87'E	1470	x	KOL	disturbed
SO202-11-2	53°06.67'N	178°53.99'E	2703		KOL	
SO202-12-1	54°03.04'N	179°05.24'E	2109	x	KAL	33 ±2
SO202-12-3	54°03.04'N	179°05.24'E	2109	x	KOL	12 ±1
SO202-13-5*	54°58.72'N	177°57.42'E	1382		KOL	
SO202-14-3	56°47.19'N	178°49.45'E	3821		KOL	
SO202-15-5	59°30.76'N	179°51.00'W	3129		KOL	
SO202-17-1	60°07.39'N	179°27.95'W	1066	x	KOL	910 ±11
SO202-18-3	60°07.60'N	179°26.67'W	1111	x	KOL	1990 ±22
SO202-18-6	60°07.60'N	179°26.61'W	1107	x	KAL	997 ±16
SO202-19-2	57°39.05'N	175°40.69'W	1752	x	KOL	622 ±6
SO202-20-1	55°08.68'N	171°04.95'W	2984		KOL	
SO202-21-1	54°47.35'N	170°19.68'W	1911	x	KOL	45 ±1
SO202-22-2	54°34.45'N	168°48.66'W	1482	x	KOL	357 ±4
SO202-22-4	54°34.41'N	168°48.62'W	1476	x	KAL	656 ±5

* Cores disturbed during retrieval or upper 15 ka missing, according to magnetic susceptibility (Gersonde, 2012). Kol: piston corer, KAL: kasten corer.

2.2 Methods

2.2.1 X-ray-fluorescence measurements

X-ray-fluorescence (XRF) logging is a common method to gain high resolution data of the relative element composition on split sediment cores (Jansen et al., 1998). The method of XRF logging was developed in 1988 and has many advantages compared to other chemical analysis, as it allows rapid, continuous and non-destructive analysis of several element concentrations with less time consuming sample preparation (Jansen et al., 1998; Richter et al., 2006). The principle of this method is adequately described by Jenkins and De Vires (1970) and Tjallingii (2006). Basically, the X-ray radiation leads to the ionization of atoms by the ejection of inner shell electrons. As a result electrons from outer shells fall back to fill the vacancies, leading to the emission of electromagnetic radiation. It has a wavelength that is characteristic for each element and the amplitude in the XRF spectral peaks is proportional to the concentration of the corresponding element (Richter et al., 2006).

Two different XRF core scanners were used for sediment core analysis. First, I scanned all Bering Sea sediment cores with 1 cm resolution with an Avaatech XRF core scanner at the Alfred-Wegener-Institute (AWI), Bremerhaven. Before scanning the split sediment cores were covered with 4 μm thin SpexCerti Prep Ultralene® foil to prevent contamination of the detector unit and the desiccation of the

sediment cores (Tjallingii, 2006). Each core segment was scanned three times with constant 1 mA electric current, Rh-tube voltages of 10 kV (Al, Si, P, S, Cl, K, Ca, Ti, Cr, Mn, Fe, Rh), 30 kV (Cu, Zn, Ga, Br, Rb, Sr, Y, Zr, Nb, Mo, Pb, Bi), 50 kV (Ag, Cd, Sn, Te, Ba) and counting times of 10 s, 15 s and 30 s respectively (Richter et al., 2006). The software packages WinAxil and WinBatch from Canberra were used for data processing. The measured results are given in counts per second (cps).

Additionally, I performed ultra-high resolution scans of the laminated sediment sections with a resolution of up to 200 µm. Therefore I used an ITRAX core scanner from Cox Analytical Systems at the Leibniz Institute for Baltic Sea Research, Warnemuende. Before scanning the cores surface was covered with a 6 µm thin polypropylene film. The XRF detection system is different compared to the Avaatech system, as it is mounted to a vertical motorized stage that adjusts itself according to the topography of the core surface (Croudace et al., 2006). XRF scans were performed with a Cr-tube voltage of 45 kV and 15 seconds counting time. The measured elements were comparable to the Avaatech scanner but additionally the ITRAX system also detected Mg, Ar, Co, Ni, Sb, Ce, Ta, Th, U. The data were processed with the Q-Spec and ReDiCore software packages and the XRF results are given in cps.

The XRF measurements were used to establish the chronostratigraphy and core-to-core correlation (*Chapter 3* and *Chapter 5*), to get information on biological productivity changes (*Chapter 3* and *Chapter 5*), to study the composition of single laminae (*Chapter 3*) and for spectral analysis of laminated intervals (*Chapter 4*).

2.2.2 X-ray images

For the kasten cores X-ray images were obtained by cutting out 25x10x0.5 cm sediment slices that were subsequently wrapped into plastic foil and sealed vacuum tight. The cabinet X-ray system Faxitron Series from Hewlett Packard at the AWI, Bremerhaven was used to produce the X-ray images. The system was set at 40 kV, 3 A and 3 min exposure time. For X-ray images of the piston cores I used the ITRAX scanner at the Leibniz Institute for Baltic Sea Research. The X-ray images were taken on split sediment cores before the XRF scan, with tube voltages of 50 to 60 kV, 30 mA, and exposure times between 700 to 1200 ms, depending on sediment thickness and density. In contrast to the system of Hewlett Packard, the radiographies of the ITRAX core scanner are radiographic positives, in which core segments of lower density appear as light intervals and vice versa (Fig. 2.2).

The X-ray images helped to identify laminated sediment sections and were used for layer counting (*Chapter 3*) and spectral analysis (*Chapter 4*).

2.2.3 Layer counting

Layer counting was an essential part for the establishment of the age model (*Chapter 3*). I performed layer counts manually on the radiographies, as the single laminae are clearly visible in these images due to their density differences. Additionally, the radiographies were combined with the high resolution chlorine counts from the ITRAX core scanner, which responded very sensible to the density changes between the laminae (Fig. 2.2). Always couplets of one light and dark laminae were counted until single laminae were no longer distinguishable in the X-ray images. The counting error was estimated by repetitive laminae counts of the same sediment interval by different investigators. The estimated error was ±5 laminae couplets for ca. 1 m long laminated sections (Tab. 2.1). For laminated core SO202-10-5 layer counts could not be performed due to core disturbances (Gersonde, 2012).

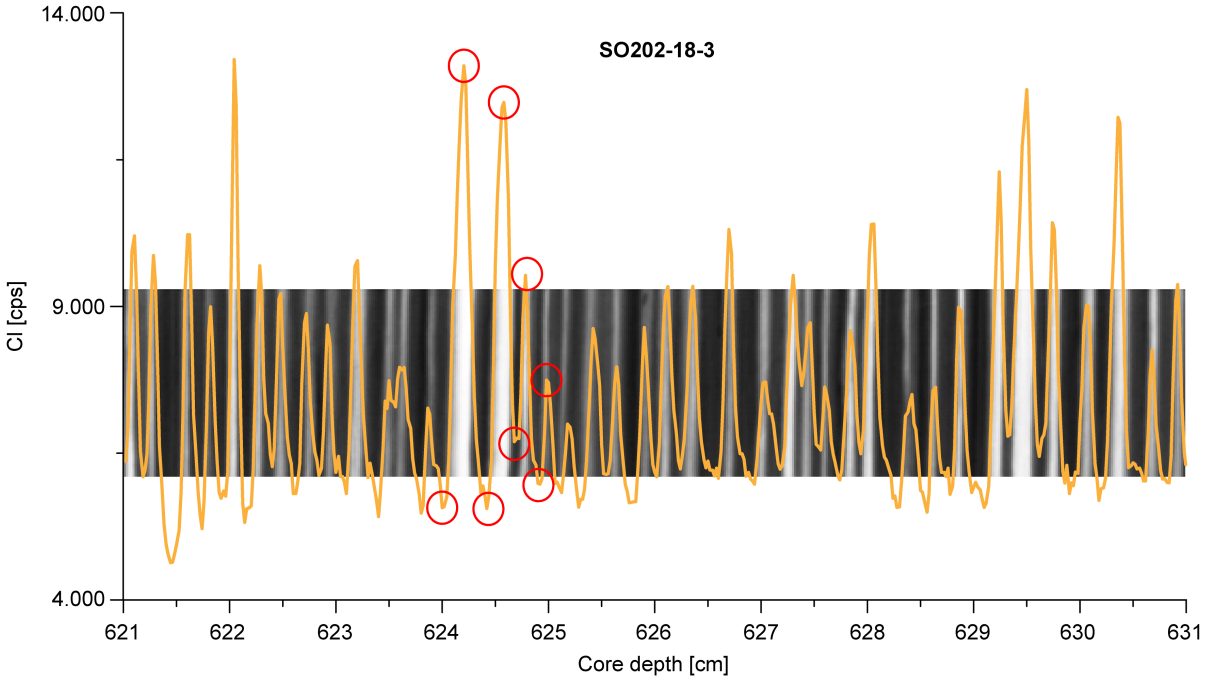

Figure 2.2: Example of a laminated section of piston core SO202-18-3 from the northern Bering Slope. Less dense, diatom rich laminae are shown in light colors and denser, terrigenous laminae in black. Results of high resolution Cl counts from the ITRAX core scanner are shown by the orange graph. Red circles give examples of single lamina Cl-maxima and minima, used for spectral analysis.

2.2.4 Radiocarbon measurements

Planktic and benthic radiocarbon ages helped to establish the age model and provided information on paleo-ventilation changes, by calculating the difference between the benthic and planktic ^{14}C age from the same sample depth. The results, including the construction of the age models, are discussed in

detail in *Chapters 3* and *5* and also contributed to age models and ventilation estimations shown in *Appendix 1* and *2*. For planktic ^{14}C dates monospecific samples of *Neogloboquadrina pachyderma* sinistral were picked from the 125 – 250 µm fraction. For benthic radiocarbon dates mostly mixed benthic foraminfera were picked from the fraction >250 µm. All samples of cores SO202-18-3 and SO202-18-6 were washed and picked by myself, while for cores SO202-12-1 and SO202-22-4 either student assistants or technicians prepared and picked the samples. Measurements were performed by the National Ocean Science Accelerator Mass Spectrometry (NOSAMS) facility at the Woods Hole Oceanographic Institution and at Beta Analytic Inc., Miami. The age models for cores SO202-18-6, SO202-18-3 and SO202-12-1 were compiled by myself and for core SO202-22-4 in collaboration with Wenshen Xiao from Tongji University, Shanghai.

2.2.5 Spectral analyses

I used the results of high resolution XRF-based Cl counts (200 µm) for spectral analysis of varved intervals in reference core SO202-18-3, spanning the Bølling–Allerød and early Holocene (*Chapter 4*). The combination of the XRF data with X-ray images allowed the identification of single laminae (Fig. 2.2). The amplitude modulation of the Cl counts was investigated by assigning the corresponding maximum and minimum Cl value to every light (= diatom rich) and dark (= terrigenous) laminae (Fig. 2.2). With this procedure an evenly spaced data set was generated with annual resolution, that was used for spectral analysis. The Cl values were used as productivity proxies, as they depend on sediment density and thus pore water content, which is influenced by the amount of preserved diatom frustules. The applied methods were a Fast Fourier Transformation, the Maximum Entropy Method and after Blackman and Tukey. Spectral analysis was performed in collaboration with Gerrit Lohmann and Oliver Esper from AWI, using a FORTRAN program routine and the AnalySeries software package (Paillard et al., 1996).

2.2.6 Organic carbon, total nitrogen and $CaCO_3$ measurements

Total carbon (TC) and total nitrogen were measured with an Elementar Vario III CNS analyzer, and total organic carbon (TOC) content with an Eltra CS-2000 Carbon Sulfur element analyzer after carbonate removal at the Alfred-Wegener-Institute, Bremerhaven (relative precision of ±3 %). Additionally, the samples were also corrected for the pore water salt content (Kuhn, 2013). The carbonate content was calculated following the equation:

$CaCO_3 = (TC-TOC) \times 8.333$

The measurements were carried out by technicians and the results provided information on changes of marine productivity (*Chapters 3* and *5*), and were used to gain information on the organic carbon-input into the Bering Sea since the Last Glacial Maximum (*Chapter 5*).

2.2.7 Biogenic opal measurements

Biogenic opal was measured at the AWI, Bremerhaven by technicians with the sequential leaching method after Müller and Schneider, (1993). The opal was extracted with 1M NaOH in a water bath at 85 °C and the opal concentrations were measured by continuous flow analysis with molybdate-blue spectrophotometry (relative precision of ±5 %). Also a correction for the pore water salt content was applied (Kuhn, 2013).

The results were used to estimate changes in the marine productivity (*Chapter 3* and *Chapter 5*) and to show the correlation between XRF-based Cl values and biogenic opal (*Chapter 4*).

2.2.8 Smear slides and diatom counts

Smear slides were prepared according to the standard method of the AWI, Bremerhaven (Gersonde and Zielinski, 2000) and the counting of diatoms followed methods of Schrader and Gersonde (1978). I prepared the smear slides and performed the diatom counts in collaboration with Oliver Esper.

The results provided information of the composition of single laminae (*Chapter 3*).

2.2.9 *Additional measurements not presented in Chapters 3 to 5*

I performed additional measurements using the Inductively Coupled Plasma-Optical Emission Spectrometer (ICP-OES) “Iris Intrepid” from Thermo Elemental at the AWI, Bremerhaven, to gain information on quantitative element variations. The sample treatment followed established methods (Wilhelms-Dick et al., 2012). Both, bulk sediment and single laminae were analyzed. To separate single laminae from each other, a 8x7x7 cm block of laminated sediment was cut out of kasten core SO202-18-6 with metal blades that were cleaned previously with ethanol and acetone. Subsequently, the sediment block was dried at ca. 30 °C for 48 hours. After this procedure the laminae could be easily distinguished, as the less dense laminae appeared as white layers in the sediment. The single laminae were carefully separated with acetone-cleaned ceramic scalpels. The results of the ICP measurements of the laminae are shown in *Chapter 6*. Additionally, stable isotope analysis were carried out in core SO202-18-6 on the endobenthic foraminifera *Uvigerina peregrina,* as no specimens

of the epibenthic genus *Cibicidoides* were found. Most samples were picked from the fraction 250-310 µm and measured at the AWI, Bremerhaven, on a Finnigan MAT 251 mass spectrometer (cf. Max, 2012). However, in the laminated intervals no *Uvigerina peregrina* were found. The results are not further discussed in this thesis.

3. Laminated sediments in the Bering Sea reveal atmospheric teleconnections to Greenland climate on millennial to decadal timescales during the last deglaciation

Hartmut Kuehn[1,2], Lester Lembke-Jene[1], Rainer Gersonde[1,2], Oliver Esper[1,2], Frank Lamy[1,2], Helge Arz[3], Gerhard Kuhn[1], Ralf Tiedemann[1]

[1] Alfred-Wegener-Institut Helmholtz-Zentrum für Polar- und Meeresforschung, Bremerhaven, Germany

[2] MARUM Zentrum für Marine Umweltwissenschaften, Bremen, Germany

[3] IOW - Leibniz Institut für Ostseeforschung, Warnemünde, Germany

Published in Climate of the Past (2014), doi:10.5194/cp-10-2215-2014

Abstract

During the last glacial termination, the upper North Pacific Ocean underwent dramatic and rapid changes in oxygenation that lead to the transient intensification of Oxygen Minimum Zones (OMZs), recorded by the widespread occurrence of laminated sediments on circum-Pacific continental margins. We present a new laminated sediment record from the mid-depth (1100 m) northern Bering Sea margin that provides insight into these deglacial OMZ maxima with exceptional, decadal-scale detail. Combined ultrahigh-resolution micro-X-ray-fluorescense (micro-XRF) data and sediment facies analysis of laminae reveal an alternation between predominantly terrigenous and diatom-dominated opal sedimentation. The diatomaceous laminae are interpreted to represent spring/summer productivity events related to the retreating sea ice margin. We identified five laminated sections in the deglacial part of our site. Lamina counts were carried out on these sections and correlated to the Bølling–Allerød and Preboreal phases in North Greenland Ice Core (NGRIP) oxygen isotope record, indicating an annual deposition of individual lamina couplets (varves). The observed rapid decadal intensifications of anoxia, in particular within the Bølling–Allerød, are tightly coupled to short-term warm events through increases in regional export production. This dependence of laminae formation on warmer temperatures is underlined by a correlation with published Bering Sea sea surface temperature records and $\delta^{18}O$ data of planktic foraminifera from the Gulf of Alaska. The rapidity of the observed changes strongly implies a close atmospheric teleconnection between North Pacific and

North Atlantic regions. We suggest that concomitant increases in export production and subsequent remineralization of organic matter in the Bering Sea, in combination with oxygen-poor waters entering the Being Sea, drove down oxygen concentrations to values below 0.1ml/l and caused laminae preservation. Calculated benthic-planktic ventilation ages show no significant variations throughout the last deglaciation, indicating that changes in formation rates or differing sources of North Pacific mid-depth waters are not prime candidates for strengthening the OMZ at our site. The age models established by our correlation procedure allow for the determination of calendar age control points for the Bølling–Allerød and the Preboreal that are independent of the initial radiocarbon-based chronology. Resulting surface reservoir ages range between 730 yr – 990 yr during the Bølling–Allerød, 800 yr – 1100 yr in the Younger Drays and 765 yr – 775 yr for the Preboreal.

3.1 Introduction

The last glacial termination is characterized by the widespread decrease of oxygen concentrations at mid-depth in the world ocean (Jaccard and Galbraith, 2012). In the North Pacific, this prominent reduction led to the expansion of Oxygen Minimum Zones (OMZs), culminating in the formation of anoxic, laminated sediment sequences at several continental margin locations (Fig. 3.1). Examples include the Santa Barbara Basin (e.g. Behl and Kennett, 1996), the Gulf of California (e.g. Kennett and Ingram, 1995; Zheng et al., 2000), the continental margins off Japan (Ikehara et al., 2006; Shibahara et al., 2007), the southeast Alaska margin (Davies et al., 2011), and multiple sites located at intermediate depth in the Bering Sea (Fig 3.1, Table 3.1 and cf. e.g. Cook et al., 2005; Itaki et al., 2009; Schlung et al., 2013).

The causes for the occurrence of laminations and hence significant decreases in oxygen concentration of bottom waters are discussed controversially. While some studies propose changes in the ventilation of intermediate waters and see no unambiguous evidence for higher export production (Kennett and Ingram, 1995; Zheng et al., 2000), other argue for increased export productivity that would contribute to anoxic conditions (Mix et al., 1999; Ortiz et al., 2004; Davies et al., 2011), or an interaction of both higher export production and ventilation changes (Cook et al., 2005; Shibahara et al., 2007). In records from lower North Pacific latitudes a strong coupling to North Atlantic climate was observed on millennial timescales in laminated sediments from the Santa Barbara Basin, which closely resemble Dansgaard-Oeschger-type temperature changes of the Greenland Ice Sheet Project 2 (GISP2) ice core during the past 60 kyr (Kennett and Ingram, 1995; Hendy et al., 2002). Furthermore, a close atmospheric climate teleconnection between the North Atlantic and North Pacific has been proposed in several modeling studies (Mikolajewicz et al., 1997; Okumura et al., 2009). For the Bering Sea, it

was shown that laminated sediments formed during warm phases of the Bølling–Allerød (14.64 – 12.85 ka) and the early Holocene (10.3 – 11.7 ka; e.g. Cook et al., 2005; Schlung et al., 2013). However, how closely laminated high-resolution sequences in the subarctic North Pacific are in fact linked to Greenland climate on shorter-than-millennial-scale changes remains unknown.

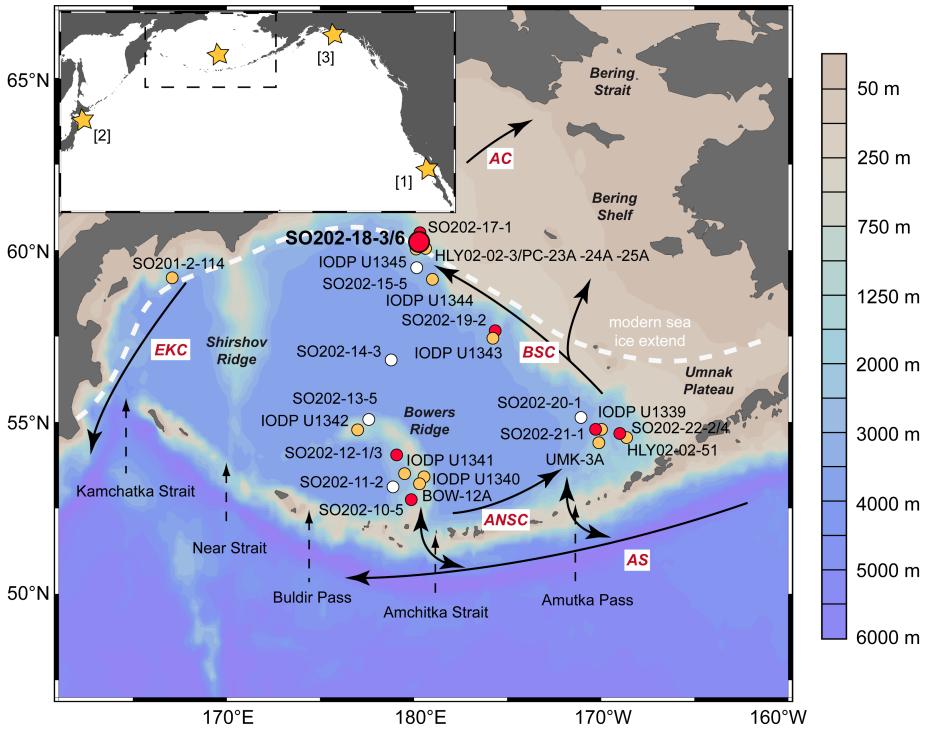

Figure 3.1: Bathymetric map of the Bering Sea with the position of laminated INOPEX cores (red circles) and INOPEX cores without laminations (white circles). Yellow circles mark the position of published laminated records in the Bering Sea (see Table 3.1 for details). The surface circulation shown by black arrows. [AC]: Anadyr Current; [AS]: Alaska Stream; [ANSC]: Aleutian North Slope Current; [BSC]: Bering Slope Current; [EKC]: East Kamchatka Current. Dashed white line shows modern maximum sea ice extension (Reynolds et al., 2002). Dashed black arrows mark the gateways between the Bering Sea and North Pacific. Yellow stars on the small map mark location of laminated sediment records in [1] Gulf of California and Santa Barbara Basin, (e.g., Behl and Kennett, 1996 ; Zheng et al., 2000), near the Island of Hokkaido (Ikehara et al., 2006; Shibahara et al., 2007), and [3] the southeast Alaska margin (Davies et al., 2011). Map drawn with Ocean Data View (Schlitzer, 2002).

In principle, laminated sediments bear the potential to provide insights into climatic evolution and hemispheric coupling mechanisms with an extremely high temporal resolution (Hughen et al., 2000; Bronk Ramsey et al., 2012; Nakagawa et al., 2012). While it has been shown for laminated sediments from the Santa Barbara Basin and Saanich Inlet on Vancouver Island (Nederbragt and Thurow, 2001, 2005) that each pair of laminae represents one year of deposition, the nature of laminations in the Bering Sea is largely unconstrained, with cases being made in previous studies for them either

representing annual depositional events (Cook et al., 2005) or with no evidence found for such annual resolution (Caissie et al., 2010). Unfortunately, no laminae counts from Bering Sea sequences exist so far that shed light on this question.

Table 3.1: Sediment cores from the Bering Sea shown in Fig. 3.1. Depths are given in meter below sea level (mbsl).

Sediment Core	Latitude	Longitude	Depth (mbsl)	Literature
SO202-10-5	52°44.57'N	179°50.87'E	1470	Gersonde,R 2012
SO202-11-2	53°06.67'N	178°53.99'E	2703	Gersonde,R 2012
SO202-12-1	54°03.04'N	179°05.24'E	2109	Gersonde,R 2012
SO202-12-3	54°03.04'N	179°05.24'E	2109	Gersonde,R 2012
SO202-13-5*	54°58.72'N	177°57.42'E	1382	Gersonde,R 2012
SO202-14-3	56°47.19'N	178°49.45'E	3821	Gersonde,R 2012
SO202-15-5	59°30.76'N	179°51.00'W	3129	Gersonde,R 2012
SO202-17-1	60°07.39'N	179°27.95'W	1066	Gersonde,R 2012
SO202-18-3	60°07.60'N	179°26.67'W	1111	Gersonde, R 2012; this study
SO202-18-6	60°07.60'N	179°26.61'W	1107	Gersonde, R 2012; this study
SO202-19-2	57°39.05'N	175°40.69'W	1752	Gersonde,R 2012
SO202-20-1	55°08.68'N	171°04.95'W	2984	Gersonde,R 2012
SO202-21-1	54°47.35'N	170°19.68'W	1911	Gersonde,R 2012
SO202-22-2	54°34.45'N	168°48.66'W	1482	Gersonde,R 2012
SO202-22-4	54°34.41'N	168°48.62'W	1476	Gersonde,R 2012
SO201-2-114	59°13.87'N	166°59.32'E	1376	Max et al., 2012
IODP U1339	54°40.02'N	169°58.902'W	1867.5	Takahashi et al., 2011
IODP U1340	53°24.001'N	179°31.297'W	1294.6	Takahashi et al., 2011; Schlung et al., 2013
IODP U1341	54°02.0025'N	179°0.49992'E	2139.5	Takahashi et al., 2011
IODP U1342	54°49.699'N	176°55.003'E	818.6	Takahashi et al., 2011
IODP U1343	57°33.399'N	175°48.966'W	1952.9	Takahashi et al., 2011
IODP U1344	59°03.0005'N	179°12.201'W	3173.1	Takahashi et al., 2011
IODP U1345	60°09.1917'N	179°28.204'W	1007.8	Takahashi et al., 2011
HLY02-02-3JPC	60°07.674'N	179°26.508'W	1132	Cook et al., 2005
HLY02-02-51JPC	54°33.192'N	168°40.014'W	1467	Cook et al., 2005; Caissie et al., 2010
PC-23A	60°09.52'N	179°27.82'W	1002	Itaki et al., 2009; Kim et al., 2011
PC-24A	60°15.70'N	179°25.34'W	852	Kim et al., 2011
PC-25A	60°04.48'N	179°27.78'W	1152	Kim et al., 2011
BOW-12A	53°23.47'N	179°33.47'W	1287	Okada et al., 2005; Tanaka and Takahashi et al., 2005
UMK-3A	54°25.22'N	170°13.38'W	1892	Okada et al., 2005; Tanaka and Takahashi et al., 2005

* Magnetic susceptibility pattern and XRF data suggest that upper 15 ka are missing (Gersonde, 2012)

In this paper, we investigate two episodically laminated sediment records from almost identical locations on the northern Bering slope with high temporal resolution. These sites were selected from a collection of sediment cores retrieved during expedition SO202 INOPEX (Gersonde, 2012) to decipher deglacial changes in OMZ dynamics. With an accelerator mass spectrometry (AMS) ^{14}C-anchored core chronology and detailed laminae counts, we give information if laminae were likely deposited annually and to which extend our records correspond to North Greenland Ice Core (NGRIP) δ^{18}O time series, especially during the warm phases of the Bølling–Allerød (GI-1; Andersen et al., 2006; Rasmussen et al., 2006) and the Preboreal (11.65 – 10.70 ka, Mangerud et al., 1974; van der Plicht et al., 2004). High-resolution X-ray-fluorescence (micro-XRF) data and sediment X-ray images provide information about formation processes of discrete laminae. We compare our results to existing seasonal sea surface temperature (SST) records from the Bering Sea and Greenland ice core data to deduce connections between hemispheric temperature changes and anoxia occurrence. Calculated benthic-planktic (B-P) ventilation ages will show whether water mass changes contribute to laminae formation.

3.2 Study area and oceanographic setting

The Bering Sea is the third-largest marginal sea in the world and comprises a broad continental shelf (Fig. 3.1). This shelf is seasonally covered with sea ice, with maximum extension occurring between March and April, including our core location, and minimum sea ice extension between July and September (Niebauer, 1980; Danielson et al., 2011). These strong seasonal contrasts are reflected in the SSTs, which range between 8 °C (summer) and 0.6 °C (winter) at our site (Levitus and Boyer, 1994), and are induced by the interplay between the Siberian High and the Aleutian Low (Niebauer, 1980). Surface water masses are influenced by the Alaska Stream (AS), which enters the Bering Sea through several straits between the Aleutian Islands. The surface circulation is characterized by a counterclockwise gyre, formed by the East Kamchatka Current (EKC), the Bering Slope Current (BSC), and the Aleutian Northern Slope Current (ANSC), the lattermost being the link between the inflowing water from the North Pacific and the BSC. The BSC contributes to the northward-flowing Anadyr Current (AC) and feeds the EKC. Surface waters leave the Bering Sea with the southward flowing EKC to the North Pacific. Deepwater exchange occurs via Kamchatka Strait and Near Strait, but only Kamchatka Strait is deeper than 2000 m and allows inflow of deep Pacific waters. Modern mid-depth to deep waters (ca. 200 – 2500 m water depth) within the Bering Sea itself are not well investigated but thought to be rather homogenous in their physical and chemical characteristics and mainly represent a mixture of North Pacific Deep and Intermediate Water (Tsunogai et al., 1979;

Luchin et al., 1999). Primary production is high, especially along the edge of the eastern continental shelf and is caused by tidal mixing and transverse circulation, which gave this area the name "Green Belt" (Springer et al., 1996). Biological productivity is dominated by siliceous plankton, with diatoms as major constituents of biogenic opal (Takahashi et al., 2002). Although no persistent mid-depth anoxia exist in the Bering Sea today, an OMZ develops between 900 and 1000 m water depth (Fig. 3.2, Garcia et al., 2010). In contrast to other permanent OMZs – e.g., in the eastern North and South Pacific – the one in the Bering Sea exhibits a significant seasonality, with lowest oxygen concentrations occurring during winter season (Paulmier and Ruiz-Pino, 2009). Throughout the year, oxygen concentrations in the core depth of the OMZ range between 0.4 and 0.7ml/l (Garcia et al., 2010).

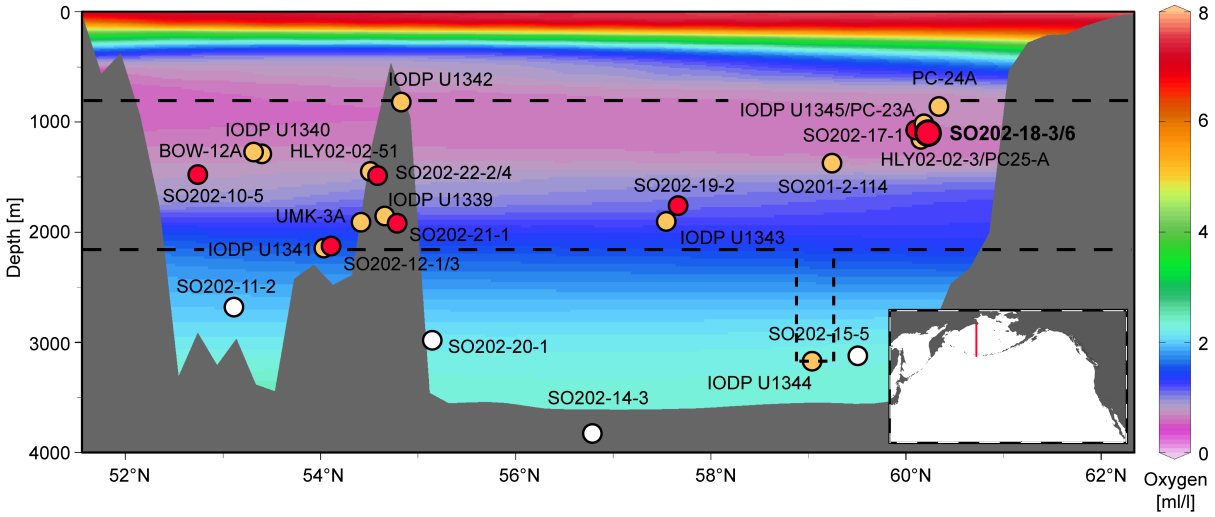

Figure 3.2: North-south profile through the Bering Sea and annual mean oxygen levels (Garcia et al., 2009). Red circles mark cores from this study containing laminated sediments; white circles mark cores from the INOPEX expedition without laminations. Core SO202-13-5 is not shown as the upper 15 kyr seems to be missing (Gersonde, 2012). Yellow circles mark published sediment records containing laminated sediments (see Table 3.1 for details). Dashed lines represent maximum and minimum water depth of the OMZ in the Bering Sea for the last deglaciation based on the occurrence of laminated sediment cores. Note that the deepening of the OMZ down to 3173 m water depth might be a local phenomenon (see text for details). Transect drawn with Ocean Data View (Schlitzer, 2002).

3.3 Material and methods

3.3.1 Sediment records

During R/V *Sonne* cruise SO202-INOPEX, 15 sediment cores were recovered from the Bering Sea in 2009 (Fig. 3.1) on a depth transect from 1066 to 3821 m water depth (Fig. 3.2). Of these cores, eight yielded laminated sequences. In this study, we use two cores from an almost identical position: piston core SO202-18-3 (60°07.60'N, 179°26.67'W; water depth: 1111 m; 10.5 cm core diameter) and neighboring kasten core SO202-18-6 (60°07.60'N, 179°26.61'W; water depth: 1107 m, 30 cm long rectangular sides). Both were retrieved off the large shelf in the northern Bering Sea, and high-resolution echo sound sub-bottom profiling data show that both coring devices penetrated to the same sediment intervals. The sediments consist of diatom-bearing silty to sandy clay. A prominent feature in both cores is the occurrence of several, meter-thick laminated sequences consisting of alternating laminae of lighter pure diatom ooze and darker diatomaceous mud. Also, several ash layers appear in both cores. Detailed core descriptions and sediment echo sounding data from the site are provided in Gersonde (2012).

3.3.2 Geochemical and X-ray image analysis

In order to obtain high-resolution geochemical data sets of major element composition, non-destructive XRF measurements were performed at the Alfred Wegener Institute with an Avaatech XRF core scanner at 1 cm resolution for both sediment cores. Each core segment was scanned three times with tube voltages of 10, 30, and 50 kV and counting times of 10, 15, and 30 s, respectively. In a second step, laminated sequences were scanned with up to 200 µm resolution at the Leibniz Institute for Baltic Sea Research using an ITRAX core scanner from Cox Analytical Systems and 45 kV Cr-tube voltage and 15 s counting time. Radiography images on the kasten core were obtained by cutting out 25x10x0.5 cm sediment slices that were wrapped into plastic foil and sealed vacuum-tight. For the radiographies, we used the cabinet X-ray system Faxitron Series from Hewlett Packard with 40 kV, 3A and 3 min exposure time. For the piston core, X-ray images were taken with the ITRAX core scanner on split sediment surfaces before the XRF scan, with tube voltages between 50 and 60 kV, a tube current of 30 mA, and exposure times between 1000 and 1200 ms depending on the thickness and density of the sediment. The radiographic images from the ITRAX scanner are radiographic positives, in which core segments of lower density appear as light intervals and vice versa (Croudace et al., 2006). Biogenic opal was measured by the sequential leaching method after Müller and Schneider (1993), total carbon content was measured with an Elementar Vario III CNS analyzer,

and total organic carbon content with an Eltra CS-2000 Carbon Sulfur element analyzer after removal of carbonate. Sediment samples were also corrected for the pore water salt content (Kuhn, 2013). $CaCO_3$ was calculated as the difference between the former two multiplied by 8.333.

3.3.3 Radiocarbon dating

For AMS ^{14}C analyses, freeze-dried sediment slices of 2 – 2.5 cm thickness were washed over a 63 μm mesh-size sieve and dried after washing at 30 °C. At least 1.7 mg of monospecific samples of the planktic foraminifera *Neogloboquadrina pachyderma* sinistral were picked from the 125 – 250 μm fraction. This foraminifera is a subsurface-dwelling species that lives in the North Pacific between 50 and 200m water depth (Kuroyanagi et al., 2002; Bauch et al., 2002). Radiocarbon dating on benthic foraminifera were carried out on mixed benthic, mostly shallow infaunal species (like *Uvigerina* spp., *Elphidium* spp, *Nonionella* spp.; cf. Bubenshchikova et al., 2008) from the fraction >250 μm. All radiocarbon measurements were performed by the National Ocean Sciences Accelerator Mass Spectrometry (NOSAMS) facility at the Woods Hole Oceanographic Institution. Ages are reported following established conventions (Stuiver and Polach, 1977). All radiocarbon dates were converted into calendar ages with the calibration software Calib 7.0 (Stuiver and Reimer, 1993) and the INTCAL13 calibration curve (Reimer et al., 2013). For the initial age conversion, a planktic reservoir age of R=700 yr was chosen, in line with previous works (Max et al., 2012; Rella et al., 2012; Itaki et al., 2009; Cook et al., 2005). Changes in deep-water ventilation ages were derived by calculating benthic-planktic ventilation ages, which are the difference between coeval benthic and planktic foraminiferal ^{14}C ages from the same respective core depth. All AMS ^{14}C measurements and calibration results are provided in Table 3.2. One ^{14}C result of the depth interval 180 – 182.5 cm in SO202-18-6 was discarded from further analysis, as it shows an age reversal that is likely attributed to a localized, bioturbation feature, which is clearly visible in the X-ray image from this depth interval (cf. Fig. 3.3a). For our other laminated cores from the Bering Sea an initial age model to determine Termination I was constructed based on correlation of XRF results (Fig. S3.1).

Table 3.2: AMS ^{14}C ages, calibrated calendar ages with 1-σ ranges, reservoir ages (res. age), and calculated benthic-planktic ventilation ages (ventil. age). Marked bold/italic res. ages are deduced by NGRIP correlation/layer counting. For comparison calendar ages with a constant reservoir age of R=700 yr are also shown. Nps: *Neogloboquadrina pachyderma* sinistral, Uvi: *Uvigerina* spp., mb: mixed benthic foraminifera.

Core	Sample ID	Depth (cm)	Species	^{14}C age (yr)	Res. age (yr)	Ventil. ages (yr)	Error ventil. ages ± (yr)	Calendar age (yr)	Calendar age (yr) 1-σ range	Calendar age (yr) with 700 yr res.age
SO202-18-3	OS-93967	530-532	Nps	12600±50	***870***	650	100	13539	13472-13579	13710
	OS-93973	530-532	mb	13250±50						
	OS-93968	542-544	Nps	12600±45	***820***	850	100	13612	13551-13711	13712
	OS-93881	542-544	mb	13450±55						
	OS-93978	601-603	Nps	12800±65	***730***	700	115	13918	13809-14005	13954
	OS-93969	601-603	mb	13500±50						
	OS-92056	747.5-750	Nps	13350±55	***880***	600	110	14640	14419-14856	15049
	OS-92023	747.5-750	Uvi	13950±55						
SO202-18-6	OS-96110	150-152.5	Nps	9280±65	770	680	115	9505	9476-9539	9550
	OS-96032	150-152.5	mb	9960±50						
	OS-93972	170-172.5	Nps	9650±35	770	800	85	10029	9917-10150	10075
	OS-93974	170-172.5	mb	10450±50						
	OS-94161*	180-182.5	Nps	9520±80	770	1030	130	9766	9604-9890	9884
	OS-96033	180-182.5	mb	10550±50						
	OS-85754	240-242.5	Nps	10050±25	770	450	80	10476	10422-10518	10566
	OS-90768	240-242.5	mb	10500±55						
	OS-90732	305-307.5	Nps	10450±40	770	600	90	11126	10907-11194	11195
	OS-92014	305-307.5	mb	11050±50						
	OS-85755	364-366.5	Nps	10700±35	***765***	700	80	11324	11263-11388	11470
	OS-90699	364-366.5	mb	11400±45						
	OS-85756**	415-417.5	Nps	10850±25	***775***	450	75	11650	11506-11750	11828
	OS-90698**	415-417.5	mb	11300±50						
	OS-96111**	432-434.5	Nps	10950±55	830	600	115	11745	11614-11946	11992
	OS-96112**	432-434.5	mb	11550±60						
	OS-94120**	512-514.5	Nps	11150±65	800	650	125	12210	12083-12382	12348
	OS-96034**	512-514.5	mb	11800±60						
	OS-96095**	592-594.5	Nps	11850±60	1100	450	140	12685	12654-12724	13020
	OS-96035**	592-594.5	mb	12300±80						
	OS-85757	622-624.5	Nps	12000±35	***990***	650	100	12869	12795-12935	13144
	OS-90733	622-624.5	mb	12650±65						
	OS-85758	650-652.5	Nps	12050±30	***970***	700	75	12955	12897-13028	13194
	OS-92049	650-652.5	mb	12750±45						
	OS-96107	680-682.5	Nps	12250±70	860	600	140	13230	13150-13293	13384
	OS-96106	680-682.5	mb	12850±70						
	OS-85759	690-692.5	Nps	12350±30	***880***	650	90	13318	13274-13353	13483
	OS-92057	690-692.5	mb	13000±60						

* age reversal

** derived from Max et al., 2014

3.3.4 Sediment classification and laminae counts

Laminae counts were performed manually on X-ray images, as the single laminae, due to their varying densities, are clearly visible in these images, compared to digital photos of the core surface. In addition, we combined the X-ray images with chlorine (Cl) counts from micro-XRF scans as a proxy for water contents (Tjallingii et al., 2007). These counts responded sensitively to density changes within the different laminae, as light and dark laminae contain different amounts of pore water. The combination of X-ray images and high resolution ITRAX data has been previously used and shown to be a suitable method for laminae countings (e.g., Staff et al., 2012). We always counted couplets of one light and one dark lamina. Laminae counting proceeded until no single laminae were visible anymore in the X-ray images, e.g., through the effect of bioturbation. The deeper laminated sequences were counted on piston core SO202-18-3, as they were not fully recovered in core SO202-18-6. For the upper laminated sections, we concentrated on core SO202-18-6, which has a better core quality during this interval. Based on repetitive laminae counts from different core section and by different investigators, the counting error is estimated to be ±5 laminae couplets for respective, ca. 1 m long, laminated sequences. This error estimation is used as counting uncertainties for the prominent laminated units that we identified in our cores (cf. Sect. 3.4.3). As we do not have a continuous record of laminated sediments, we cannot estimate a cumulative maximum counting error, which increases with depth, as done for the Greenland ice core record (Rasmussen et al., 2006).

For this study, the sediment was classified into four different types of sediment facies: (1) “Laminated Facies”, (2) “Layered Facies”, (3) “Bioturbated Lamination Facies”, and a (4) “Bioturbated Facies”. A comparable approach was applied previously in other Pacific locations on laminated sediments from the Santa Barbara Basin (Behl and Kennett, 1996) and the Japan Sea (Watanabe et al., 2007) in order to assign different types of sediment to different oxygen concentrations. The differentiation into these categories was done by visual inspection of the X-ray images (Fig. 3.3): the Laminated Facies consists of distinct and undisturbed sub-millimeter-scale up to 6 mm thick laminations with clear boundaries that can be counted and do not show signs of burrowing or other disturbances. In the Layered Facies, boundaries between biogenic and siliciclastic parts of the laminations are not clearly discernible or disappearing and centimeter-thick, undisturbed layers of mostly siliciclastic material are formed instead of clearly alternating sedimentary patterns as in the Laminated Facies. The thickness of these facies in our sediment core ranges from several centimeters down to 1 cm. In the Bioturbated Lamination Facies, originally laminated structure is partially disturbed through burrowing organisms. Lastly, the Bioturbated Facies does not show any traces of laminations or layers, since it has been completely homogenized by benthic organisms.

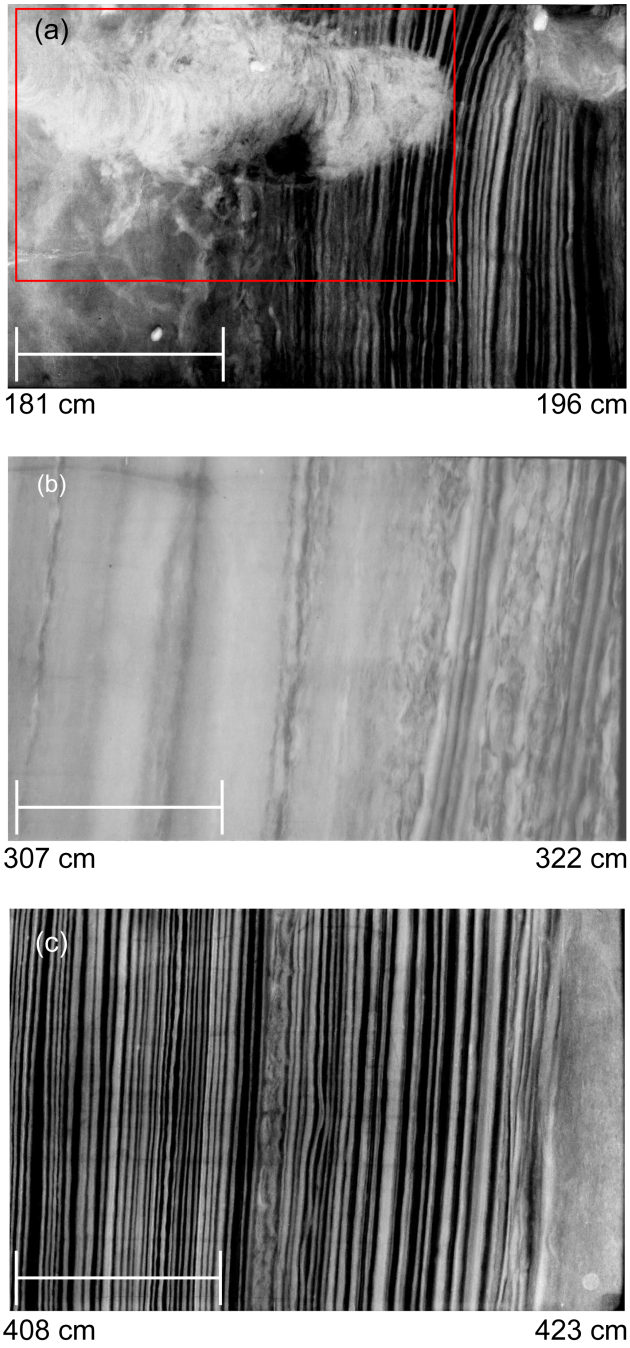

Figure 3.3: Examples of three different sediment facies in SO202-18-3/6 as shown in radiographs. (a) Bioturbated Facies (left side) and Bioturbated Lamination Facies (middle section) at the end of Preboreal laminations, (b) Layered Facies, and (c) Laminated Facies during the Preboreal. All radiographs are shown with increasing core depth to the right. The core depths of each radiograph sections are indicated below the images. The red box in (a) marks a bioturbational feature that led to an age reversal in a ^{14}C age in core SO202-18-6, 180 – 182.5 cm. The scale bar on each radiograph marks a 5 cm interval.

3.4 Results and discussion

3.4.1 Initial ^{14}C-supported age model and regional stratigraphic context

In order to correlate cores SO202-18-3 and SO202-18-6, the occurrence of two distinct ash layers, Ca/Ti ratios, and Ti counts from XRF scanning, as well as the occurrence of the laminated sections, were used (Fig. 3.4). In the XRF scans the laminated and layered sequences in both cores are characterized by higher Ca/Ti ratios and lower Ti counts (Fig. 3.4), with similar peak structure especially in the Ca/Ti ratios. Due to the shorter length of the kasten core, the lowermost laminated section was only partly recovered in core SO202-18-6. In total, piston core SO202-18-3 contains 461 cm of low-oxygen sediment sequences (i.e., Laminated and Layered Facies), and kasten core SO202-18-6 about 300 cm. We correlated the onset of laminated and non-laminated sections as basic lithostratigraphic units, by visual inspection and XRF-scanning records between cores SO202-18-3 and SO202-18-6. As an independent correlation marker we used two tephra layers identified in both cores (Table 3.3 and Gersonde, 2012). This enabled us to transfer ^{14}C ages of core SO202-18-6 to corresponding depths of core SO202-18-3, where the upper part was not sampled. The correlated core depths of core SO202-18-3 are given in supplement Table S3.1. An overview of the different sedimentary facies with according core depths is given in Table 3.3; the correlation pattern is shown in Fig. 3.4. Other laminated INOPEX cores from the Bering Sea reveal similar trends in the XRF data (Fig. S3.1).

To establish a chronostratigraphic framework for the combined core SO202-18-3/6, we converted the individual planktic AMS ^{14}C ages to calendar ages by using the INTCAL13 calibration curve (Reimer et al., 2013). In this first age control step, we used a constant reservoir age of R=700 yr (Table 3.2), in line with most previous studies (Gorbarenko et al., 2005; Itaki et al., 2009; Max et al., 2012). However, marine reservoir ages likely have varied over the glacial termination in the western North Pacific (Sarnthein et al., 2007). We address the potential changes in local reservoir ages in the discussion of Sect. 3.4.3. An age-depth relationship (Fig. 3.5) was established by linear interpolation between individual planktic AMS ^{14}C age control points through their reported median probability ages (Telford et al., 2004). According to this age model, linear sedimentation rates mostly range between 150 and 250 cm ka^{-1}.

Table 3.3: Core depths of the different facies types occurring in cores SO202-18-3 and SO202-18-6: lam: Laminated Facies, lay: Layered Facies, biolam: Bioturbated Lamination Facies, bio: Bioturbated Facies, ash: ash layer. Depth intervals of prominent laminated units (TI-BLU1-5) are marked bold/italic.

Core	Depth (cm)	Facies	Core	Depth (cm)	Facies
SO202-18-3	0-111.82	bio	SO202-18-6	0-183.91	bio
	111.82-120.07	biolam		183.91-191.84	biolam
	120.07-125.52	lam		191.84-193.5	lam
	125.52-126.6	lay		193.5-208.57	biolam
	126.6-128.31	lam		208.57-214	lam
	128.31-132.57	lay		214-256.42	lay
	132.57-137.1	lam		256.42-258.49	lam
	137.7-157.45	lay		258.49-261.04	lay
	157.45-159.62	lam		261.04-263.09	lam
	159.62-163.47	lay		263.09-269.33	lay
	163.47-169.37	lam		269.33-270.18	lam
	169.37-173.4	lay		270.18-280.83	lay
	173.4-174.28	lam		280.83-300.33	lam
	174.28-180.66	lay		300.33-317.67	lay
	180.66-196.91	lam		317.67-322	lam
	196.91-200.62	lay		322-324.84	lay
	200.62-201.99	lam		***324.84-360.25***	***lam***
	201.99-203.92	lay		***360.25-362.49***	***ash***
	203.92-226.7	***lam***		***362.49-421.05***	***lam***
	226.7-231.39	***ash***		421.05-448	bio
	231.39-266.27	***lam***		448-453.57	ash
	266.27-282.2	bio		453.57-620.02	bio
	282.2-287.5	ash		620.02-629.85	biolam
	287.5-415.75	bio		***629.85-647.39***	***lam***
	415.75-421.18	biolam		647.39-651.74	bio
	421.18-423.43	***lam***		651.74-665.68	biolam
	423.43-424.89	***lay***		665.68-690.75	bio
	424.89-440.78	***lam***		690.75-698.8	biolam
	440.78-444.08	bio		698.8-725	lam
	444.08-458.83	biolam			
	458.83-476.15	bio			
	476.15-483.59	biolam			
	483.59-503.4	***lam***			
	503.4-504.52	***lay***			
	504.52-509.7	***lam***			
	509.7-510.36	***lay***			
	510.36-527.42	***lam***			
	527.42-528.85	lay			
	528.85-532.46	lam			
	532.46-533.48	lay			
	533.48-535.33	lam			
	535.33-536	lay			
	536-538.5	lam			
	538.5-540.73	lay			
	540.73-542.72	lam			
	542.72-543.84	lay			
	543.84-561.75	***lam***			
	561.75-563.2	***lay***			
	563.2-580.76	***lam***			
	580.76-581.77	***lay***			
	581.77-602.81	***lam***			
	602.81-608.87	lay			
	608.87-615.45	lam			
	615.45-618.16	lay			
	618.16-747.08	***lam***			
	747.08-1849	bio			

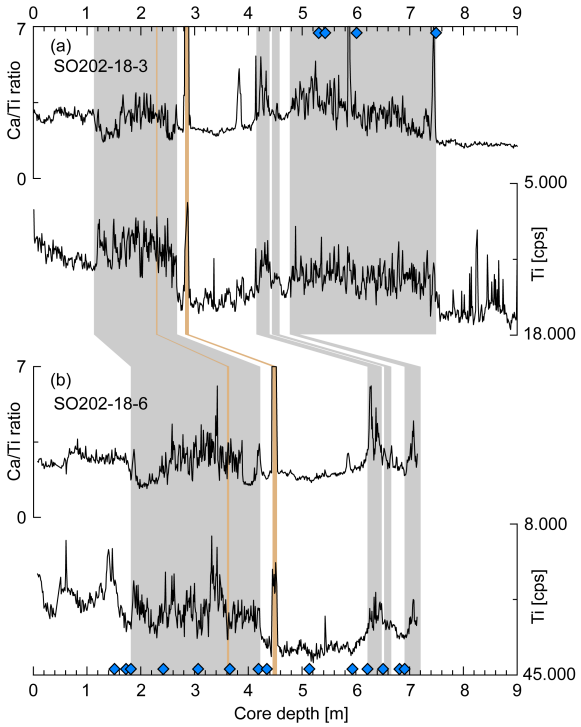

Figure 3.4: Inter-core correlation between piston core SO202-18-3 (a) and kasten core SO202-18-6 (b) based on XRF-scanning data of the Ca/Ti ratio and Ti concentrations (given in counts per second). Gray bars mark the occurrence of Layered and Laminated Facies; brown bars mark ash layers. Note inverse scale of Ti concentrations. Blue diamonds mark planktic AMS ^{14}C ages.

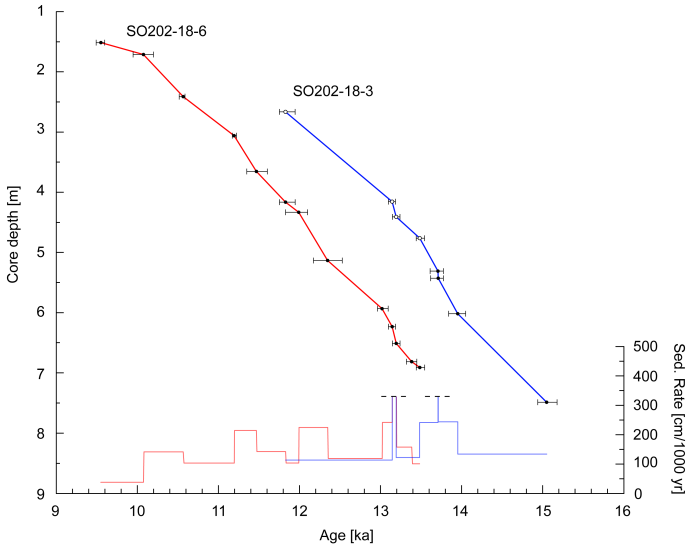

Figure 3.5: Age-depth relationship of cores SO202-18-3 (blue curve) and SO202-18-6 (red curve) based on use of constant reservoir ages of 700 yr. Error bars show 1-σ ranges of ^{14}C results. White circles in blue curve show ages derived by core-to-core correlation. Light red and blue curves show sedimentation rates. Note the cut-off in the sedimentation rate at 325 cm 1000 yr^{-1} marked by a dashed line.

To incorporate the radiocarbon-based age model of our sediment record into an established regional stratigraphic framework for the last deglaciation, we used calcium carbonate concentrations, represented by Ca-XRF counts in our records and compared those with earlier published sediment records. Deglacial sediment sequences in the North Pacific region are characterized by the occurrence of two prominent calcium carbonate peaks that have been radiocarbon-dated and assigned to glacial terminations Ia and Ib in the open North Pacific (Keigwin et al., 1992; Galbraith et al., 2007), the Bering Sea (Gorbarenko et al., 2005), and the Okhotsk Sea (Keigwin, 1998; Max et al., 2012). Our Ca concentration records closely correspond to previously published carbonate data (Itaki et al., 2009; Max et al., 2012; Rella et al., 2012). In those studies, following other published records (Cook et al., 2005; Kim et al., 2011; Schlung et al., 2013), the lower laminated sequence was assigned to the Bølling–Allerød interstadial, whereas the upper laminated interval was identified to represent the early Holocene. In particular, the 11-point smoothed Ca counts curve of core SO202-18-3 (Fig. 3.6a) closely resembles the lower-resolved $CaCO_3$ record of nearby core PC23A (Fig. 3.6b, Itaki et al., 2009; Rella et al., 2012) in the laminated intervals, with similar peak structures. The corresponding uncorrected AMS ^{14}C ages of planktic foraminifera measured on the individual carbonate peaks in SO202-18-3 and SO202-18-6 are nearly identical to those dated in core PC23A, i.e., mostly differing by less than 100 ^{14}C yr. Though it is less densely dated, core SO201-2-114 with laminated sediment sections from the western Bering Sea margin (Max et al., 2012) also closely matches our carbonate peak pattern and uncorrected ^{14}C ages (Fig. 3.6c).

The observed close similarities between the cores of this study and previously published records give us confidence to assign our Laminated and Layered Facies sections to the deglacial phases of the Bølling–Allerød and Preboreal, and the bioturbated intermediary sediment sections to the Younger Dryas (GS-1) interval. Based on this assumption we progressed to subsequent laminae counts and analyses, in order to assess the nature of deglacial and Preboreal anoxia occurrences on the Bering Sea margin and their temporal relationship with regional ocean proxy time series and the NGRIP ice core reference record (NGRIP-Members et al., 2004).

The comparison to other laminated sediment cores from the Bering Sea also reveals that the OMZ expanded to greater water depths, as sediment cores that lie below the lower boundary of the modern moderate OMZ of 900 m water depth show laminations during the last deglaciation (Fig. 3.2). The maximum vertical expansion of the OMZ according to the lamination occurrence in sediment cores extended from 818 m (laminated core U1342; Takahashi et al., 2011) to a maximum of 3173 m (laminated core U1344; Takahashi et al., 2011). However, such deep expansion of the deglacial OMZ might be a localized phenomenon of the core U1344 site, as a comparable depth was not recorded as

laminated in cores retrieved during the INOPEX cruise. There, the deepest laminated cores are from 2109 m (SO202-12), during the last deglaciation (Figs. 3.1, 3.2; Gersonde, 2012).

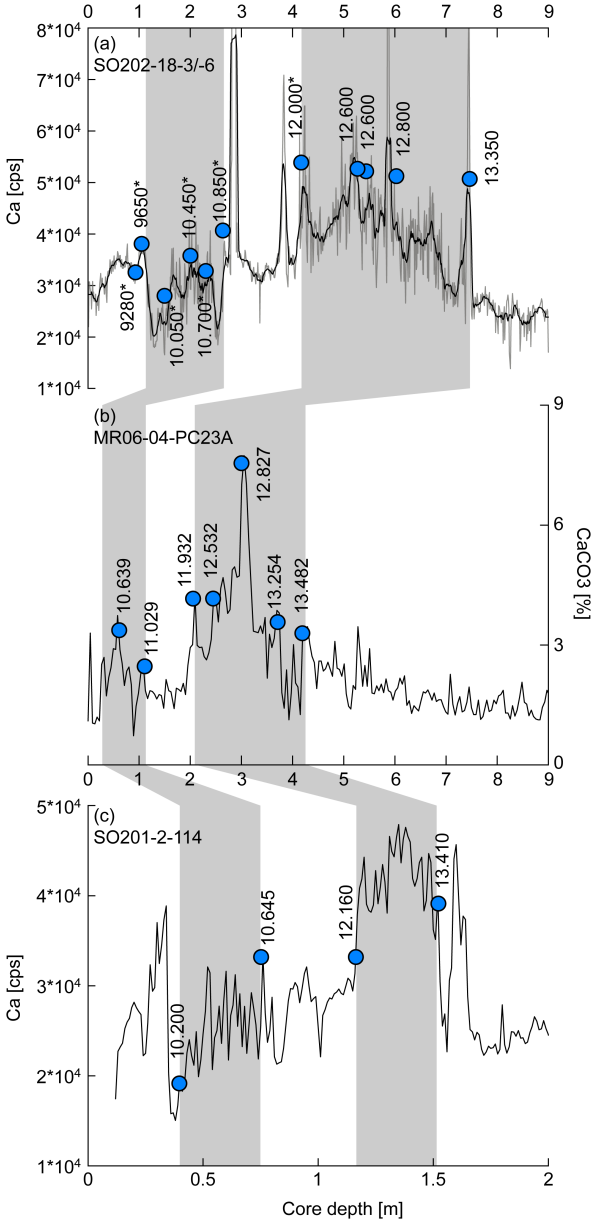

Figure 3.6: Regional stratigraphic framework based on established basin-wide carbonate peak patterns (Max et al., 2012; Keigwin et al., 1992). Comparison of core SO202-18-3 (this study) to published Bering Sea records with radiocarbon age control and laminated sediment sections. (a) Ca XRF counts of SO202-18-3; thick black line shows the 11-point moving average of the Ca data. ^{14}C ages in this graph marked with asterisks are from SO202-18-6 and were transferred to the corresponding depths of SO202-18-3 through core-core correlation. One ^{14}C age is not plotted, as it shows an age reversal (see text for details). (b) Core MR06-04-PC23A (Itaki et al., 2009; Rella et al., 2012). (c) Core SO201-2-114 (Max et al., 2012). Blue circles denote radiocarbon dates age with raw, uncalibrated ^{14}C ages. Gray shading indicates anoxic (laminated/layered) core sections.

3.4.2 Core site lamination pattern based on XRF and X-ray results

The micro-XRF data and radiographs reveal that the laminae of pure diatom ooze have a lower density due to the high concentration of well-preserved diatoms. This also leads to higher Si/Ti ratios and Cl counts (Fig. 3.7), the latter being the effect of the high porosity of the material and thus higher pore water content. Through the effect of dilution, the diatom-rich laminated sequences also lead to generally lower Ti counts within these intervals (Fig. 3.4). Microscopic analyses of selected smear slides from both cores indicate that Si-rich laminae comprise well-preserved diatom species such as *Fragilariopsis oceanica*, *F. cylindrus*, *Bacterosira bathyomphala* and *Porosira glacialis*, which are sea-ice- or cold-water-related species in the modern Bering Sea (Fig. S3.2; Ren et al., 2014). Preliminary diatom countings revealed concentrations of up to 76 % for the sea-ice-related diatoms *F. oceanica* and *F. cylindrus* in the diatom species assemblages of these laminae. Detailed counting results of selected smear slides are given in supplement Table S3.2. Phytoplankton blooms at ice edges during spring are common in the Bering Sea today (Niebauer and Alexander, 1985). Accordingly, we interpret the Si-rich layers as diatom-productivity-dominated time intervals related to the spring/summer sea ice break up phase, whereas their denser counterparts are lower in biogenic Si and contain relatively large amounts of terrigenous detrital material, rather reflecting the autumn/winter sedimentation.

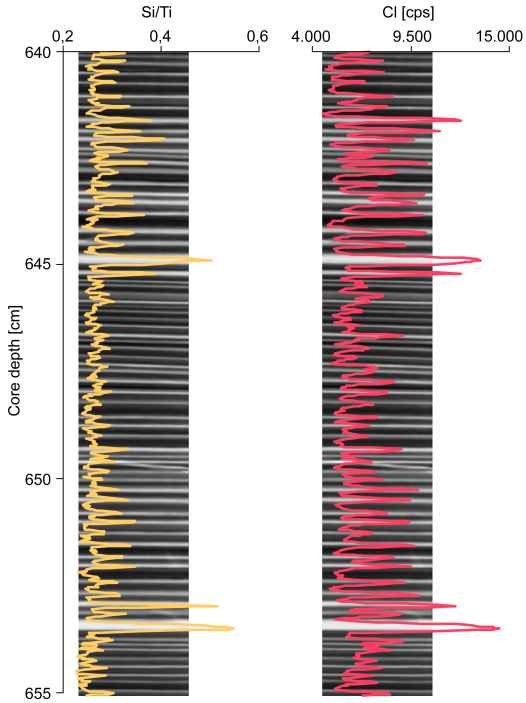

Figure 3.7: Example micro-XRF Si/Ti and Cl counts and X-ray images of SO202-18-3, 640 – 655 cm core depth. Note that less dense laminae are shown in white. The white laminae with high amounts of well-preserved diatoms represent the spring/summer bloom, while the dark, denser laminae contain high amounts of terrigenous material.

The X-ray images further reveal that the transition from bioturbated sediment to laminations occurs abruptly, especially at the Younger Dryas–Holocene transition in both cores and at the onset of the Bølling in core SO202-18-3. However, traces of bioturbation can reach several centimeters downcore at the transition from laminated to bioturbated sediment (Fig. 3.3a). According to our sediment analysis there are repeated, thicker intervals of laminated sediment sequences in our cores. We call these "Termination I Bering Sea Lamination Units" with consecutive numbering from the younger to older sequences (TI-BLU1–5). In core SO202-18-3, TI-BLU3–5 are separated by thinner sediment sequences containing additional Layered Facies sediments, while the Bioturbated Laminae Facies as well as the Bioturbated Facies intermittently occur in both cores between TI-BLU1 and TI-BLU3 (Fig. 3.8). Small intervals of laminated sediments occur also above TI-BLU1; however we did not include those parts as separately numbered units in the deglacial terminology presented here. At the current stage, we decided to concentrate our efforts on the deglacial section of our record.

3.4.3 A floating laminae-counted chronology anchored to the NGRP δ18O time series

Based on our initially established radiocarbon-anchored and regionally correlated stratigraphic framework for site SO202-18-3/6, we performed a detailed counting of the lamination pattern in the deglacial section of site SO202-18-3/6, assuming one laminae couplet represents 1 year of deposition. Following this assumption we refer to a laminae couplet as a "varve" hereafter. We compared the occurrences of the identified five TI-BLU sections, and the number of varves counted therein, to the NGRIP oxygen stable isotope record (20 yr resolution) as a Northern Hemisphere climatic reference record. For this exercise, we used two anchor dates for the marine-ice-core correlation: (1) the onset of laminations (TI-BLU5) at the start of the Bølling (or GI-1e) and (2) the re-establishment of laminations at the Younger Dryas–Holocene boundary (onset TI-BLU1). In addition, we follow the established assumption that laminated sediments correspond to the warmest interstadial phases (e.g., Behl and Kennett, 1996; Rella et al., 2012). In contrast, layered and bioturbated sediments correspond to colder periods.

The results of the varve counts in the sections TI-BLU1–5 are illustrated in Fig. 3.8. Our observed alternation of laminated TI-BLU intervals and Layered or Bioturbated Facies sections closely resemble submillennial-scale warm-cold oscillation originally identified in the Greenland ice core $\delta^{18}O$ record and described in the deglacial chronology by the INTIMATE working group (Rasmussen et al., 2006; Blockley et al., 2011). The number of counted varves seemingly corresponds to time intervals that lie above a certain minimum in the $\delta^{18}O$ NGRIP data of around 39 ‰ (Fig. 3.8). In the following, we compared our deglacial time series of Bering Sea events with the respective Greenland

sequence of events (GI-1e to GS-1/Holocene). From the older towards the younger section of our cores we counted the following intervals.

Section TI-BLU5 consists of 556±6 varves. Based on our defined first chronostratigraphic anchor point, these TI-BLU5 varves correspond to the Bølling (GI-1e, Fig. 3.8), which comprises 617 yr on the GICC05 timescale. This ca. 90 % temporal coverage argues for the occurrence of annually deposited, laminated sediments at our site. Based on the assessment that cold intervals are not laminated, the following mainly Layered Facies section between TI-BLU5 and TI-BLU4 would then be assigned to the small cooling of the Older Dryas (GI-1d) in the GICC05 chronology.

Section TI-BLU4 consists of 289±3 varves and correlates to a first warm phase in the NGRIP Allerød (GI-1c), ranging from 13.90 to 13.62 ka, thus indicating a nearly complete overlap with our laminae counts. While no formal subdivision has been established within the Allerød (GI-1c) so far (e.g., by the INTIMATE working group; Blockley et al., 2011), we partition this time interval as we can identify short cold periods within this warm phase, which are imprinted as Layered Facies intersections in otherwise Laminated Facies parts in our core and can be correlated with short cold spells in the 20 yr averaged NGRIP $\delta^{18}O$ time series. The following sequence between TI-BLU4 and TI-BLU3 contains several Layered Facies intervals and is assigned to a short, intra-GI-1c cooling period in the NGRIP $\delta^{18}O$ record that lasts about 85 yr (13.62 – 13.53 ka) and which we tentatively call Early Allerød Cooling (EAC, Fig. 3.9). Despite the intermittent accumulation of Layered Facies sediments within the EAC, we counted 60±1 varves and thus cover 80 % of the potential reference time. The detailed inspection of TI-BLU4 before the EAC and TI-BLU3 after the EAC reveals that these two intervals are both interrupted by multiple, thin (i.e., less than 2 cm thick) Layered Facies sediment sections at ca. 13.80, 13.72, 13.44, and 13.42 ka (Fig. 3.9). Based on our varve counts these short intervals correspond to rapid, inter-decadal cooling intervals in GI-1c with durations of less than 60 yr each. This lamination pattern is surprisingly similar to the distant NGRIP record, in particular with regard to the bidecadal resolution of the ice core record's $\delta^{18}O$ time series. This might also be a reason for the slight differences between the temperatures decreases in NGRIP and the position of these thin Layered Facies sections.

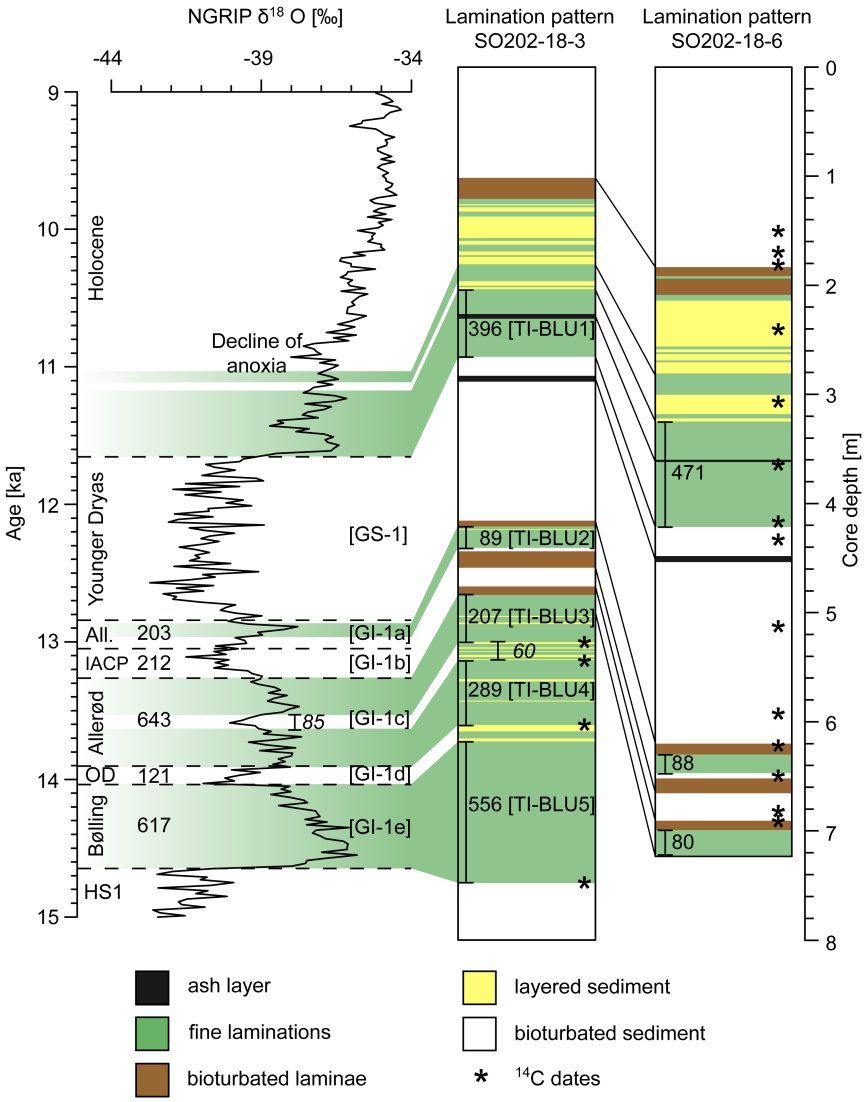

Figure 3.8: Correlation between lamination pattern in cores SO202-18-3/6 to 20 yr average NGRIP ice core data (Rasmussen et al., 2006). Dashed lines and captions on the right side of NGRIP data mark the events according to the GICC05 chronology, and their duration is given with the numerical numbers between the dashed lines. The left side of the stable isotope graph shows the commonly used terminology of the Blytt-Sernander sequence (Mangerud et al., 1974) for comparison. The italic number inside GI-1c gives the duration of a short cold period inside the Allerød that we also identified in our core SO202-18-3. Green colors in the NGRIP data mark warm phases that correspond to the laminated sediment intervals of our sediment cores. On the right side the lamination patterns of SO202-18-3 and SO202-18-6 are shown. Bioturbated Facies are shown in white, Bioturbated Lamination Facies in brown, Layered Facies in yellow, Laminated Facies in green, and ash layers in black. Black lines between both cores mark correlated sediment facies. Laminated sections that were correlated with warm periods in the ice core record are labeled TI-BLU1–5. Asterisk mark ^{14}C dates, and numbers and vertical black lines inside the lamination patterns give results of laminae counts for the TI-BLU intervals. Additionally, laminae countings of a short cold period between TI-BLU4 and TI-BLU3 that was identified during our correlation are given in italic letters (see text for details). Note that thick laminated sections do not occur after 11 ka. (All.): Allerød; (IACP): Intra-Allerød Cold Period; (HS1): Heinrich Stadial I; (OD): Older Dryas.

Within the uppermost part of interval TI-BLU3 (Fig. 3.8) the effect of downward bioturbation slightly decreases the precision of laminae counts. In total, 207±2 varves were counted in this interval. However, when correlated with the upper part of the Allerød (GI-1c), ranging from 13.53 to 13.26 ka, our counts still cover more than 77 % of the NGRIP reference time interval under an annual deposition scenario. We acknowledge that varves might have been lost in the counting process due to the upper completely bioturbated boundary. The cold period on top of TI-BLU3 matches the entire Intra-Allerød Cold Period, or IACP (GI-1b). This colder interval in its youngest part shows the first Bioturbated Facies sediments and a short interval of Bioturbated Laminae Facies.

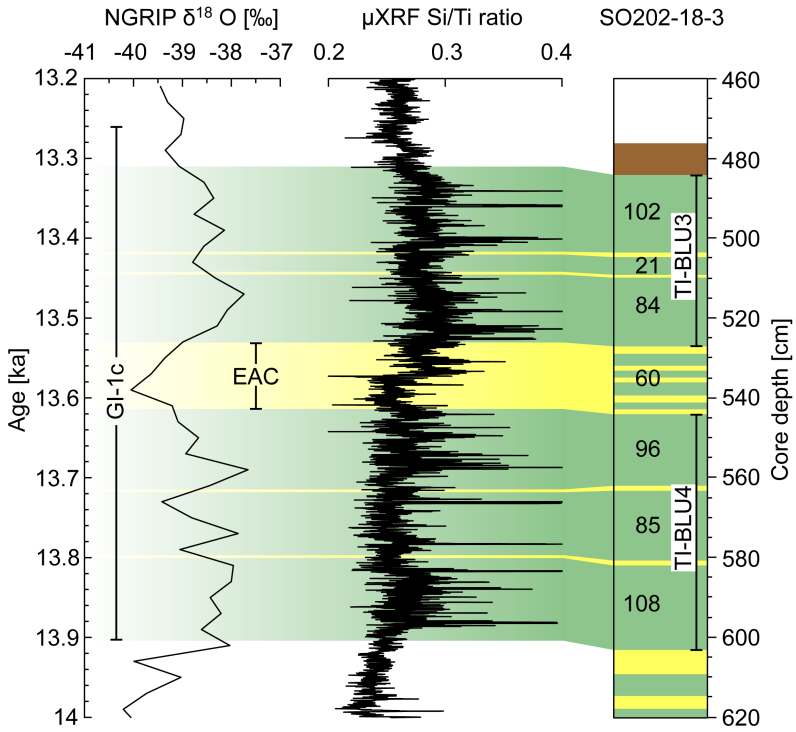

Figure 3.9. Detailed lamination pattern of core SO202-18-3 covering the Allerød (GI-1c) interval with a correlation with NGRIP ice core data. Left panel: NGRIP 20 yr average $\delta^{18}O$ record. EAC marks the "Early Allerød Cooling", a small cooling event not named in the GICC05 chronology. Middle panel: micro-XRF Si/Ti ratios as a proxy for productivity, with higher ratios indicative of higher productivity. Right panel: Bering Sea lamination pattern with varve counts. Bioturbated Facies is shown in white, Bioturbated Lamination Facies in brown, Layered Facies in yellow, and Laminated Facies in green as in Fig. 3.8.

Thereafter, the Laminated Facies section begins, identified as TI-BLU2 (Fig. 3.8). We counted 89 (±1) varves in this section and assigned these to NGRIP Allerød (GI-1a). Compared to the GICC05 chronology that provides a duration of 203±71 yr for this time interval, our TI-BLU2 section is at face value lacking a considerable part of preserved laminae, or years. To resolve this discrepancy, we

consider the following explanation: the TI-BLU2 interval is bound both on the upper and lower boundary by intervals with the Bioturbated Laminae Facies, which we were not able to count reliably. Thus, we presume that our reported varve counts in TI-BLU2 are skewed towards lower numbers than have been deposited originally. In fact, for a "true" count of all originally deposited varves, we would have to add the neighboring upper and lower core intervals of the Bioturbated Laminae Facies (5.43 and 18.75 cm, respectively; cf. Table 3.3) to our counts in the Laminated Facies section (18.13 cm, Table 3.3, all values taken from core SO202-18-3). If we roughly extrapolated the potential number of "uncounted varves" from these Bioturbated Laminae Facies based on core depths and average sedimentation rate/thickness of laminae within the Laminated Facies, we would have to add ca. 119±12 varves to our counted 89 varves (in depth interval 421.18 – 440.78 cm, Table 3.3, core SO202-18-3), thus bringing the total of originally deposited varves to 208±13. This value would then be in excellent agreement with the GICC05-based duration of 203 yr for GI-1a. As a result, we are rather confident that the proposed annual sedimentation regime for the laminae persisted throughout the entire warm phases of the Bølling–Allerød (GI-1). Moreover, a potentially slightly diachronous GS-1 inception as shown by differing proxy time series within the NGRIP ice core might hamper a direct annual one-to-one correlation in this particular time interval (e.g., Ruth et al., 2007; Steffensen et al., 2008). The subsequent interval between TI-BLU2 and TI-BLU1 corresponds to the Younger Dryas (GS-1), and the occurrence of the Bioturbated Facies during this cold interval prevented laminae counts.

For the onset of TI-BLU1 we assume an age of 11.65 ka, based on the GICC05 chronology (Fig. 3.8), in line with our defined anchor point. For TI-BLU1 (11.65 – 11.18 ka) we,unfortunately, cannot establish a clear upper chronostratigraphic boundary, because cold and warm oscillations identified in the NGRIP ice core during the Preboreal are at present difficult to reconcile with our Bering Sea time series (Fig. 3.8). We note, however, that neither are all early Holocene climatic oscillations unambiguously recorded in all Greenland ice cores (Rasmussen et al., 2007). Thus, we defined the upper end of TI-BLU1 through laminae counts with a total number of 471±4 varves (Fig. 3.8). Taken together, our laminae counts show strong support for the hypothesis that laminae are deposited annually. As a result, our achieved correlation allows for the defining of sections which are directly tied to GICC05-derived calendar ages. These independent calendar ages deduced by correlation with the NGRIP record can in turn be used to estimate regional surface reservoir ages (i.e., R) for radiocarbon dating (Table 3.2). Our calculated reservoir ages range within 730 – 990 yr in the Bølling–Allerød (mean reservoir age: 875 yr), 800 – 1100 yr in the Younger Dryas (mean reservoir age: 910 yr) and 765 – 775 yr in the Preboreal (mean reservoir age: 770 yr) (cf. Table 3.2, directly calculated R values in bold/italic letters). These are qualitatively consistent with earlier studies that

suggested varying reservoir ages in the North Pacific during the last deglaciation (Gebhardt et al., 2008; Sarnthein et al., 2007). Our calculated values for local reservoir ages are in line with studies that inferred surface reservoir ages close to 730 yr during the last deglaciation, with variations of about ±200 yr in the eastern North Pacific (Lund et al., 2011), and with reservoir age estimates of 700 – 800 yr for the British Columbia coast (Southon and Fedje, 2003). However, we note that regional reservoir ages reconstructed for the eastern North Pacific and wester North Pacific during the Bølling–Allerød (GI-1) derived by the "plateau tuning method" (Sarnthein et al., 2007) are younger than our results – with 440 and 720 yr, respectively – pointing to the possibility of distinct regional or even localized oceanographic reorganizations in the upper and mid-depth water column during the last deglaciation (Sarnthein et al., 2013).

3.4.4 Teleconnections and forcing mechanisms for rapid climate signal transfer

As a result of the close correspondence between the counted lamination patterns and the Greenland ice core data (Figs. 3.8, 3.9), we assume that the preservation of laminations is tied to warm surface temperature intervals concomitant with higher export production, superimposed on the already-warm background temperature within GI-1. This co-occurrence of higher export production with warmer temperatures is also evident on decadal timescales by a slight decline of the Si/Ti ratios in our proposed EAC (Fig. 3.9) and on centennial scales during the Older Dryas (GI-1d) and IACP (GI-1b; Fig. 3.10a). The Si/Ti ratios are robust indicators of bio-siliceous export production, as they are not susceptible to post-depositional alteration by sedimentary redox conditions.

To further test the relationship between lamination occurrence and SST, we used lower-resolved alkenone-based SST reconstructions of three cores from the Shirshov Ridge in the western Bering Sea (Max et al., 2012) to infer SST information at least on a basin scale. We used these SSTs as no data are available directly from Laminated and Layered Facies sediment intervals of our sites. We are aware that the alkenone data may represent a seasonal signal, most likely a summer temperature signal (Seki et al., 2007). We merged the individual site reconstructions presented in Max et al. (2012) into one stacked, three-point running mean SST record (Fig. 3.10b) to consolidate the regional signal. Hereby, we used the published age model of Max et al. (2012). This age model is mainly based on high-resolution scans of color b*values, a proven proxy for biogenic productivity variations (Nürnberg and Tiedemann, 2004). The close correlation between high color b*values and lamination occurrence during the last deglaciation was also shown for nearby core PC23A (Kim et al., 2011). The standard error of the originally used SST calibration is ±1.5 °C (Max et al., 2012). Despite the lower resolution, these SST data indicate corresponding temperature variations throughout the Bølling–Allerød (GI-1),

and SST maxima broadly correlate with the occurrence of laminated intervals and warmer Greenland air temperatures. The stacked SST record from the Bølling–Allerød (GI-1) reveals temperature differences between the cold phases of the Older Dryas (GI-1d), the small EAC as well as the IACP (GI-1b), and the warm laminated periods. Mean SSTs during the colder Bølling–Allerød intervals in the Bering Sea were around 5 °C, and increased to 6 °C in the warmer phases (Fig. 3.10b). Further support comes from a stacked $\delta^{18}O$ record of the planktic foraminifera *Neogloboquadrina pachyderma* sinistral of the Gulf of Alaska (GoA), which was interpreted as a proxy for changes of annual SSTs (Fig. 3.10c; Praetorius and Mix, 2014). This record with decadal-scale resolution clearly shows the warm-cold oscillations during the Bølling–Allerød (GI-1) that are visible in our lamination sequence and in the NGRIP record (Fig. 3.10d). We observe a close correspondence between the GoA and our Bering Sea record even for short-term events like the observed EAC event, reflected in higher $\delta^{18}O$ GoA values (i.e., lower SSTs). These temperature trends from several locations in the North Pacific in principle support our assumption that anoxia occurrence is connected to warmer SSTs; however, additional annually resolved SST proxy time series from our sites would be needed to prove a causal relationship between higher SSTs and the occurrence of anoxia.

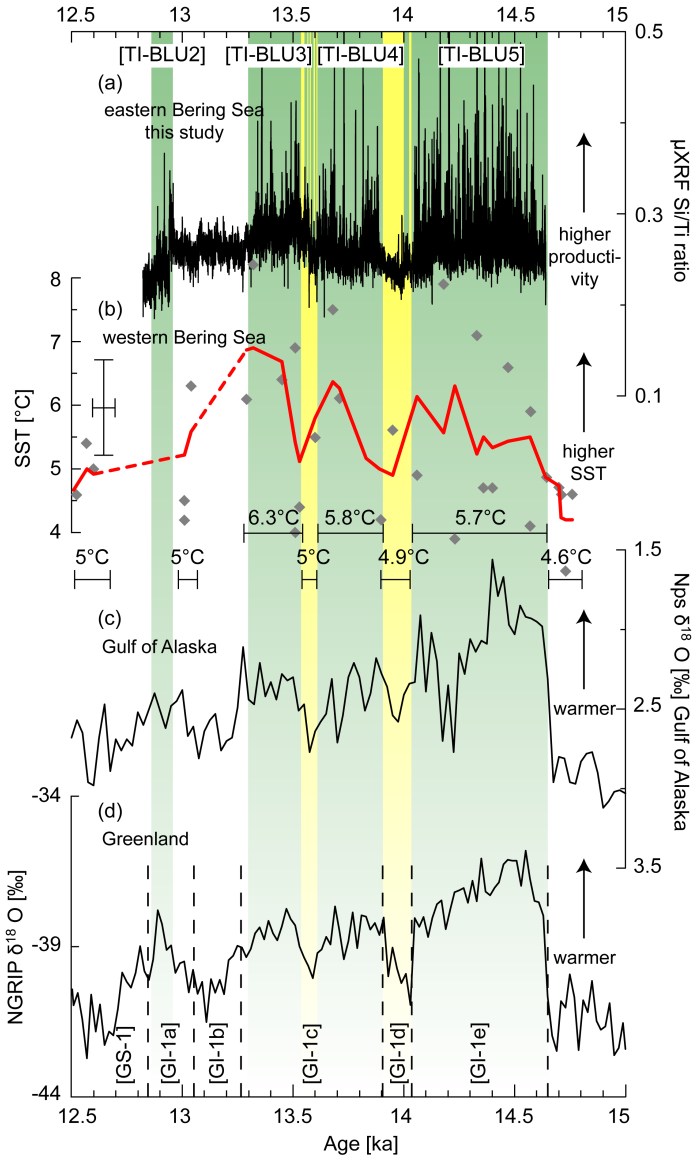

Figure 3.10: Comparison of laminated core SO202-18-3 with Bering Sea SST records, planktic $\delta^{18}O$ data from the Gulf of Alaska, and Greenland temperature changes across the Bølling–Allerød time interval. (a) Micro-XRF Si/Ti ratios of SO202-18-3. (b) In red the stacked SST record (three-point running mean) of cores SO201-2-77, SO201-2-2-85, and SO201-2-101 from the Shirshov Ridge, western Bering Sea. The gray squares depict the individual SST measurements (Max et al., 2012). Dashed parts in the SST record indicate intervals with insufficient temperature data. The age model used in this plot is the published model of Max et al. (2012). The numerical temperatures below graph (b) are the calculated mean SSTs from the marked warm and cold intervals, and the horizontal bars indicate the temporal range of the average SST. The error bars on the left side of (b) show the uncertainties of SST measurements and radiocarbon datings. (c) $\delta^{18}O$ data of planktic foraminifera *Neogloboquadrina pachyderma* sinistral from the Gulf of Alaska as a proxy of long-term changes in annual average SST (Praetorius and Mix, 2014). Note that we used the age model after Praetorius and Mix (2014). (d) NGRIP stable isotope data as reference record. The occurrence of mainly Laminated Facies, Layered Facies, and Bioturbated Facies in SO202-18-3 is shown in green, yellow, and white, respectively. Laminated sections in SO202-18-3 are labeled TI-BLU as in the text.

The clear imprint of even such short time periods like the low-amplitude EAC between 13.62 and 13.53 ka and the Older Dryas in the Bering Sea lamination pattern strongly argues for a close atmospheric coupling between the North Atlantic and the North Pacific without significant time lags. Several previous works have provided evidence for millennial-scale variations in Bering Sea biogenic productivity and upper-ocean characteristics during the last glacial termination that occur in phase with both Greenland and east Asian paleoclimatic reference records (Rella et al., 2012; Itaki et al., 2009; Max et al., 2012; Caissie et al., 2010; Riethdorf et al., 2013b). This in-phase behavior of laminated sediment deposition in warm phases of the deglacial Bølling–Allerød (GI-1) interstadial is also known from several locations around the North Pacific Rim (Jaccard and Galbraith, 2012), albeit not on shorter decadal timescales as implied by our study. The oceanographic changes recorded in our sediment core occur with rapidity, comparable to the fast climate changes reported from ice cores (Taylor et al., 1997; Steffensen et al., 2008) or varved lake sediments (Kossler et al., 2011; Brauer et al., 2008).

In the past, studies using general circulation models investigated the teleconnection between the North Atlantic and the North Pacific and possible linkages to changes in the Atlantic Meridional Overturning Circulation (e.g., Mikolajewicz et al., 1997; Vellinga and Wood, 2002; Okumura et al., 2009). In these numerical model experiments cold periods like Heinrich Stadial 1 and the Younger Dryas are simulated by freshwater forcing in the North Atlantic, which leads not only to a weakening of the overturning cell but also to significantly colder temperatures over both the North Atlantic and North Pacific regions. However, while the response over the North Pacific is common in many models, the transfer mechanisms are less well understood, especially on decadal timescales. One important climate determinant for variations in the Bering Sea ocean-atmosphere system is the Aleutian Low as a main action center in the circulation of the Northern Hemisphere (Rodionov et al., 2007). Changes in the strength and location of this system have a direct effect on winter air and sea surface temperatures and thus sea ice occurrence, which in turn influence the strength of the phytoplankton bloom season. Several studies suggest a strong Aleutian Low is associated with warm winters in the Bering Sea (Niebauer, 1983), and that winter temperatures in the Bering Sea are sensitive to the position of the Aleutian Low (Rodionov et al., 2007). It has further been shown that the Aleutian Low varies on decadal timescales and is also associated with variability of the Arctic Oscillation (Overland et al., 1999). We suggest that decadal changes in position and strength of the Aleutian Low lead to colder and warmer winters on decadal timescales. The colder (warmer) winters are connected with increased (decreased) sea ice cover, which is highly sensitive to temperature changes and fosters decreased (increased) diatom blooming events.

3.4.5 Characteristics and causes of millennial- to decadal-scale OMZ development

The occurrence of laminations serve as a direct indicator for oxygenation decreases below the threshold for most marine benthic life and the development of severe and persistent anoxia in Pacific intermediate water masses. We follow previous works (Behl and Kennett, 1996) in assigning different oxygen concentrations to the different facies in our record. These are as follows: <0.1ml/l O_2 excluding any burrowing macrofauna for Laminated Facies; 0.1 ml/l O_2 for Layered Facies, which allows only meiofaunal bioturbation that just diffuses the laminations on millimeter scales but does not lead to deeper bioturbation by larger organisms; 0.1 – 0.2 ml/l O_2 for Bioturbated Laminae permitting partial homogenization; and >0.3 ml/l O_2 for the Bioturbated Facies allowing bioturbating macrofauna (Behl and Kennett, 1996).

3.4.5.1 Deglacial strengthening and Holocene decline of anoxia in the Bering Sea

Our facies analysis reveals millennial-scale changes between stadial, well-oxygenated (bioturbated) phases and interstadial, mainly anoxic (laminated/layered) phases during the last glacial termination, consistent with recent assessments (Jaccard and Galbraith, 2012). In our records, Bioturbated Facies occur on millenial scales during the cold stadial Younger Dryas (GS-1) phase and the relatively cold IACP (GI-1b), indicating improved oxygen concentrations in the bottom water at our site. These periods are contrasted with the two interstadial dysoxic – anoxic sediment facies during the entire Bølling (GI-1e) – Allerød (GI-1c) and Preboreal (Fig. 3.8).

Notably, superimposed on these interstadial warm phases we recorded multiple, rapid facies changes on inter-decadal timescales between Layered and Laminated Facies (Fig. 3.9). These changes exhibit a shorter-term, subtler process that modulates the mid-depth deglacial Bering Sea oxygen concentration. Though Layered Facies do not show a clear expression of alternating seasonal laminae like in laminated sections, they are devoid of major bioturbation, thus evidencing persistent anoxic to dysoxic conditions. These patterns lead us to distinguish between millennial-scale larger oxygenation changes (between oxic and dysoxic – anoxic) and superimposed decadal-scale smaller fluctuations (between dysoxic and anoxic) as distinct patterns in OMZ strength.

The Laminated and Layered Facies disappear after the Preboreal in the Holocene, indicating both a vertically contracting and abating OMZ in the Bering Sea compared to deglacial conditions (Fig. 3.8). As the increasing NGRIP $\delta^{18}O$ data would suggest ongoing deposition of laminations, changes in the environmental background conditions must have been distinct. Multiple causes are likely. Firstly, alkenone-based SST data show a temperature decrease of more than 3 °C in the Bering Sea throughout

the early Holocene, which might lead to reduced phytoplankton productivity due to shorter and colder summers (Caissie et al., 2010; Riethdorf et al., 2013a). However, SSTs are still higher compared to the Bølling–Allerød, pointing to additional factors besides SSTs that might influence the Holocene OMZ development. Secondly, another potential cause could be a change in the characteristics of mid-depth water masses at our sites in the Bering Sea, either in age (and thus nutrient inventories) or in oxygenation compared to the mid-late Holocene. Published ventilation ages reveal no clear Holocene changes in the North Pacific (Duplessy et al., 1989; Ahagon et al., 2003), and the occurrence of oxygen-poor, Layered Facies together with rather unchanged B-P ventilation ages suggests that oxygen depletion of mid-depth waters is not caused by the presence of upwelled older, oxygen-poor North Pacific deep-water masses (cf. 3.4.5.2). In support of this notion, evidence from Gulf of Alaska sites that lie in the upstream part of waters entering the Bering Sea show oxygenation increases from anoxic – suboxic towards suboxic – oxic conditions around 10.9 – 9.2 ka (Addison et al., 2012; Davies et al., 2011), broadly in line with ceasing anoxia at our site SO202-18-3/6.

An additional factor for the establishment of higher oxygenation potentially is the opening of the Bering Strait at around 11 ka (Elias et al., 1996; Hu et al., 2010). Today, the northward annual through-flow of relatively warm, nutrientrich North Pacific water into the Arctic Ocean is around 0.8 sverdrup (Woodgate et al., 2010). Roughly, during the time of the Bering Strait opening at 11 ka the occurrence of Layered Facies increases until laminations finally disappear at 10 ka. As Layered Facies represent slightly higher oxygen concentrations compared to laminated sequences, this change might represent a trend towards decreasing productivity, beginning with the opening of the Bering Strait. Likely, the effect of this gateway opening was not instantaneous but rather steadily increasing and amplified with ongoing sea level rise. Today the gateway influences the lower productivity ecosystems of the Chukchi and Beaufort seas with the advection of high nutrient Pacific waters (Grebmeier et al., 2006). As it has further been suggested that higher primary production in the Chukchi Sea also during the Holocene could result from the greater nutrient supply from the Bering Sea (e.g., Keigwin et al., 2006), we suggest the following mechanism: before 11 ka Bering Sea surface ocean circulation was substantially different from modern patterns, with an absent or weakened Anadyr Current and differing expression of the Bering Slope Current, also leading to different interactions with the Alaskan Stream and the open North Pacific. These changes potentially caused a more intense gyre circulation within the Bering Sea, enhanced trapping and re-circulation of nutrients and thus higher productivity. We further suggest that the opening of this shallow gateway also led to a decline in the surface stratification as warm, nutrientrich surface waters were transported to the Arctic Sea. Such a trend for declining stratification after the Preboreal in the Bering Sea can be tentatively assumed based on differences between alkenone and Mg/Ca-based SST starting at about 9 ka

(Riethdorf et al., 2013a). As a second factor, the coastline retreated significantly further away from the core position during the flooding of the shallow northern shelf areas in connection with ongoing sea level rise. Thus, the influence of the fluvial input, delivering nutrients and enhancing surface stratification, diminished.

3.4.5.2 Millennial-scale changes in intermediate water ventilation

To identify the potential impact of North Pacific intermediate water circulation and ventilation changes on longer-term, millennial-scale oxygen variations on our sites, we calculated benthic-planktic ventilation ages (Fig. 3.11). In principle, older B-P ages could indicate the transport of highernutrient, lower-oxygen water masses, such as North Pacific Deep Water (NPDW) to the Bering Sea and their entrainment into the upper, mid-depth waters, thereby supporting OMZ strengthening. However, our B-P ages show only moderate oscillations throughout the deglacial sequence, with values between 470 and 700 ^{14}C yr, all significantly below values reported for Pacific Deep Water of 1530±230 ^{14}C yr (Lund et al., 2011). Additionally, B-P age oscillations at our sites do not reflect stadial-interstadial changes in ventilation and are with variations of 100 – 200 yr substantially smaller in amplitude than those reported from distant, more southern mid-depth locations, e.g., off Japan and the Santa Barbara Basin for the same time interval (Fig. 3.11; cf. Duplessy et al., 1989; Ahagon et al., 2003; Roark et al., 2003; Kennett and Ingram, 1995). Note that for this comparison planktic ^{14}C ages of Japan and the Santa Barbara Basin were recalculated using the new INTCAL13 calibration curve and reservoir ages of Sarnthein et al. (2007) for the Santa Barbara Basin. One potential reason for the small oscillations could be that the Bering Sea is remote from the formation area of the most prominent mid-depth water mass, North Pacific Intermediate Water (NPIW), which has a strong influence on the ventilation off Japan. Our B-P ventilation age data do not support a collapse of subarctic North Pacific mid-depth water circulation during GI-1 and the Preboreal. As a result, we do not consider that physical forcing leading to NPIW formation rate or source region changes play a decisive role in the development and vertical expansion of interstadial anoxia at mid-depth in the Bering Sea.

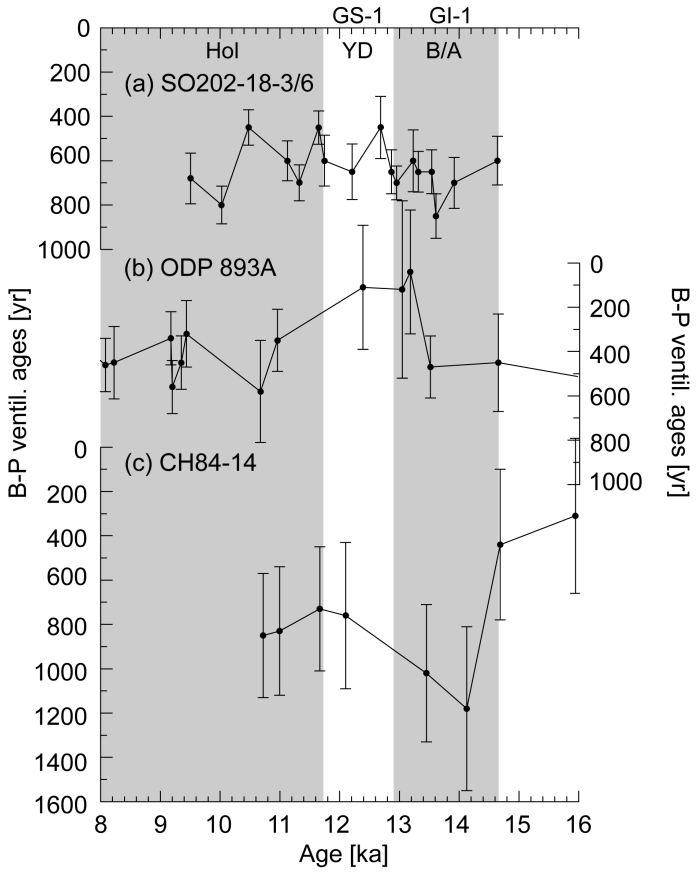

Figure 3.11: Compilation of ^{14}C paleo-ventilation ages (a) for core SO202-18-3/6, derived from benthic-planktic foraminifera age differences compared to results from (b) the Santa Barbara Basin (Ingram and Kennett, 1995; Roark et al., 2003) and (c) off Japan (Duplessy et al., 1989). Error bars show radiocarbon dating errors. For this comparison, planktic 14C ages of Japan and the Santa Barbara Basin were recalculated using the new INTCAL13 calibration curve and reservoir ages of Sarnthein et al. (2007) for the Santa Barbara Basin. Hol: Holocene; YD: Younger Dryas; B/A: Bølling–Allerød.

However, for the Gulf of California and the Santa Barbara Basin it was suggested that phases of oxic and dysoxic conditions were controlled by changes in oxygen concentration of upper intermediate water (Kennett and Ingram, 1995; Hendy et al., 2002). Based on analyses of laminated sediments from the North American continental margin, Zheng et al. (2000) suggested suppressed ventilation at higher latitudes of the North Pacific during the Bølling–Allerød. In line with these assumptions, epibenthic $\delta^{13}C$ data from the Alaska Margin (Davies et al., 2011) and from the modern formation regions of NPIW (Max et al., 2014) show major decreases in mid-depth oxygenation during the Bølling–Allerød. We thus assume that changes in NPIW oxygen concentrations are an important factor for conditioning the mid-depth waters in the Bering Sea on millennial timescales. Oxygen decreases can be caused by high export production and subsequent higher mid-depth remineralization of exported organic matter along the pathway of NPIW in the Pacific subarctic gyre without significant changes in the formation

rate of NPIW (Crusius et al., 2004). This scenario would be in line with our radiocarbon B-P age ventilation data and is supported by a number of studies indicating widespread export productivity peaks during the Bølling–Allerød and the Preboreal throughout the North Pacific (Brunelle et al., 2010; Kohfeld and Chase, 2011), combined with reductions in oxygen concentrations along the pathway of NPIW throughout the North Pacific (Hendy and Pedersen, 2006; McKay et al., 2005).

3.4.5.3 Modulation of OMZ strength during the Bølling–Allerød (GI-1) and Preboreal

Increased export production through higher biogenic productivity leads to an intensification of the OMZ through organic matter degradation. Generally, higher primary productivity is indicated by various productivity proxies. Increased Ca/Ti ratios (Fig. 3.4) and carbonate mass accumulation rates (Fig. S3.3) might be caused by higher carbonate production through coccolithophorids (Okazaki et al., 2005; Khim et al., 2010). Further, the low Ti concentrations during the laminated intervals, higher biogenic opal mass accumulation rate (Fig. S3.3), and high Si/Ti ratios in the biogenic laminae (Fig. 3.7) point to increased seasonal export production. Regionally increased bio-siliceous productivity during the Preboreal and Bølling–Allerød was also shown for the southern Bering Sea (Gorbarenko et al., 2005) and in nearby, partly laminated, core PC23A (Fig. 3.1; Khim et al., 2010; Katsuki et al., 2014). Several environmental factors can influence the biological productivity and OMZ development.

1. Higher bottom water temperatures at our site during the warmer Bølling–Allerød phases would increase the remineralization of organic matter at the seafloor, as metabolic rates of organisms increase with higher temperatures (Matsumoto et al., 2007). Such a process could work independently of surface ocean processes as a positive feedback, contributing to elevated oxygen consumption in intermediate waters. Unfortunately, regional bottom water temperature reconstructions from North Pacific sites are to our knowledge not available to provide information on the importance of such a process. However, a qualitative assessment of potential temperature changes based on published benthic oxygen isotope records from comparable water depths shows no unambiguous trends. On Shirshov Ridge, values show a glacial-interglacial amplitude change of 1.95 ‰ (Riethdorf et al., 2013), and in the eastern Bering Sea of ca. 1.4 ‰ (Rella et al., 2012).

2. During peak glaciation, the biological productivity was restricted by a shorter and colder summer that led to the spatial extension of sea ice (Takahashi, 2005; Nakatsuka et al., 1995). Higher temperatures during the Bølling–Allerød and since the onset of the Holocene (Max et al., 2012; Riethdorf et al., 2013a) would have supported an earlier retreat of sea ice and a change from longer and more pronounced, sometimes multi-year sea ice cover during cold phases like Heinrich Stadial 1 and Younger Dryas to shorter, seasonal sea ice seasons. This is in line with evidence based on diatom

assemblages from the Umnak Plateau (Caissie et al., 2010), which indicates during the Bølling–Allerød a shift from perennial to seasonal sea ice and a pattern similar to the ice-related bloom in the marginal ice zone on the Bering Shelf today.

3. Regionally elevated rates of primary productivity ultimately require high-nutrient surface water concentrations. On the NE Bering Sea margin, these can be delivered through several sources. High meltwater input by fluvial runoff from retreating North American hinterland glaciers would provide additional nutrients through lateral transport of terrigenous material, most likely delivered during warmer episodes (Sancetta et al., 1984; Itaki et al., 2009). In addition, nutrient increase was likely enhanced to a significant extent by the deglacial sea level rise, leading to the flooding of the previously exposed, wide, shallow proximal northern Bering Sea shelf. This process would have provided additional nutrients compared to the modern situation, as suggested for similar settings with laminated sediments from the southeast Alaska Margin (Davies et al., 2011). Another process influencing the amount of biological productivity is light, depending on upper ocean stratification, which can constitute the limiting factor in biogenic productivity especially in high latitudes (Kohfeld et al., 2005). Before the Bølling–Allerød, enhanced upper-ocean mixing potentially increased light limitation by a deeper mixed layer. With the onset of the Bølling, input of meltwater from the North American ice sheets stratified the upper water column and fostered biological productivity (Lam et al., 2013; Katsuki et al., 2014) as it would enable phytoplankton to prolong their growth season and better use the more abundant bio-available nutrients in the upper photic zone (Niebauer et al., 1995; Niebauer and Alexander, 1985). Such changes in freshwater-induced stratification might also work fast enough to explain the observed decadal-scale correspondence of fine laminations to higher temperatures (Fig. 3.10).

In summary, we presume that major forcing of OMZ was likely a combination of sea ice changes, with less sea ice during the warm phases and variations in ocean stratification with a more stratified upper water due to freshwater input.

However, the anoxic – dysoxic bottom waters during the Older Dryas (GI-1d) and the EAC did not ameliorate to a point that would permit strong bioturbation, but just enabled the observed meiofauna-induced dispersal of annual layer structures on millimeter scales. Had instead the former been the case, the layered structure of the sediment would have been destroyed by larger-scale macrofauna bioturbation. A further increase in oxygenation, despite the lower productivity in these cold phases, was likely prevented by the still comparably low oxygen concentrations of mid-depth water entering the Bering Sea.

Taken together, we see two major processes that contribute to the strengthening of the OMZ in the Bering Sea and thus the formation of laminated sediments. Based on rather constant ventilation ages, we observe millennial-scale changes in the NPIW oxygen concentrations without significant variations in the formation rate of NPIW. This millennial-scale pattern, however, apparently did not drive oxygen concentrations below the critical threshold for anoxic conditions and lamina formation (i.e., <0.1ml/l). Oxygen concentrations decreased to that extent only in combination with higher regional export production and subsequent remineralization of organic matter during the warm phases of the Bølling–Allerød. Our results corroborate earlier hypotheses that argued for oxygen drawdown in the North Pacific by a combination of higher organic matter export and lower O_2 concentrations at intermediate waters (Zheng et al., 2000; Crusius et al., 2004). Other possible forcing mechanisms connected to indices like the Pacific Decadal Oscillation or to solar forcing are currently under discussion (e.g., Katsuki et al., 2014) and at present cannot be corroborated based on the data presented in this story.

3.5 Summary and conclusions

Two laminated cores from the northern Bering Slope located in intermediate water depths allow for a tight coupling to Greenland ice core data on decadal timescales, especially for the deglacial Bølling–Allerød phase (GI-1, 14.64 – 12.85 ka). By correlating a suite of laminated sediment intervals to NGRIP oxygen isotope data, we established an age model partly independent from radiocarbon dating, which in turn was used to calculate marine reservoir ages. Mean reservoir ages are 875 yr for the Bølling–Allerød (GI-1), 910 yr for the Younger Dryas (GS-1), and 770 yr for the Preboreal. The correlation and laminae counts implied the presence of annually layered sediment sections (varves). The combined information from sediment facies analysis and microscale high-resolution XRF-scanning showed that the laminations represent an annual alternation of high bio-siliceous spring/summer blooming events driven by the sea ice retreat and a rather siliciclastic background sedimentation.

Our results show for the first time that the mid-depth water column in the Bering Sea reacted quickly on inter-decadal timescales to changes in upper-ocean characteristics, particularly in regard to sea ice dynamics, surface water stratification, and sea surface temperatures. Potential implications for the future arise from these observations of rapid changes. It is unclear whether oxygen concentrations could drop again to anoxic levels if temperature increases and sea ice decreases continue along present trends (e.g., Brown and Arrigo, 2012; Grebmeier, 2006), leading to the expansion of subarctic Pacific “death zones”. This would create significant consequences and large-scale ecosystem readjustments.

On millennial, or stadial to interstadial, timescales relatively constant benthic-planktic ventilation ages reveal that the OMZ development is more likely caused by basin-wide mid-depth remineralization of organic matter in intermediate waters, rather than changes in formation rate or sources of intermediate water masses. On decadal timescales, the formation of laminated sediments during the Bølling–Allerød seems to be effectively coupled to warm temperatures, as expressed in NGRIP ice core $\delta^{18}O$ and Bering Sea SST data. This tight correlation with warm phases during the Bølling–Allerød in the ice core data implies a close atmospheric teleconnection to North Atlantic and Greenland climate. During these warm intervals, rapid sea ice and temperature-induced decadal-interannual-scale export productivity changes lead to fine modulations of OMZ strength between anoxic and dysoxic conditions. Comparison with other laminated cores from the Bering Sea shows that during the last deglaciation the OMZ expanded to greater water depths, possibly of more than 3000 m at some locations. The disappearance of the laminations during the Holocene might be coupled to the opening of the Bering Strait.

Acknowledgements

We thank the captain, crew, and scientific party of R/V *Sonne* for their support during cruise SO-202 (INOPEX). Lars Max and Jian Ren provided comments and suggestions that improved this paper. We thank Susanne Wiebe, Ute Bock, and Rita Fröhlking (AWI) for technical support, and Sascha Plewe and Rainer Bahlo (IOW) for support with the ITRAX core scanner. We acknowledge financial support by the Alfred-Wegener-Institute, Helmholtz Centre for Polar and Marine Research; the MARUM – Center for Marine Environmental Sciences (Project OC 3); and funding by the German Federal Ministry of Education and Research (BMBF Grant no. 03G0202A) for the INOPEX (Innovative NOrth Pacific EXperiment) project.

Supporting Information

Laminated sediments in the Bering Sea reveal atmospheric teleconnections to Greenland climate on millennial to decadal timescales during the last deglaciation

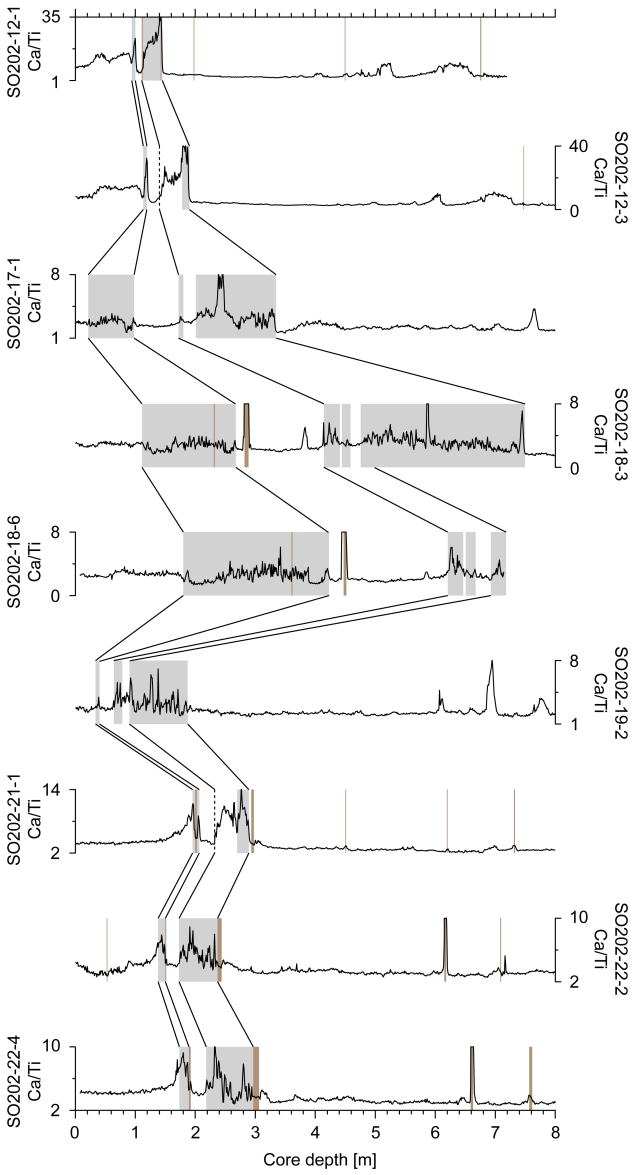

Fig. S3.1: XRF derived Ca/Ti counts of laminated INOPEX cores in the Bering Sea (see Table 3.1 for details) and core-core correlation. Laminated intervals of the early Holocene and the Bølling–Allerød are marked with gray bars. Ash layers are shown with brown bars. In cores SO202-12-3 and SO202-21-1 only the first part of the Bølling–Allerød seems to be laminated and the end of the Bølling–Allerød is indicated by a dashed line. The cores are shown with increasing station number. The deepest core with laminations is SO202-12 with 2109 m water depth, while the shallowest core is SO202-17-1 with 1066 m water depth.

Table S3.1: Depth intervals of ^{14}C age samples of core SO202-18-6 and the corresponding core depths of SO202-18-3. The depths were derived by the inter-core correlation, based on the appearances of the laminations and ash layers in both cores.

Core depths of ^{14}C ages SO202-18-6 [cm]	Corresponding core depths SO202-18-3 [cm]
150-152.5	96
170-172.5	111
180-182.5	112
240-242.5	152
305-307.5	198
364-366.5	230
415-417.5	266
432-434.5	273
512-514.5	328
592-594.5	393
622-624.5	417
650-652.5	444
680-682.5	468

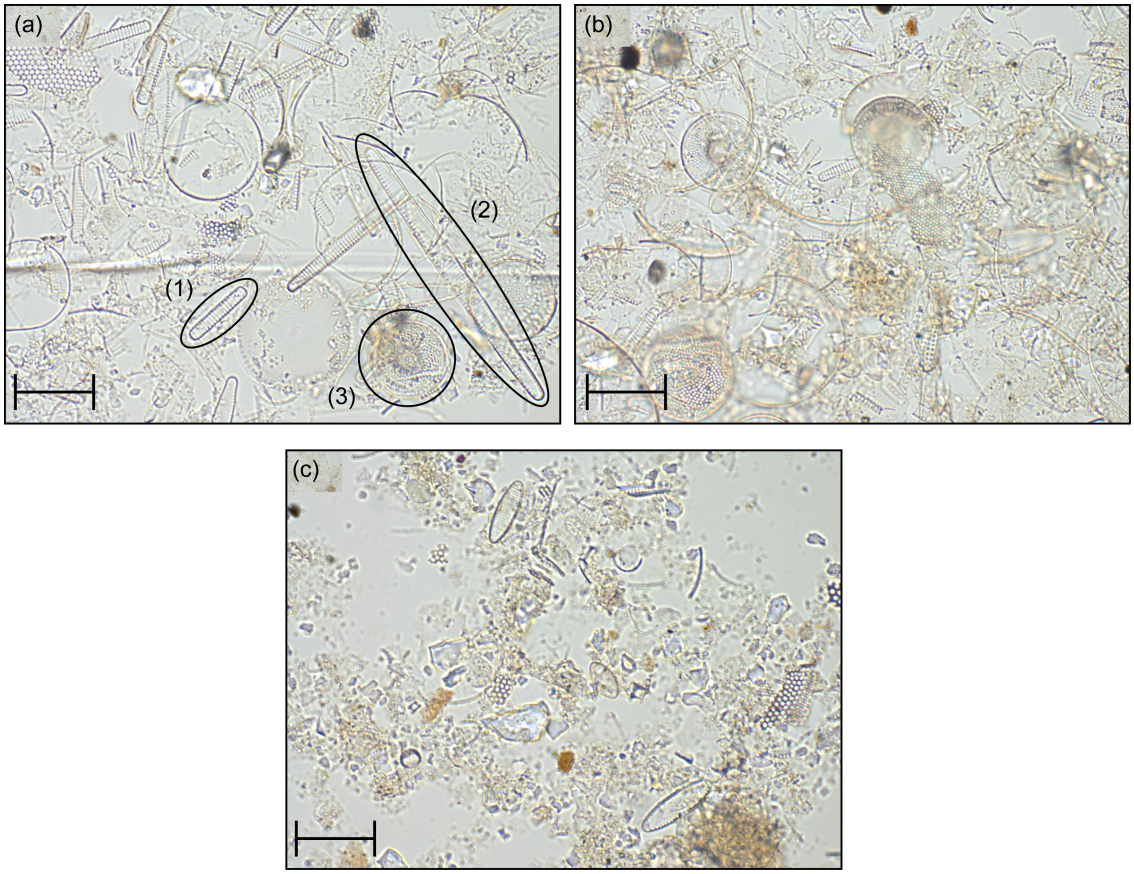

Fig. S3.2: Smear slides of single laminae from core SO202-18-3. (a): Holocene biogenic lamina from 234.3 cm core depth. Marked (1) to (2) are sea ice related diatom species *Fragilariopsis cylindrus* and *F. oceanica* and (3) cold-water related species *Bacterosira bathyomphala*. Diatom counts revealed ca. 76 % of sea ice related species. (b): Biogenic lamina from the Bølling at 686.8 cm core depth. In this slide ca. 63 % of the counted diatom assemblage represent sea ice related species. (c): Terrigeneous lamina from the Bølling (623.9 cm core depth). This slide reveals only moderate preservation of diatoms, while the preservation in the biogenic laminae is good and ca. 35 % of the counted diatom assemblage are sea ice related species. The scale in all images represents 20 µm. Detailed results of diatom counts are given in supplement Table S3.2.

Table S3.2: Exemplary diatom counts of the smear slides (Fig. S3.2). Blue background and bold species names are sea-ice-related taxa (note high abundance).

Diatom species	SO202-18-3, 234.3 cm	SO202-18-3, 686.8 cm	SO202-18-3, 623.9 cm
Actinoptychus senarius			1
Asteromphalus brookei	1		
Bacterosira bathyomphala	6	18	4
Chaetoceros spp. (spores)	46	36	47
Chaetoceros spp. (vegetative)			35
Coscinodiscus marginatus		1	4
Coscinodiscus radiatus	2		
Coscinodiscus oculus-iridis			1
Delphineis surirella			18
Fragilariopsis cylindrus	300	200	32
Fragilariopsis oceanica	22	55	68
***Fragilariopsis oceanica* (long)**	13	11	2
Navicula spp.	1		
Neodenticula seminae		1	19
Nitzschia spp.	1		3
Odontella aurita	1	2	1
Paralia sulcata			2
Porosira glacialis	17	67	8
Thalassionema nitzschioides	2		8
Thalassiosira antarcitca var. *borealis*	17	15	6
Thalassiosira antarcitca var. *borealis* r.sp.			1
Thalassiosira nordenskioeldii		2	
Thalassiosira trifulta		2	4
Thalassiosira spp.	14	10	25

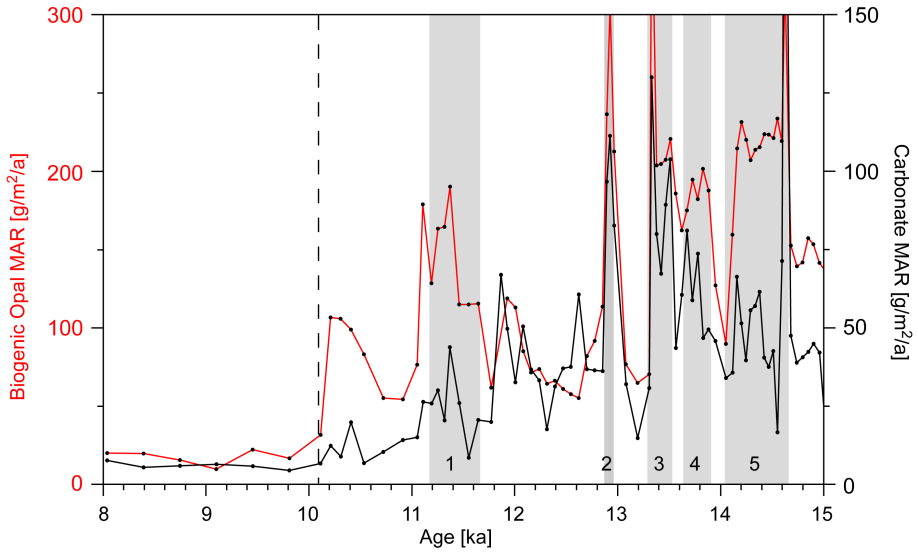

Fig. S3.3: Biogenic opal mass accumulation rate (MAR, in red) and carbonate MAR in black of core SO202-18-3. The shaded sections mark the laminated units (TI-BLU1–5) that were derived by our correlation to the NGRIP record (see text for details). The dashed line indicates the disappearance of laminations in the Holocene. Higher biosiliceous productivity during the laminated units TI-BLU1–5 (marked by numbers 1–5) is indicated by higher biogenic opal MAR. Carbonate MAR shows the same trend as the biogenic opal MAR.

4. Tidal forcing and ocean-atmosphere dynamics drive productivity variations in the deglacial Bering Sea

Hartmut Kuehn[1,2], Lester Lembke-Jene[1], Gerrit Lohmann[1], Rainer Gersonde[1,2], Oliver Esper[1,2], Helge Arz[3], and Ralf Tiedemann[1]

[1] Alfred-Wegener-Institut Helmholtz-Zentrum für Polar- und Meeresforschung, Bremerhaven, Germany

[2] MARUM Zentrum für Marine Umweltwissenschaften, Bremen, Germany

[3] IOW - Leibniz Institut für Ostseeforschung, Warnemuende, Germany

To be submitted to Geophysical Research Letters

Abstract

We analyzed a sediment record from the northeastern Bering Sea, with annually laminated sections covering the Bølling–Allerød and early Holocene. By using micro-X-ray-fluorescence-derived Chlorine data, which represent semi-quantitative biogenic opal concentrations, we established an annually-resolved proxy time series. We discovered cyclic variations in the amplitude of the Cl counts that indicate changes in the biosiliceous (opal) productivity. Spectral analyses revealed a sharp 18.8-year spectral peak and a second, broader peak in the range of 30 – 60 yr. We ascribe the first peak to the 18.6 yr nodal tidal cycle and the latter to variations of the Pacific Decadal Oscillation. These two forcing systems influence primary productivity through nutrient supply to the mixed layer via tidal mixing, variations in sea surface temperature and stratification. While the identified processes have been previously inferred from instrumental data and modelling studies for the modern setting, our results show the persistence of these mechanisims through deglacial times. We suggest that productivity variations in the subarctic Pacific are consistently influenced by a combination of external and internal forcing mechanisms.

4.1 Introduction

The subarctic North Pacific is subject to substantial natural variations in biogeochemistry and ecology on decadal timescales (e.g. Minobe, 97; Mantua and Hare, 2002). The causes for this variability are

still largely unknown, partly due to the insufficient temporal length of most instrumental datasets covering just about 100 years (e.g. Overland et al., 2012), the complexity of the potential forcings and their interactions. Both, factors internal to ocean-atmosphere dynamics, and externally generated features like solar- or tidally-induced variations have been suggested as forcing candidates (e.g. Keeling and Whorf, 2000), with differing consequences for the long-term characteristics and persistence of natural environmental variations in these sensitive ecosystems, and their potential impending anthropogenic alteration (e.g. Grebmeier et al., 2006; Latif, 2006; van Loon et al., 2007). Hence, longer-term reconstructions back in geological time from well-resolved archives help to better understand mechanisms of interdecadal oceanographic dynamics and the dynamics of the involved processes.

In the marine setting, analyses of long, annually laminated sediments provide the opportunity to study decadal scale oceanographic changes, as they combine the critically needed, precise age control with sufficient temporal resolution. Laminated records, mostly from the last glacial termination, have been studied from various sites in the North Pacific and Bering Sea (e.g. Cook et al., 2005; Caissie et al., 2010). The Bering Sea is of particular interest as it is one of the most productive marginal seas in the world and has a very sensitive ecosystem that has been recently proposed to undergo a fundamental and probably non-reversible change towards warmer, more subarctic conditions (Grebmeier et al., 2006). In the Bering Sea, the deglacial strengthening of the oxygen minimum zone that led to the deposition of laminated sediments has been ascribed mainly to increases in biological productivity with subsequent maxima in export and remineralization of organic matter (OM), supported by oxygen-poor waters entering the Bering Sea (Kuehn et al., 2014). However, the laminated records so far have mostly been used to study longer, millennial- to centennial-scale changes, and not for analyzing prominent decadal-scale dynamics.

Here, we present results from a partially laminated sediment core from the northeastern Bering Sea slope that covers parts of the last deglaciation with annual resolution (Kuehn et al., 2014). We use micro-X-ray-fluorescence (XRF)-derived Chlorine data as indicator for biological productivity and spectral analyses to investigate whether cyclic variations can be detected in our record. We discuss if these productivity variations are driven by external forcing mechanisms or originate internally from the ocean-atmosphere system. These results will advance our understanding of the persistence of major climate drivers in the subarctic North Pacific.

4.2 Material and methods

In this study, we used the partly varved piston core SO202-18-3 (60°07.60'N, 179°26.67'W, water depth 1111 m) from the northeastern Bering Sea slope (Fig. 4.1; Gersonde, 2012). The age model for the last 15 ka has been established based on ^{14}C dating of planktic foraminifera, layer counting and a correlation of prominent laminated sediment sections to the NGRIP ice core oxygen isotope record. It has further been shown that the occurrence of laminations is tightly coupled to the warm phases of the Bølling–Allerød (B/A) and early Holocene (Fig. 4.2; Kuehn et al., 2014). The laminations consist of alternations between low-density, biosiliceous productivity-dominated layers, and denser layers consisting of mainly terrigenous detrital material. The diatom layers represent the spring/summer sea ice break-up phase, with larger amounts of biogenic material being produced, whereas the latter reflect the autumn/winter sedimentation, leading to the deposition of annual layers (or varves) as shown in a previous study (Kuehn et al., 2014).

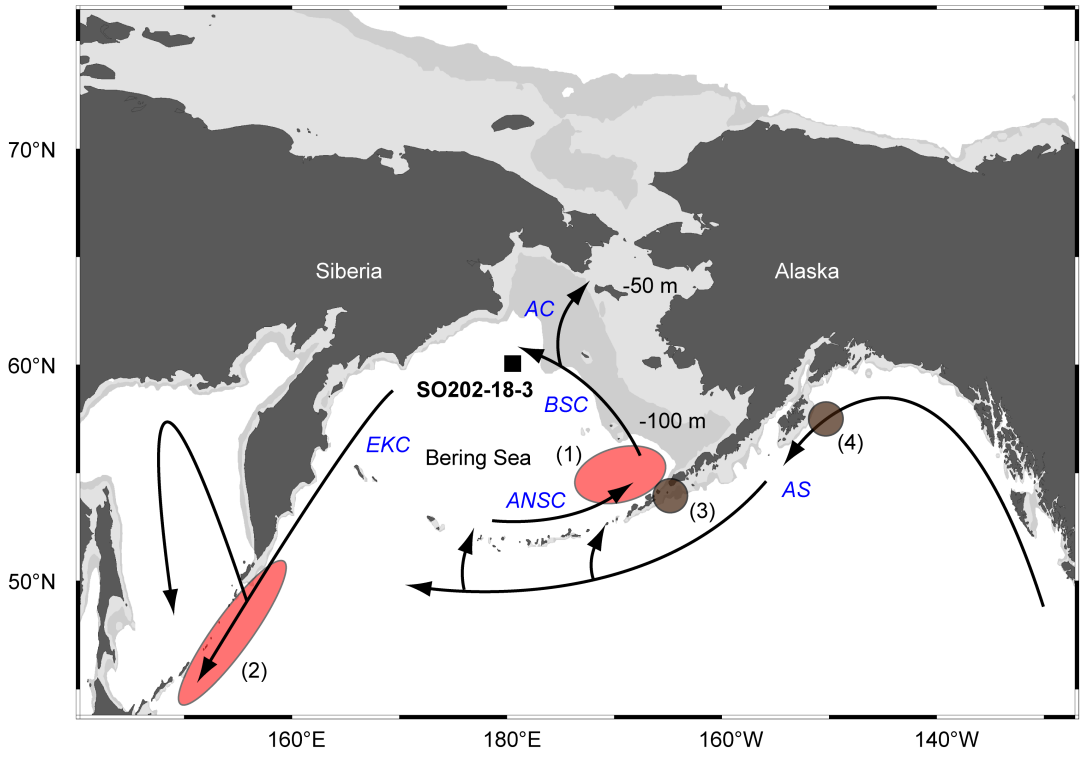

Figure 4.1: Map showing the core position (black square) and shelf areas that were aerially exposed by a deglacial sea level of -50 m (light gray) and -100 m (dark gray). Surface circulation shown with black arrows and currents labeled blue. AS: Alaska Stream; ANSC: Aleutian North Slope Current; BSC: Bering Slope Current; AC: Anadyr Current; EKC: East Kamchatka Current. Red circles (1) and (2) mark areas where the 18.6 yr nodal tidal cycle was reported to effect surface- and intermediate water properties (*Osafune and Yasuda*, 2006; *Osafune and Yasuda* 2010). Brown circles (3) and (4) mark areas where strong tidal mixing was observed (*Stabeno et al.*, 2005; *Ladd et al.*, 2005). Map generated with Ocean Data View (*Schlitzer*, 2002).

For spectral analyses of varves characteristics we used micro-XRF-based Cl counts with 200 µm resolution as indicator for biosiliceous productivity. XRF measurements with 200 µm resolution were performed with the ITRAX scanner from COX Analytical Systems at the Leibniz Institut für Ostseeforschung, Warnemuende and with 1 cm resolution with the Avaatech XRF core scanner at the AWI, Bremerhaven (see text S4.1). Additional biogenic opal measurements on bulk sediment were measured following the leaching method of Müller and Schneider (1993), results were corrected for the porewater salt content (Kuhn, 2013).

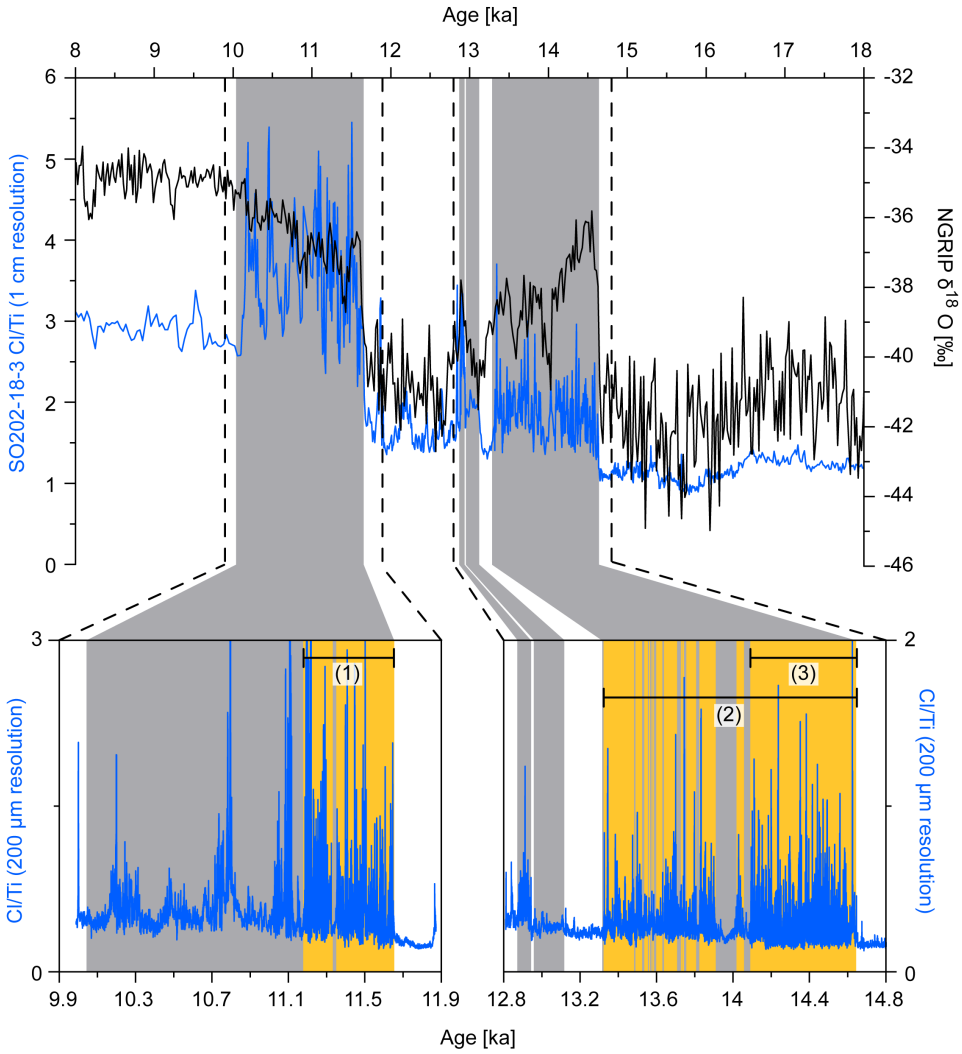

Figure 4.2: Deglacial XRF-derived Cl/Ti ratios (1 cm resolution, measured with the Avaatech core scanner) of core SO202-18-3 (blue) in comparison to NGRIP $\delta^{18}O$ data (black; NGRIP members, 2004). Gray bars mark intervals with layered to laminated sediments during times of oxygen depletion. Cutout sections below show XRF-scan with 200 µm resolution (measured with the ITRAX core scanner) of the early Holocene and B/A. Horizontal lines (1) to (3) show the time slices of the (1) Holocene, the (2) Bølling–Allerød and (3) Bølling where we performed spectral analyses. The exact laminated sequences for spectral analyses are shown in orange.

Today, the Bering Sea is one of the most biologically productive oceanic regions, with siliceous photoautotrophs, especially diatoms, as main contributors to primary production (Takahashi et al., 2002). In the sediment record, the pore water content and thus Cl concentration depends on the density of the sediment. Especially in the Bering Sea the latter is closely related to the preservation of diatom frustules with large diatom contents resulting in a lower density (Hamilton, 1970). Accordingly, the biosiliceous laminae parts reveal comparably higher Cl contents as they contain high amounts of well preserved diatoms, as previously shown in smear slide analyses of discrete laminae (Kuehn et al., 2014). This assumed tight relation is corroborated by (1) comparative analyses of X-ray images and micro-XRF results of single laminae with both high Cl counts and high Si/Ti ratios that co-occur in less dense, more biosiliceous laminae (Fig. 4.3a and 4.3b); and (2) the high correlation of single laminae Cl contents and sediment density, derived from X-ray-based gray values (Fig. 4.3c). Lastly, a validation test successfully showed good correlation between bulk sediment biogenic opal concentrations and XRF-based Cl counts from the exact same sample depths (Fig 4.3d). In summary, we suggest it is reasonable to use XRF-based Cl data as indicator for biosiliceous primary productivity.

The X-ray images in combination with the micro-XRF data enabled us to identify single laminae and their corresponding Cl values (Fig. 4.3). We investigated the seasonal amplitude modulation of the Cl values by assigning the corresponding maximum Cl value to every biogenic laminae and the minimum value to every terrigenous laminae. The result is an evenly spaced data set with seasonal resolution, which can be analyzed with respect to its frequencies. For the spectral analyses of our time series we used a Fast Fourier Transformation (FFT) with the confidence interval set at 95 % and the spectra being obtained by averaging 2 bins of the periodogram. Additionally, we applied spectral analyses following Blackman and Tukey, and the Maximum Entropy method (see text S4.1). In this study we focus on spectral peaks that are visible in three time slices from the Bølling, the B/A and the early Holocene (Fig. 4.2). For the Bølling interval we analyzed an uninterrupted sequence of laminations covering 559 yr, for the B/A we combined laminae to construct a longer, “composite” time series of 1006 yr, and for the early Holocene we analyzed an uninterrupted laminated sequence of 391 yr length.

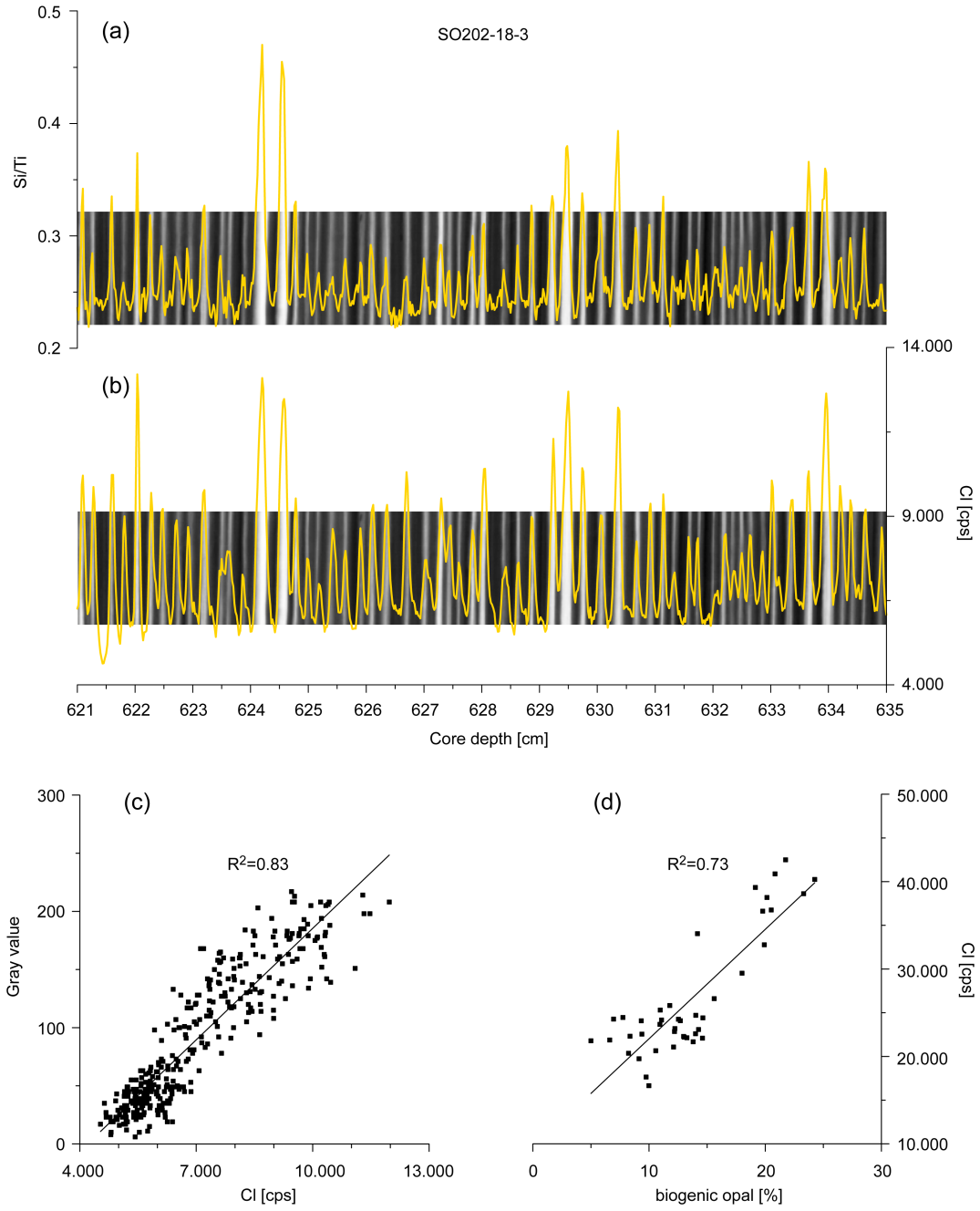

Figure 4.3: (a) X-ray showing an example of laminations within the Bølling interstadial and an overlay of XRF derived Si/Ti ratios, (b) XRF derived Cl values (given in counts per second) and the corresponding X-ray image of the same interval shown in (a). Note phases of enhanced opal deposition at 624.5 cm, 629.5 cm and 634 cm core depth, with higher Cl counts and increased Si/Ti ratios. Biosiliceous, less dense laminae are shown in light gray. (c) Correlation coefficient R^2 of XRF-derived Cl values (given in counts per second) and X-ray-derived gray values of single laminae from the Bølling interval. (d) Correlation coefficient R^2 of bulk sediment biogenic opal and the corresponding Cl values (in counts per second) of the same sample depths from the Holocene to Bølling-Allerød. Note XRF measurements in (a) to (c) were performed with the ITRAX core scanner and in (d) with the Avaatech core scanner.

4.3 Results and discussion

The FFT spectrogram of the Bølling time series reveals (1) a significant sharp spectral peak in the range of 18.9 years and (2) a broad, three-peak spectral maximum between 30 – 60 years (Fig. 4.4a). These spectral peaks are confirmed by our additional spectral analyses (Fig. S4.1a). Less distinct spectral peaks are apparent at 3.8 yr and 8 yr (Fig. 4.4a).

In the time series from the B/A the main spectral peaks retain their overall structure and are similar to those of the Bølling interval, with the 18.8 year spectral peak becoming even more pronounced (Fig. 4.4b, Fig. S4.1b, Fig. S4.2). The previously identified spectral peak at 30 – 60 yr remains statistically significant. In the early Holocene record, covering a shorter time span of 391 yr, significant peaks occur at 13 yr, 18 yr, 30 – 40 yr (Fig. 4.4c; Fig. S4.1c).

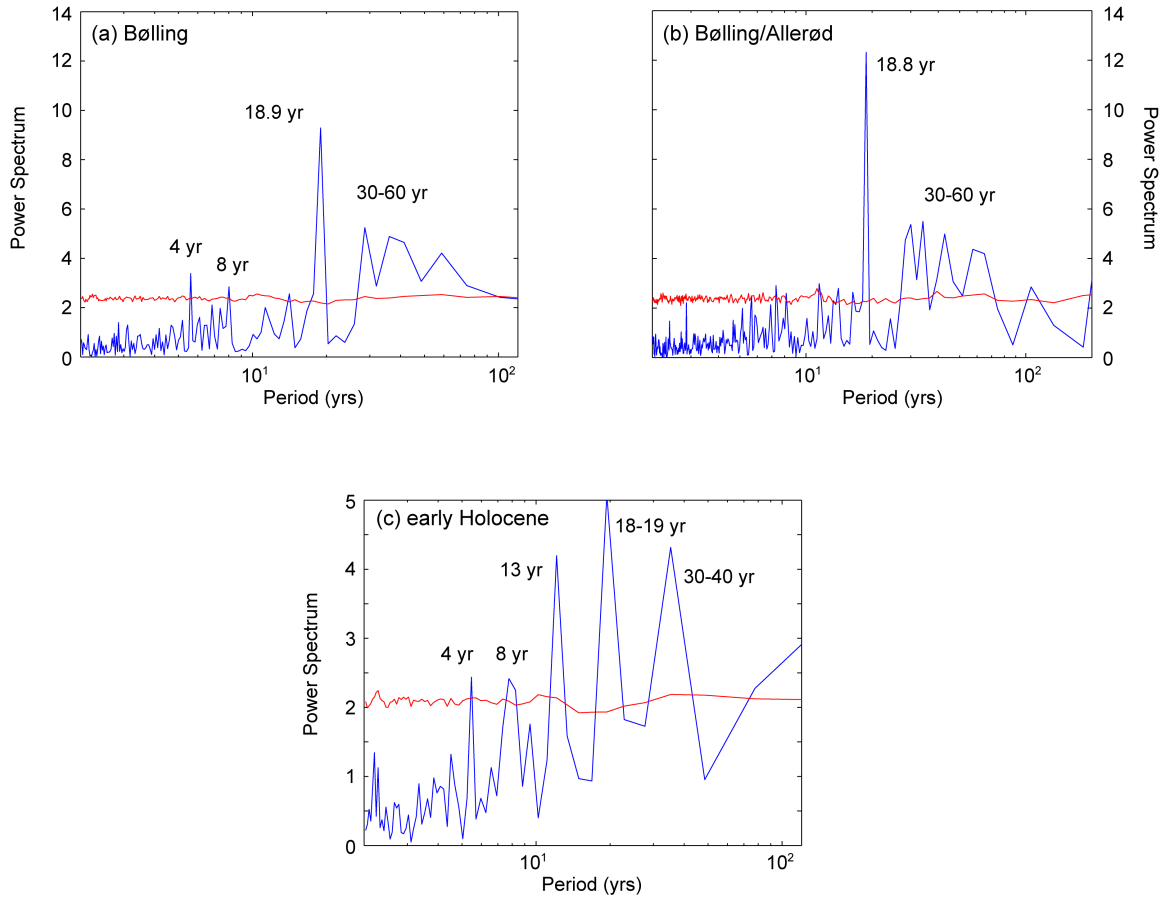

Figure 4.4: Fast Fourier transformation power spectral analysis on single laminae of the last deglaciation (blue line). Red lines denote the 95 % highest spectrum of 1000 AR(1) processes with the same autocorrelation. (a): Results from the Bølling interval. Significant peaks occur at 18.9 yr and a broad spectral peak at 30 – 60 yr and minor spectral peaks at 4 yr and 8 yr. (b) Results from the composite data set from the Bølling–Allerød. Most significant peaks occur at 18.8 yr and 30 – 60 yr respectively. (c) Results from the early Holocene with spectral peaks at 18–19 yr, 30 – 40 yr, 13 yr and 4 yr.

The consistent strong appearance of a sharp spectral peak of ~18.8 yr indicates an external forcing mechanism as these processes are characterized by narrow spectral lines (Munk et al., 2002). We propose that the prominent spectral peak of 18.9 yr in our data is connected to the 18.6 yr nodal tidal cycle. It is caused by variations in the inclination of the moons orbit to the equator, causing fluctuations of oceanic tides (e.g. Loder and Garrett, 1978; Foreman et al., 2006; Yasuda, 2009). This cycle is known to have strong influences on the North Pacific upper to mid-depth ocean, mostly through increased vertical mixing during times of strong diurnal tides, based on both instrumental and modeling studies (e.g. Osafune and Yasuda, 2006). It induces bidecadal variations in surface- and intermediate water temperatures (Royer, 1993; Loder and Garrett, 1978) and nutrient inventories through tidal mixing (Osafune and Yasuda, 2006; Osafune and Yasuda, 2010). We suggest that in years of enhanced tidal mixing more nutrients were supplied to the surface from intermediate depths, resulting in a regime of comparably higher, sustained biological productivity in the summer season and higher diatom frustule and OM burial at the sea floor. This enhanced OM- and diatom frustule burial lowers the sediment density, which leads to a higher pore water content and also results in higher Si/Ti ratios and an increase in the thickness of the biosiliceous laminae (Fig. 4.3).

Such a connection of higher productivity induced by nutrient supply through enhanced tidal mixing was previously proposed for the modern western North Pacific, with North Pacific Intermediate Water acting as an important nutrient source (Nishioka et al., 2007; Tadokoro et al., 2009). In addition, the Aleutian and Kuril island passes as well as the Gulf of Alaska were probable locations of strong nutrient entrainment into the mixed layer, with subsequent transport to the NE Bering Sea shelf via the North Pacific gyre circulation (Fig. 4.1), as today tidal mixing is observed in both areas (Ladd et al., 2005; Stabeno et al., 2005). Especially strong tidal mixing over the Aleutian island passages are considered to be an important source of nutrients for the Bering Sea ecosystem (Stabeno et al., 2005). Furthermore, modelling results have shown that tidal energy dissipation and mixing is localized in regions with pronounced bathymetric features and is strong especially in the Bering Sea (Nakamura et al., 2000; Haigh et al., 2011). During the B/A the tidal mixing was probably intensified through lower sea level and a coastline closer to the core position (Fig. 4.1).

The broader 30 – 60 yr multi-decadal spectral peak is assigned to the Pacific Decadal Oscillation (PDO), which has been described as a leading mode of SST anomalies in the extratropical North Pacific, and varies in the same multi-decadal band (Mantua et al., 1997; Minobe, 1997). We suggest that during the last deglaciation the PDO influenced the productivity through SST variations and mixed layer dynamics, with warmer SSTs and increased stratification and thus higher productivity during times of a positive PDO and most extensive sea ice coinciding with a strong negative PDO.

These influences of the PDO are known from the modern North Pacific (Stabeno et al., 2001; Chavez et al., 2003). In contrast to most North Pacific PDO records, which are based on tree rings (e.g. Wilson et al., 2007), our results show that the PDO had a strong, persistent influence on ocean ecosystem variability and thus OM export back through the warm phases of the last deglaciation.

The PDO and nodal tidal cycle may not be acting completely independent of each other, as the PDO has been earlier proposed to comprise a 18.6 yr tidal signal, as reported from North American tree-ring data (Yasuda, 2009). It was hypothesized that the large-scale thermocline ocean mixing processes induced by the nodal tidal cycle make it a potential candidate for causing bidecadal ocean-atmosphere variability in the North Pacific (Yasuda et al., 2006). The sharp 18.8 yr and the broad 30 – 60 yr spectral variability in our data provides, however, evidence for a distinction between a nodal tidal cycle and internal variability (most likely the PDO) both as fundamental forcing mechanisms for Bering Sea upper ocean changes. The less distinct 3 – 8 yr spectral peaks resemble cyclic variations known from low-latitude El Niño Southern Oscillation (ENSO) dynamics. Interestingly, like for the PDO, a relation has been suggested between the nodal tidal cycle and ENSO (Cerveny and Shaffer, 2001).

While a recent study, which analyzed laminae thickness variations and microfossil flux rates in a nearby sediment core also showed an, albeit weaker, 18 yr spectral peak, the analyzed cyclic variations were mainly assigned to the 11 yr sunspot cycle (Katsuki et al., 2014). However, the physical connection between such relatively small-scale solar forcing and the oceanic response perhaps remains to be validated. Our results alternatively suggest that decadal-scale oscillations during the Deglacial and Early Holocene were primarily driven by a mix of internal ocean-atmosphere dynamics as evidenced by the PDO, and external tidally-induced forcing. Both mechanisms have been independently shown by instrumental and modelling results to operate in present-day settings and influence primary production and nutrient supply (e.g. Mantua and Hare, 2002; Osafune and Yasuda, 2006).

4.4 Summary and conclusions

We showed by spectral analyses of varved sediments that deglacial Bering Sea primary productivity and, by inference, carbon export is modulated on interdecadal timescales by a combination of external and internal cyclic climate forcing mechanisms. The investigated time series comprise the Bølling, the Bølling–Allerød, and the early Holocene. We found spectral peaks that are related to the 18.6 yr nodal tidal cycle, the PDO and possibly ENSO. Especially the nodal tidal cycle shows a consistently sharp spectral appearance throughout the investigated time series. We hypothesize that tidal mixing

influenced primary productivity through variations in nutrient supply to the mixed layer. During years of enhanced tidal mixing the mainly diatom-based blooming season intensified, as more nutrients were supplied from intermediate depths, or were transported from areas of strong tidal mixing through the North Pacific gyre circulation to our study site. The PDO most likely affected the deglacial biological productivity via variations in sea surface temperature, sea ice cover and winter mixed layer stratification. Comparable processes to the ones proposed here are known from the modern North Pacific for the nodal tidal cycle and the PDO. Our results imply that both internal variability, originating from coupled ocean-atmosphere dynamics, and external forcing through the sharply expressed nodal cycle have been persistent features of the inter-decadal ocean-climate system in the subarctic North Pacific since the last glacial and are not limited to modern observations. The identified cyclic forcing mechanisms in our study over geological time scales may help to predict future climate and ecosystem changes, and aid in distinguishing natural variations from anthropogenic induced changes.

Acknowledgements

We acknowledge the professional help of the crew and shipboard science party of R/V during SO202 cruise. We thank Sascha Plewe and Rainer Bahlo at IOW for the technical support during XRF measurements. This paper is a contribution to Topic 3.1 “Circumpolar climate variability and global teleconnections at seasonal to orbital time scales” of the AWI PACES II research program. The study was funded through the “Innovative North Pacific Experiment (INOPEX)” by the German Federal Ministry of Education and Research (BMBF Grant no. 03G0202A) and by funding to LLJ, GL, OE and RT through the bilateral “Sino-German Pacific Ocean Experiment (SIGEPAX)” project (BMBF grant no. 03F0704A). Additional financial support came from the MARUM – Center for Marine Environmental Sciences (Project OC 3) and AWI through the Helmholtz REKLIM Initiative.

Supporting Information

Tidal forcing and ocean-atmosphere dynamics drive productivity variations in the deglacial Bering Sea

Text S4.1:

For high-resolution with XRF scanning (200 µm) with the ITRAX scanner from Cox Analytical Systems we used a counting time of 15 s and a Cr-tube voltage of 45 kV. XRF scanning with the Avaatech XRF scanner was performed with tube voltages of 10, 30, 50 kV and counting times of 10, 15, 30 s respectively (Kuehn et al., 2014).

Additional spectral analyses were performed following the method of Blackman and Tukey (1958) and with the Maximum Entropy Method (e.g. Haykin, 1983). The first method was used for the high confidence of the results and the latter for its high resolution. These spectral analyses were carried out with the AnalySeries software package (Paillard et al., 1996), with the confidence interval set at 95 % for Blackman-Tukey analysis. Detailed settings for spectral analysis are given in the figure caption of Fig. S4.1. For further visualization of the main spectral frequency, we applied a Gaussian 18.65 yr filter on the Cl-data from the Bølling–Allerød and show both plots in Fig. S4.2.

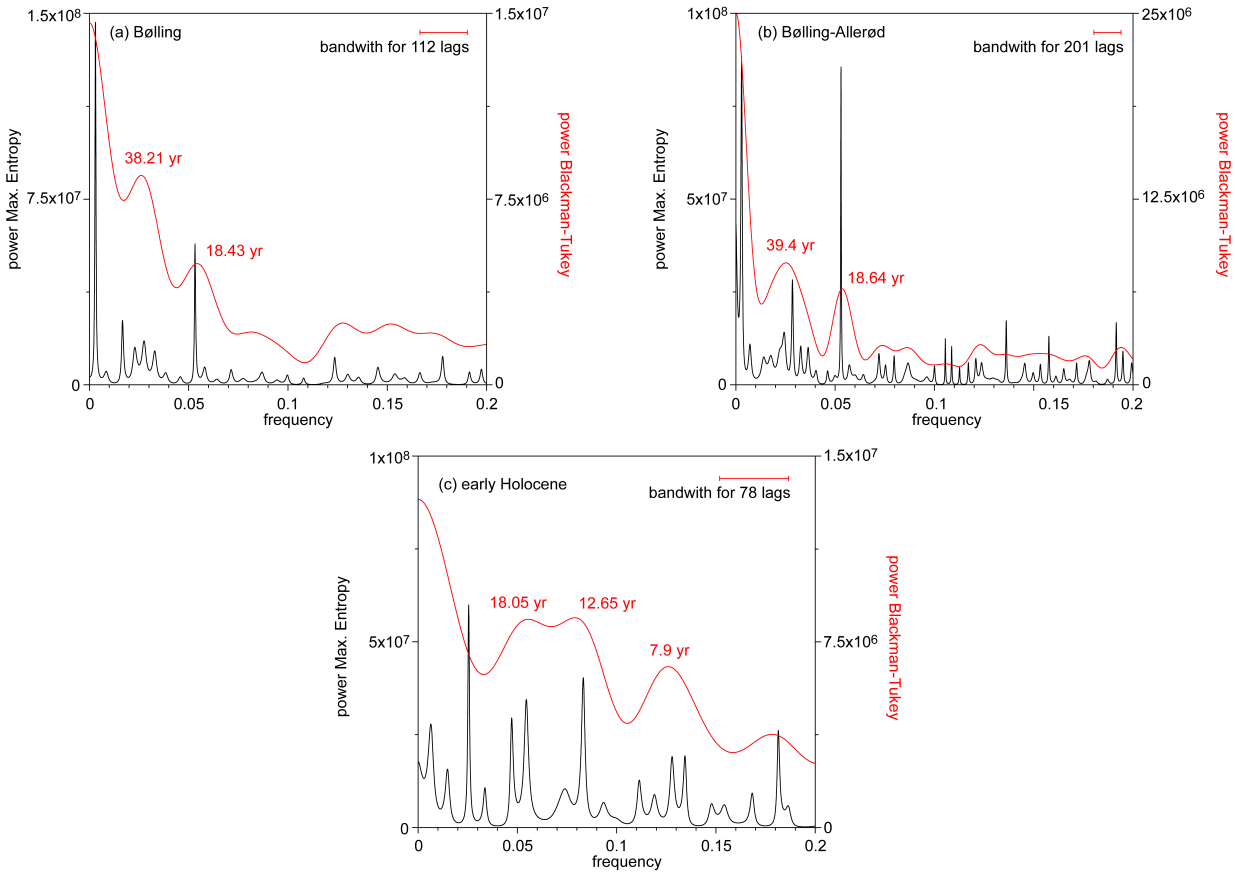

Figure S4.1: Additional spectral analyses methods on the different time slices from the last deglaciation. The method after Blackman and Tukey, using a Tukey, window is shown in red and results of the maximum entropy method in black. (a): Results from the Bølling interval. Blackman/Tukey confidence interval at 95 % given by 0.623<DP/P<1.861. (b) Results of the composite data from the Bølling/Allerød. Blackman/Tukey confidence interval at 95 % given by 0.624<DP/P<1.86. (c) Results from the early Holocene. Blackman/Tukey confidence interval at 95% given by 0.623<DP/P<1.862.

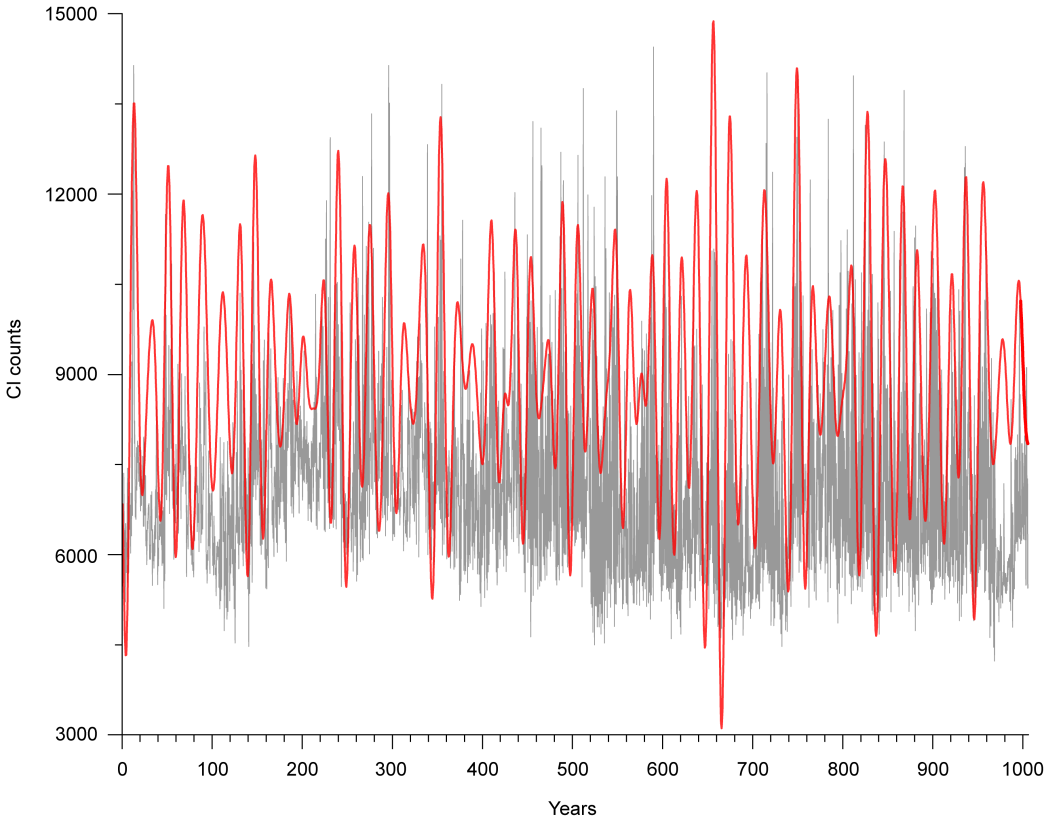

Figure S4.2: Overlay of the plotted XRF-derived Cl data (in gray) and of the filtered data from the Bølling–Allerød, using a 18.65 yr Gaussian filter (in red) to point out the variation in the data set, caused by the nodal tidal cycle.

5. Timing and forcing mechanisms of anoxia in the Bering Sea during the last deglaciation

Hartmut Kuehn[1,2], Lester Lembke-Jene[1], Rainer Gersonde[1,2], Andrea Abelmann[1], Wenshen Xiao[3], Oliver Esper[1,2], Gerhard Kuhn[1] and Ralf Tiedemann[1]

[1] Alfred-Wegener-Institut Helmholtz-Zentrum für Polar- und Meeresforschung, Bremerhaven, Germany

[2] MARUM Zentrum für Marine Umweltwissenschaften, Bremen, Germany

[3] State Key Laboratory of Marine Geology, Tongji University, Shanghai, China

To be submitted to Journal of Quaternary Science

Abstract

A comprehensive suite of high-resolution sediment cores from the Bering Sea, which are partially laminated and cover a depth transect from 1100 m to 2700 m, is used to study deglacial oxygen minimum zone (OMZ) dynamics. We apply a combination of planktic ^{14}C ages, X-ray fluorescense (XRF)-derived elemental ratios and biogenic mass accumulation rates. Severe oxygen depletions occurred during the Bølling/Allerød (B/A) and early Holocene, which is in strong accordance with other locations in the North Pacific, especially the Gulf of Alaska margin. Detailed analysis of the timing of lamination occurrence between the sediment core transects revealed that the onset of severe anoxia at the beginning of the B/A and early Holocene is a synchronous event, within the errors of the developed stratigraphic framework. Thus, we propose that the onset of laminations can be used as lithostratigraphic markers in future studies. In contrast, the disappearance of laminations and amelioration of bottom water oxygen conditions is revealed as being a more diachronic process. The deglacial OMZ strengthening is mainly driven by increased remineralization of organic matter in the deglacial mesopelagic water column, likely caused by a combination of processes: export production, visible in XRF-derived elemental ratios, and corresponding high accumulation rates of biogenic components. The export production is driven by higher sea surface temperatures, decreased sea ice cover and increased thermal stratification. One major nutrient- and organic carbon source was the eastern continental shelf, which was flooded during the global sea level rise. However, as the sediment cores lie in different proximity to the shelf, this led to different amounts of delivered nutrient and

organic carbon at the core sites, resulting in the varying durations of anoxia and their absence on the Shirshov Ridge.

5.1 Introduction

The oxygenation of the world ocean has received increasing attention over the past decades, as models predict that the average oxygen content will decrease with ongoing global warming (e.g. Keeling et al., 2010, Schmittner et al., 2008; Shaffer et al., 2009). Measurements at several mid-depth (i.e. about 600 – 2000 m) North Pacific regions have recorded oxygen decreases and shoaling of hypoxia depths (e.g. Watanabe et al., 2003; Whitney et al., 2007). Also, in the Atlantic and Indian Ocean decreases in dissolved oxygen over the last 50 years have been reported (Stramma et al., 2010). In its extreme expression, oxygen drawdowns lead to the formation of oxygen minimum zones (OMZs) that can reach anoxic conditions with complete oxygen consumption (Keeling et al., 2010; Jaccard and Galbraith, 2012). Such oceanic "death zones" have a strong impact on marine ecology, the faunal habitats and therefore also on human economy through changes in marine living resources. Oxygen declines, e.g. off Oregon in 2002 led to mass die-offs of invertebrates and fish (Grantham et al., 2004). Thus, as a forecasting of future OMZ development in the world ocean is important, so is the need for a better understanding of the involved processes and their natural variations (Keeling et al., 2010).

Severe anoxia in the Pacific have also occurred over the geological past, the most recent one being the prominent mid-depth Indo-Pacific de-oxygenation during the last glacial termination (e.g. Jaccard and Galbraith, 2012; Moffitt et al., 2015 for reviews). Such past events with natural forcing conditions provide potential analogues to better understand future ocean oxygenation changes. In addition, the last deglaciation is a time interval of particular interest, as it is marked by rapid warm-cold climate transitions (e.g. GRIP members, 1993; Steffensen et al., 2008), coupled with abrupt changes in the reorganization of the global Meridional Overturning Circulation (MOC), ocean oxygenation, sea surface temperatures (SST's) and productivity (e.g. Sarnthein et al., 1994; Behl and Kennett, 1996; Hughen et al., 1996; Sarnthein et al., 2000; Max et al., 2014)

In principal, bottom water oxygen concentrations of < 0.1 ml/l prevent the bioturbating benthic fauna to thrive and result in anoxia, and the deposition of laminated sediments (e.g. Behl and Kennett, 1996). Such sediments are found at several continental margin locations around the North Pacific for the last deglaciation. They occur near the island of Hokkaido (e.g. Ikehara et al., 2006; Shibehara et al., 2007), in the Bering Sea along the shelf break and bathymetric heights (e.g. Cook et al., 2005; Caissie et al., 2010; Kuehn et al., 2014), in the Gulf of Alaska (Davies et al., 2011; Addison et al., 2012) and the

California Margin (e.g. Keigwin and Jones, 1990; Kennett and Ingram 1995; Behl and Kennett, 1996; van Geen et al., 2003).

Of these regions, the Bering Sea is of particular interest, as it is one of the largest and most productive marginal seas in the world ocean (Springer et al ., 1996). In addition, the Bering Sea ecosystem is today influenced by global climate change, and a shift from arctic to subarctic conditions has recently been observed (Grebmeier et al., 2006). While a number of studies have used sediment records from the North American margin (Zheng et al., 2000; van Geen et al., 2003) and the temperate North Pacific (Moffitt et al., 2015) to investigate deglacial OMZ dynamics, the subarctic regions including the Bering Sea were largely under-represented from these studies.

In order to increase the knowledge of the deglacial development of Bering Sea oceanographic changes, we use a suite of sediment cores covering a depth transect from 1100 m to 2700 m water depth. We present a combination of X-ray-fluorescence (XRF)-derived elemental data, planktic ^{14}C ages and discrete geochemical measurements to provide information for the following questions: (1) what are the regional patterns and differences in the occurrence of deglacial anoxia, (2) which factors contribute to the strengthening of the OMZ and (3) is the occurrence of deglacial anoxia, expressed as laminated sediment sections, a synchronous event throughout the Being Sea and other regions of the subarctic North Pacific, and can thus be used as stratigraphic marker?

5.2 Regional setting

The Bering Sea, located near the North Pacific terminus of the global MOC features a large continental shelf (0-200 m water depth) in the eastern part that is seasonally covered with sea ice (Fig. 5.1). Maxima in sea ice extent occurs in March to April and minima between July to September (Niebauer, 1980). The seasonal sea ice and climatic variability is controlled by the interplay of the Aleutian Low and Siberian High (Niebauer, 1980) inducing strong seasonal variability in the sea ice cover and SSTs. The upper oceanic circulation in the Bering Sea consists of a cyclonic gyre, comprising the Aleutian North Slope Current (ANSC), Bering Slope Current (BSC) and the East Kamchatka Current (EKC) (Fig. 5.1). Outflow into the Arctic Ocean occurs through the shallow Bering Strait (50 m water depth) in the North with about 0.8 Sv (Woodgate and Aagaard, 2005), and into the North Pacific through several passages between the Aleutian islands, especially the deep Kamchatka Strait (Stabeno et al., 1999). Deep water exchange between the North Pacific and Bering Sea occurs mainly through the Kamchatka Strait, however, within the Bering Sea little information is available about the deep circulation (Stabeno et al., 1999).

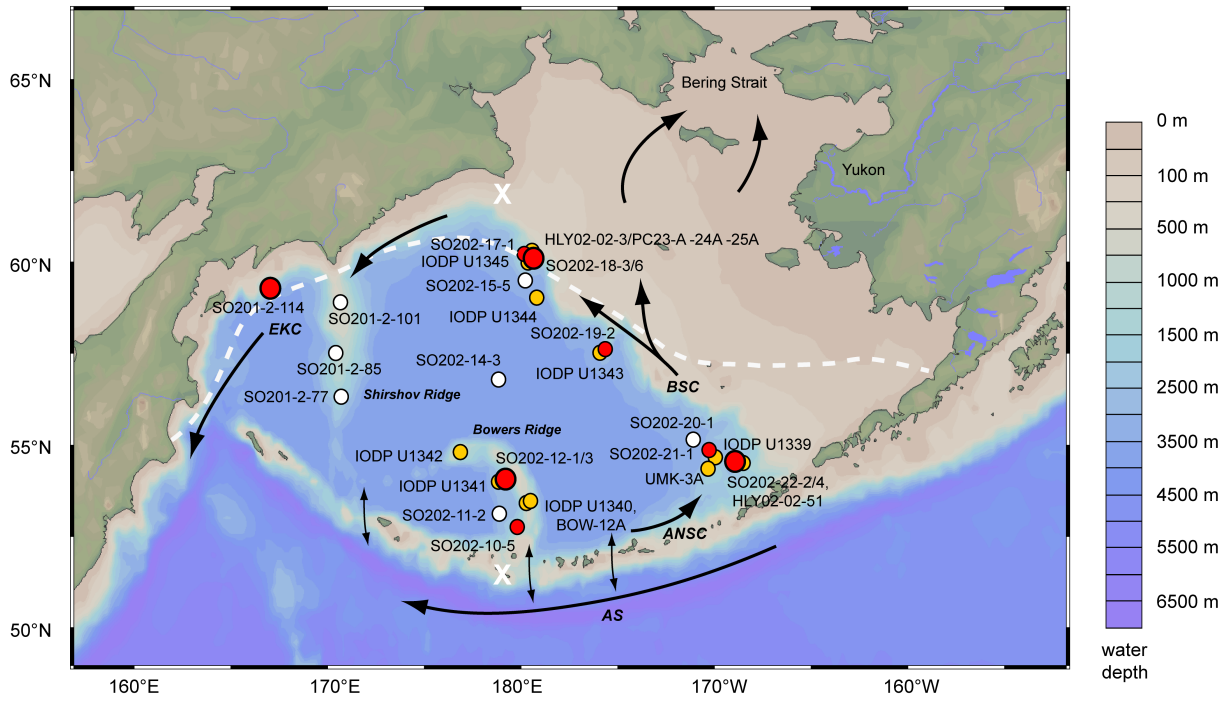

Figure 5.1: Map showing bathymetry of the Bering Sea and the location of laminated INOPEX cores (red circles). Non-laminated INOPEX cores and cores from the Shirshov Ridge without laminated sequences are shown with white circles and published records with laminations during the last deglacial are shown with orange circles. Cores discussed in more detail are shown with large red circles. Detailed information on the shown cores is provided by Table 5.1. Dashed line shows modern maximum sea ice extension (Reynolds et al., 2002) and black arrows mark the surface circulation. The transect shown in Fig. 5.2 lies between white asterisks. AS: Alaska Sream, ANSC: Aleutian North Slope Current, BSC: Bering Slope Current, EKC: East Kamchatka Current.

Primary productivity in the Bering Sea, dominated by diatoms, is one of the highest in the world ocean, with values of 175-275 $gCm^{-2}y^{-1}$ and highly productive areas are located along the shelf edges, which gave this area the term “Green Belt” (Springer et al., 1996; Takahashi et al., 2002). Though the absence of laminations in modern sediments indicate sufficient bottom water oxygen levels for sediment bioturbation by benthic macrofauna, an OMZ exists in the Bering Sea today, which is centered at ca. 900 m water depth (Cook et al., 2005; Garcia et al., 2010). The strength of the OMZ varies throughout the year, with oxygen concentrations decreasing to 0.4 ml/l during January-March (Garcia et al., 2010). In its horizontal extension and strength the OMZ is relatively uniform throughout the Bering Sea basin (Fig. 5.2).

Table 5.1: Bering Sea cores shown in Fig. 5.1. Core in italic letters were retrieved during the INOPEX cruise, in bold italic are laminated INOPEX cores. KAL: Kasten cores

Core	Latitude	Longitude	Depth (mbsl)	Reference
SO202-10-5	52°44.57'N	179°50.87'E	1470	Gersonde,R 2012, Kühn et al., 2014
SO202-11-2	53°06.67'N	178°53.99'E	2703	Gersonde,R 2012, Kühn et al., 2014
SO202-12-1 KAL	54°03.04'N	179°05.24'E	2109	Gersonde,R 2012, Kühn et al., 2014
SO202-12-3	54°03.04'N	179°05.24'E	2109	Gersonde,R 2012, Kühn et al., 2014
SO202-14-3	56°47.19'N	178°49.45'E	3821	Gersonde,R 2012
SO202-15-5	59°30.76'N	179°51.00'W	3129	Gersonde,R 2012
SO202-17-1	60°07.39'N	179°27.95'W	1066	Gersonde,R 2012, Kühn et al., 2014
SO202-18-3	60°07.60'N	179°26.67'W	1111	Gersonde, R 2012, Kühn et al., 2014
SO202-18-6 KAL	60°07.60'N	179°26.61'W	1107	Gersonde, R 2012, Kühn et al., 2014
SO202-19-2	57°39.05'N	175°40.69'W	1752	Gersonde,R 2012, Kühn et al., 2014
SO202-20-1	55°08.68'N	171°04.95'W	2984	Gersonde,R 2012
SO202-21-1	54°47.35'N	170°19.68'W	1911	Gersonde,R 2012, Kühn et al., 2014
SO202-22-2	54°34.45'N	168°48.66'W	1482	Gersonde,R 2012, Kühn et al., 2014
SO202-22-4 KAL	54°34.41'N	168°48.62'W	1476	Gersonde,R 2012, Kühn et al., 2014
SO201-2-77	56°19.83'N	170°41.98'W	2135	Max et al., 2012
SO201-2-85	57°30.30'N	170°24.77'W	968	Max et al., 2012
SO201-2-101	58°52.52'N	170°41.45'W	630	Max et al., 2012
SO201-2-114	59°13.87'N	166°59.32'E	1376	Max et al., 2012
IODP U1339	54°40.02'N	169°58.902'W	1867.5	Takahashi et al., 2011
IODP U1340	53°24.001'N	179°31.297'W	1294.6	Takahashi et al., 2011; Schlung et al., 2013
IODP U1341	54°02.0025'N	179°0.49992'E	2139.5	Takahashi et al., 2011
IODP U1342	54°49.699'N	176°55.003'E	818.6	Takahashi et al., 2011
IODP U1343	57°33.399'N	175°48.966'W	1952.9	Takahashi et al., 2011
IODP U1344	59°03.0005'N	179°12.201'W	3173.1	Takahashi et al., 2011
IODP U1345	60°09.1917'N	179°28.204'W	1007.8	Takahashi et al., 2011
HLY02-02-3JPC	60°07.674'N	179°26.508'W	1132	Cook et al., 2005
HLY02-02-51JPC	54°33.192'N	168°40.014'W	1467	Cook et al., 2005; Caissie et al., 2010
PC-23A	60°09.52'N	179°27.82'W	1002	Itaki et al., 2009; Kim et al., 2011
PC-24A	60°15.70'N	179°25.34'W	852	Kim et al., 2011
PC-25A	60°04.48'N	179°27.78'W	1152	Kim et al., 2011
BOW-12A	53°23.47'N	179°33.47'W	1287	Okada et al., 2005; Tanaka and Takahashi et al., 2005
UMK-3A	54°25.22'N	170°13.38'W	1892	Okada et al., 2005; Tanaka and Takahashi et al., 2005

5.3 Material and methods

5.3.1 Sediment records and geochemical measurements

Cruise SO202 INOPEX (Innovative NOrth Pacific EXperimnt) recovered 15 sediment cores from the Bering Sea. Together, they yield a depth transect of 1066 to 3821 m water depth (Table 5.1, Fig. 5.2; Gersonde, 2012). The used coring devices are a Piston Corer and a Kasten Corer. The latter was used to gain complementary neighboring, large-diameter cores for three piston cores. Nine of the cores from the Bering Sea feature laminated sections. They were retrieved on the Bowers Ridge, the Umnak Plateau and along the eastern Bering shelf ridge (Fig. 5.1, Table 5.1). Additionally we show core positions of published sediment cores to better constrain the expansion of the deglacial OMZ (Fig. 5.1, Fig. 5.2; Table 5.1).

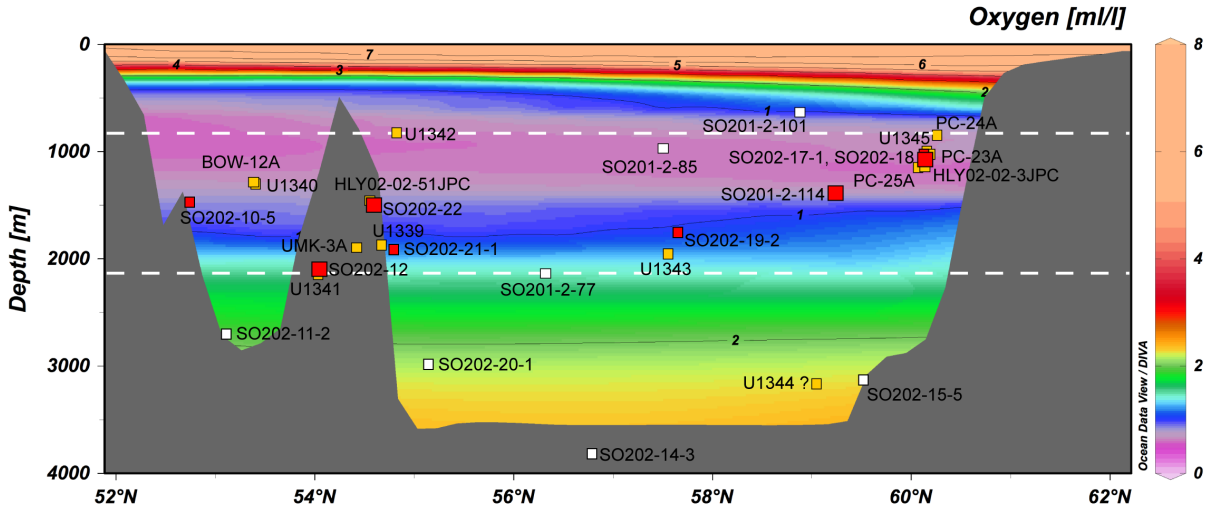

Figure 5.2: North-south transect of the Bering Sea with color-bar and iso-lines showing annual mean oxygen levels (Garcia et al., 2009). Core of todays OMZ is shown in dark purple. The colors of the sediment cores are the same as in Fig. 5.1. Cores discussed in more detail are shown with large red squares. The dashed white line depicts the OMZ expansion in the Bering Sea during the last deglaciation, based on the occurrence of laminations (Kuehn et al., 2014). Core U1344 from the northeastern Bering Sea slope was reported to contain laminated sections (Takahashi et al., 2011), but this not confirmed by sediment cores from this study.

In order to assess marine export productivity we apply a multi-proxy approach and use XRF- derived Ca/Ti and Si/Al ratios to gain information about calcareous and siliceous bio-productivity. Additionally, Br/Ti-ratios are used to provide qualitative information on marine organic matter content (Ziegler et al., 2008). These semi-quantitative XRF results are supplemented by mass accumulation rates (MAR) of biogenic opal and total organic carbon (TOC), as well as C/N-ratios for information on biological productivity versus possible effects of terrestrial carbon input, with high C/N ratios pointing

towards a terrestrial source (Riethdorf et al, 2013). To clearly identify the laminated sediment sequences we used X-ray images. For a straightforward comparison of the different sediment cores we simplified the detailed analysis of the lamination pattern in core SO202-18-3 as reported in Kuehn et al. (2014). In the approach presented here we summarize the previously subdivided three facies (laminated, layered, bioturbated laminae) now under the term anoxic intervals, representing O_2 values <0.1 – 0.1 ml/l (Behl and Kennett, 1996).

XRF scanning was performed with an Avaatech XRF core-scanner at the AWI Bremerhaven**.** We scanned with a sample spacing of 1 cm, Rh-tube voltages of 10 kV, 30 kV, 50 kV and counting times of 10 s, 15 s and 30 s, respectively (Richter et al., 2006).

We measured biogenic opal concentrations (relative precision of ±5 %) with the sequential leaching method after Müller and Schneider (1993). Total carbon content was measured with an Elementar Vario III CNS analyzer, and total organic carbon content with an Eltra CS-2000 Carbon Sulfur element analyzer, respectively, at the Alfred-Wegener-Institute after removal of carbonate (relative precision of ±3 %). Additionally, we also applied corrections for the pore water salt content (Kuhn, 2013). X-ray images were obtained at the AWI with the X-ray system Faxitron Series from Hewlett Packard for sediment slices from the Kasten core and the ITRAX core scanner on half piston core liners at the Leibniz-Institute for Baltic Sea Research, Warnemünde (see Kuehn et al., 2014 for details).

5.3.2 Radiocarbon dating and core-to-core correlation

For AMS ^{14}C dating, we picked mono-specific samples of the planktic foraminifera *Neogloboquadrina pachyderma* sinistral from the fraction > 125 µm from cores SO202-12-1, SO202-18-3 and SO202-22-4. This species is common in (sub)polar regions and a subsurface-dweller with abundance maxima between 50 and 200 m water depth (e.g. Bauch et al., 2002; Kuroyanagi et al., 2011). In case of insufficient *Neogloboquadrina pachyderma* sinistral numbers, we picked mixed planktic foraminifera from the same fraction. Measurements were carried out by the National Ocean Sciences Accelerator Mass Spectrometry (NOSAMS) Facility at the Woods Hole Oceanographic Institution for cores SO202-12-1 and SO202-18-3 and at Beta Analytic Inc., Miami for sediment core SO202-22-4 (Table 5.2).

Table 5.2: AMS ^{14}C ages, reservoir ages (res. age), calibrated calendar ages and calendar ages with 1-σ ranges.

Core	Sample ID	Depth (cm)	Species	^{14}C age (yr)	Res. age (yr)	Calendar age (yr)	Calendar age (yr) 1-σ range
SO202-12-1	OS-93970	10-12.5	Nps	3520 +/-35	770	2839	2789-2869
	OS-92051	50-52.5	Nps	7290 +/-35	770	7439	7420-7468
	OS-93966	60-62.5	Nps	8200 +/-35	770	8261	8200-8311
	OS-85934	75-77.5	Nps	9420 +/-45	770	9603	9543-9654
	OS-92042	85-87.5	Nps	10300 +/-45	770	10870	10720-11068
	OS-92043	95-97.5	Nps	10750 +/-45	770	11434	11294-11601
	OS-85933	100-102.5	Nps	10950 +/-60	770	11868	11758-11998
	OS-92045	105-107.5	Nps	11400 +/-50	910	12455	12397-12547
	OS-85929	110-112.5	Nps	12250 +/-45	875	13216	13164-13268
	OS-92046	120-122.5	Nps	12450 +/-55	875	13405	13346-13460
	OS-92052	130-132.5	Nps	13100 +/-55	875	14123	14035-14198
	OS-92044	140-142.5	Nps	13200 +/-50	875	14294	14131-14415
	OS-85932	145-147.5	Nps	13350 +/-50	875	14657	14448-14871
	OS-92040	160-162.5	Nps	14300 +/-55	1150	15799	15693-15906
	OS-92048	180-182.5	Nps	15750 +/-55	1150	17782	17685-17878
SO202-18-3	OS-94141	992-993	Nps	14050 +/-80	750	15995	15863-16120
	OS-101640	1173-1175	Nps	16600 +/-120	1560	18275	18113-18433
	OS-101641	1349-1351	Nps	20400 +/-160	1000	23359	23127-23568
	OS-101642	1517-1519	Nps	22100 +/-200	1300	25056	24754-25366
	OS-101644	1768-1771	mp	26900 +/-400	400	30647	30321-31066
SO202-22-4	364794	149-150	Nps	8920 +/-40	770	9085	9022-9123
	364795	184-185	Nps	10690 +/-60	770	11341	11236-11402
	364796	224-225	Nps	11830 +/-50	875	12803	12730-12851
	364797	279-280	Nps	13240 +/-50	875	14391	14188-14531
	364798	314-315	Nps	13490 +/-50	875	14991	14881-15127
	364799	369-370	Nps	16020 +/-60	1150	18078	17974-18173
	364800	459-460	Nps	17570 +/-70	1150	19812	19688-19933
	367266	644-645	Nps	21350 +/-90	1150	24268	24138-24397
	364802	754-755	Nps	23110 +/-100	1150	26161	26022-26274
	367267	869-870	Nps	25930 +/-140	1150	28811	28647-28963
	367268	919-920	Nps	27090 +/-150	1150	30197	29919-30466

Ages are reported following established conventions (Stuiver and Polach, 1977). For the conversion of radiocarbon dates to calendar ages we used our own published regional reservoir ages for the deglacial (Kuehn et al., 2014) and applied the Calib 7.0 software with the INTCAL 13 calibration curve (Reimer et al., 2013). All ages are reported as ^{14}C yr or ka (uncorrected ^{14}C age in years / kyr before AD 1950). For INOPEX cores that were not ^{14}C dated, we applied a core-core correlation based on XRF-derived elemental ratios and the appearance of laminated sediment sequences. For this correlation we focused on cores from 1066 m to 2703 m water depth, as deeper cores do not reveal obvious peaks in elemental ratios that can be used for correlation. Core SO202-10-5 is not shown in our correlation approach as the deglacial section was disturbed during the coring process (Gersonde, 2012).

5.4 Results and discussion

5.4.1 Stratigraphic approach and age models

To establish the stratigraphic framework for all cores in this study we used piston core SO202-18-3 from the northern Bering slope as a reference site (Fig. 5.1). This core features sedimentation rates of more than 200 cm/kyr, significantly higher compared to the other radiocarbon dated cores, which have sedimentation rates of 20-60 cm/kyr (Fig. S5.1). Further, core SO202-18-3 has a well established age model for the first 15 ka, which was based on a correlation to neighbouring, ^{14}C dated kasten core SO202-18-6 and a detailed, decadal-scale correlation of layer-counted varves and lamination patterns to the NGRIP stable isotope record (Kuehn et al., 2014). To extend the age model beyond 15 ka we correlated the Ca/Fe ratios of SO202-18-3 to the NGRIP record (NGRIP Members et al., 2004) as they show a strong resemblance to the ice core d^{18}O data (Fig. 5.3). Based on this correlation, the newly derived planktic reservoir ages for times older than 15 ka range between 750 and 1560 yr and are in good agreement with recent results from the subarctic NE Pacific (Sarnthein et al., 2015). There, plateau tuning-derived planktic reservoir ages yielded values between 550 and 1560 yr for the time interval 16 – 19 ka. This correspondence gives us additional confidence in our age model.

For the radiocarbon-dated cores SO202-12-1 and SO202-22-4 we first applied a preliminary age assessment based on the XRF derived Ca/Ti peak pattern, as it was shown that Ca-peaks show strong similarities in Bering Sea cores during the last deglaciation (Gorbarenko et al., 2005; Khim et al., 2010; Max et al., 2012). Thereafter, we used the average reservoir ages derived from reference core SO202-18-3 to convert the planktic ^{14}C ages into calendar ages. The used values were 770 years for the Holocene, 910 years for the YD, 875 years for the B/A (Kuehn et al., 2014), and 1150 years for sections older than the B/A (Table 5.2). For the calculation of the average reservoir age in the latter

case, we discarded the result of depth interval 1768-1771 cm, which seems to too low with 400 years. This might be linked to an isolated large-scale bioturbation pattern.

For core SO201-2-114 from the western Bering Sea we used the previously published age model (Max et al., 2012). It was based based on ^{14}C measurements of planktic foraminifera and correlation of high resolution color *b scans to the NGRIP oxygen isotope record, as the color *b values have been shown to be a reliable proxy for biogenic productivity changes (Nürnberg and Tiedemann, 2004; Riethdorf et al., 2013).

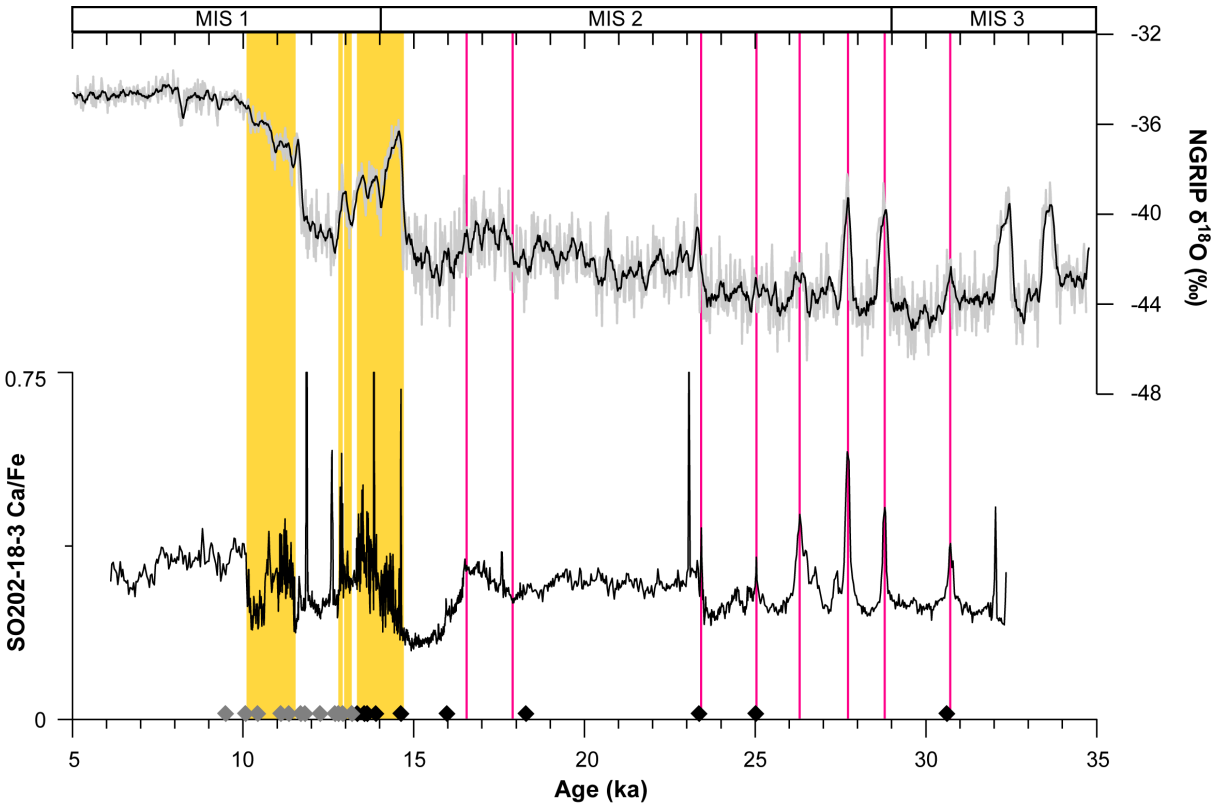

Figure 5.3: Age model of core SO202-18-3 for the last 35 ka and the correlation of XRF-based Ca/Fe ratios (11-pt running mean shown in black) to the NGRIP stable isotope record (NGRIP members, 2004). Correlation shown with red vertical lines. Anoxic sections of SO202-18-3 are shown in orange. The age model for the time interval of the B/A to Holocene was published in Kuehn et al., 2014. Black diamonds depict planktic ^{14}C dates and numbers above give calculated planktic reservoir ages. Marine Isotope Stages (MIS) are shown on top. Note that ^{14}C dates in light gray are from neighbouring core SO202-18-6 (Kühn et al., 2014).

5.4.2. Timing and appearance of Bering Sea anoxia and regional context

Based on our age model, longest intervals of anoxic conditions, and thus lamina deposition, persisted during the B/A (14.6 – 12.8 ka), with a synchrouns onset at the beginning of the Bølling interval at

14.6 ka (Fig. 5.4). While the Bølling (14.6 – 14 ka) is completely anoxic at all core sites, sediment cores SO202-18-3, SO201-2-114 and SO202-22-4 reveal short oxic (bioturbated) sequences starting at 14 ka (Fig. 5.4a-c). In core SO202-18-3 these facies variations are tightly coupled to short-term warm-cold-oscillations recorded in the NGRIP ice core during the B/A (Kuehn et al., 2014). The weakening of the OMZ at the end of the B/A, seems to be a rather diachronous process. At the end of the Allerød the re-oxygenation and thus lamina disappearance starts 400 years earlier, at 13.3 ka, in deep core SO202-12-1 from the Bowers Ridge (Fig. 5.4d) and core SO201-2-114 (Fig. 5.4b) from the western Bering Sea, compared to cores SO202-18-3 (Fig. 5.4a) and SO202-22-4 (Fig. 5.4c), which reveal a transition to bioturbates sediments at 12.8 ka. This is also reflected in the XRF data, where the Ca/Ti ratios in cores SO202-12-1 and SO201-2-114 reveal an earlier decrease near the end of the Allerød at 13.2 ka.

During the entire Younger Dryas oxic conditions and low Ca/Ti ratios persisted at all core positions. A sharp Ca/Ti peak at 11.8 ka in SO202-18-3 is related to a dispersed ash layer. With the onset of the Holocene at 11.7 ka, anoxic conditions started to occur simultaneously at all core sites. However, on Bowers Ridge core SO202-12-1 anoxic conditions persisted only for the first 200 years of the Holocene (Fig. 5.4d), compared to the 1,500 year long period of anoxia in core SO202-18-3 from the northern Bering Slope (Fig. 5.4a). In addition, the Ca/Ti ratios in SO202-12-1 show only a comparably short peak during the early Holocene. Core SO202-22-4 from the Umnak Plateau also reveals earlier re-oxygenation, starting at 10.7 ka, while the Ca/Ti ratios remained high until 10.2 ka (Fig. 5.4c); around the same time when the OMZ weakened in SO202-18-3. On the northwestern Bering Sea margin (core SO201-2-114), persistent anoxic conditions occurred until from 10.9 ka, with only intermittent episodes of anoxic conditions thereafter, until 9.7 ka (Fig. 5.4b).

Comparison of the uncorrected planktic ^{14}C ages between the sediment cores show almost similar ages, ranging between 13,350 – 13,490 ^{14}C yr and 10,950 – 10,645 ^{14}C yr at the onset of the B/A and Holocene, respectively (Fig. 5.4). In core SO202-22-4 one planktic ^{14}C sample from the Holocene lies slightly above the onset of the Holocene anoxia, but linear extrapolation to the onset of laminae reveals a raw ^{14}C age of 10,800 ^{14}C yr. In general the uncorrected planktic ^{14}C ages agree overall well, within the range of dating uncertainties and indicate that there were no large surface reservoir age variations throughout the Bering Sea. Based on these results we suggest that the disappearance of laminations (or entire length of a laminated core interval) should not be used as a stratigraphic marker (cf. van Geen et al., 2003), in contrast to the onset of laminated sequences, which represent a synchronous lithostratigraphic marker tied to the onset of the B/A and Holocene. We followed this approach in our core-core correlation (Fig. 5.5).

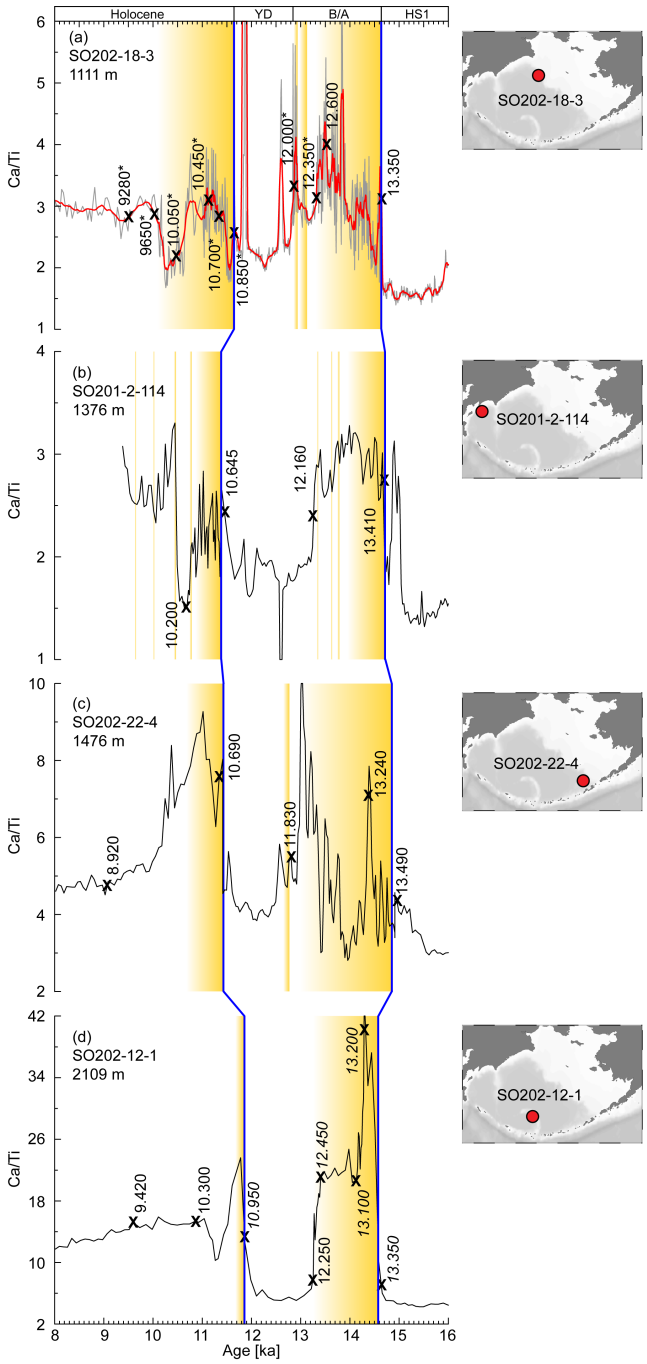

Figure 5.4: XRF-based Ca/Ti ratios and correlation of anoxic (layered to laminated) sediment sections (in orange) of several cores throughout the Bering Sea with increasing water depth from (a) to (d). (a) SO202-18-3, (b) SO201-2-114, (c) SO202-22-4, (d) SO202-12-1. Note that Ca/Ti ratios in (a) are depicted in red, as they represent a 11-pt running mean of the raw data (in gray). Exact locations of each cores are depicted on the small maps by red circles. The correlation of the onset of laminations is shown by a blue line and represents most likely a synchronous event (see text for details). Black crosses and numbers inside different graphs give uncorrected planktic ^{14}C ages. ^{14}C ages marked with asterisks in the plot of SO202-18-3 are from neighboring kasten core SO202-18-6 and where correlated to SO202-18-3, based on the similar lamination pattern analysis in both cores (Kuehn et al., 2014). YD: Younger Dryas, B/A: Bølling|/Allerød, HS1: Heinrich Stadial I.

Our XRF measurements and core-core correlation reveal that a thin sequence of Holocene laminations and comparable thicker laminated intervals during the B/A are common in all of our sediment cores. In core SO202-18-6, however, the B/A was not completely recovered (Fig. 5.5). The thickest anoxic sequence (465 cm) is recorded in core SO202-18-3 (1111 m water depth) (Kuehn et al., 2014) the thinnest anoxic interval (14 cm) occurs in core SO202-12-3 (2109 m water depth). In core SO202-11-2 (2703 m water depth) laminations are not visible any longer (Fig. 5.2, Fig. 5.5). This core was most likely located near the lower boundary of the deglacial anoxia occurrence as, despite the absence of laminations, it shows a similar peak structure in the XRF derived elemental ratios, with prominent increases in Ca/Ti, Si/Al and Br/TI during the B/A and early Holocene. Similar Ca-peaks are common in sediment records throughout the subarctic North Pacific (Keigwin et al., 1992; Keigwin, 1998; Gorbarenko et al., 2005) and allow a placement of these lithostratigrpahic features into a basin-wide deglacial context.

These results reveal, that the OMZ showed a drastic vertically expansion and intensification during the last deglaciation, with anoxic conditions reaching down to water depths between 2100 – 2700 m, much deeper than the modern depth of the OMZ core. However, one deeper core (3200 m water depth) from the northern Bering Slope was reported to bear deglacial laminations (Takahashi et al., 2011) but this is not confirmed by our sediment cores (Fig. 5.2, Fig. 5.5). Despite this strengthening of the degalcial OMZ, anoxic conditions did not occur on all major topographic heights in the Bering Sea, as sediment cores from the Bowers Ridge covering a depth transect of 630 m – 2135 m (Fig. 5.1; Max et al., 2012) are not laminated.

On a larger scale, the circulation in the Bering Sea is influenced by the Pacific Subarctic Gyre circulation and the inflowing Alaska Stream (Fig. 5.1; Stabeno et al., 1999). We thus compared our results from the Bering Sea with a well-dated, laminated record from the Gulf of Alaska. In this core from 682 m water depth, laminated sequences were assigned to the B/A and early Holocene, and uncorrected, planktic ^{14}C ages with 13,430 ^{14}C yr at the onset of the B/A and 10,600 ^{14}C yr at the early Holocene (Davies et al., 2011) are almost similar to our results from the Bering Sea. These similar ^{14}C ages indicate that surface reservoir ages in the Bering Sea and Gulf of Alaska were relatively similar during the last deglaciation. We thus feel confident that our reported Bering Sea onsets of mid-depth anoxia occur on a basin-wide scale synchronous to other, lower latitude North Pacific regions from the Japan and the North American margins, within the errors of the respective age models (Zheng et al., 2000; Moffitt et al., 2015).

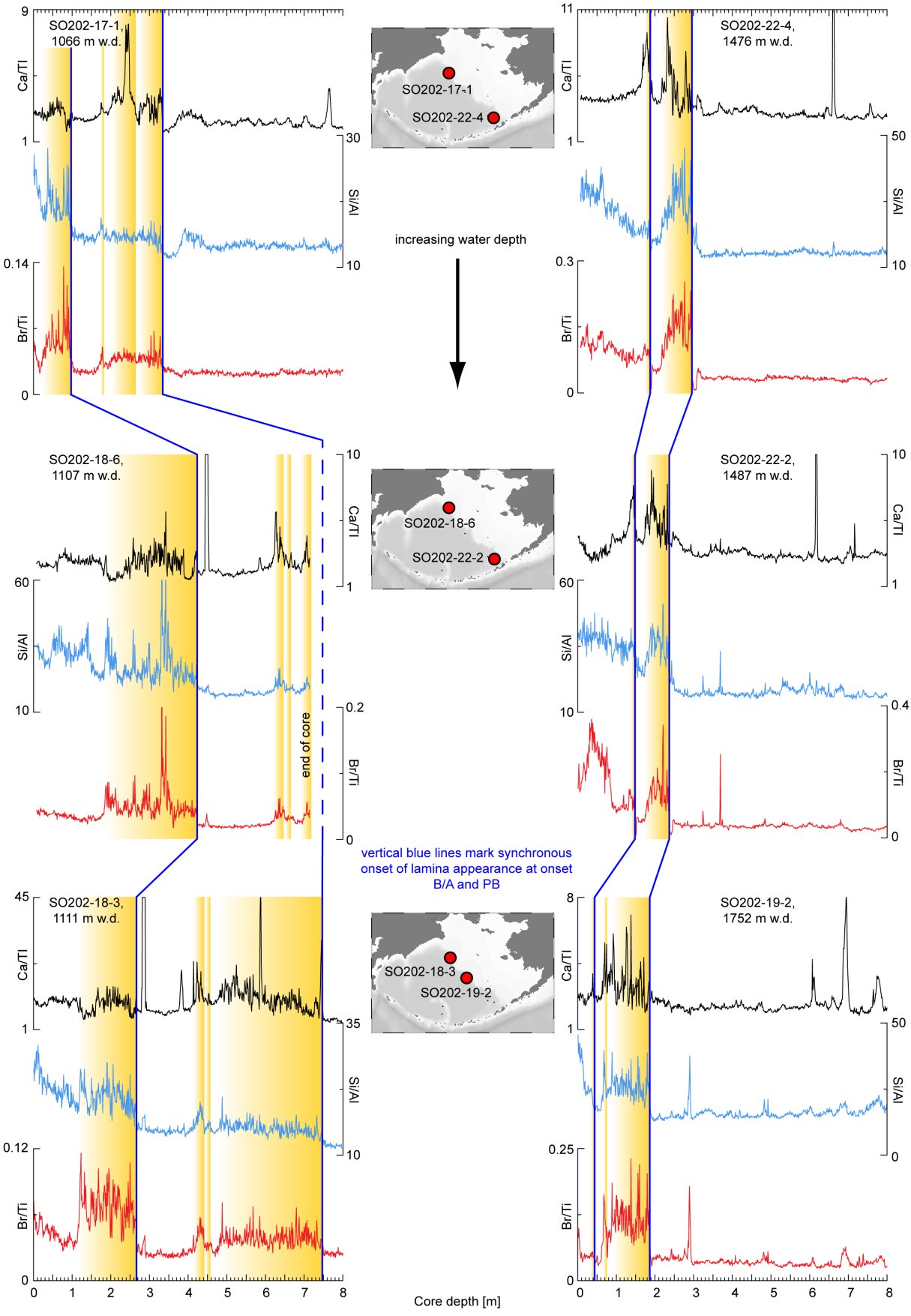
SO202-17-1, 1066 m w.d.
SO202-22-4, 1476 m w.d.
SO202-18-6, 1107 m w.d.
SO202-22-2, 1487 m w.d.
SO202-18-3, 1111 m w.d.
SO202-19-2, 1752 m w.d.
Ca/Ti
Si/Al
Br/Ti
increasing water depth
end of core
vertical blue lines mark synchronous onset of lamina appearance at onset B/A and PB
Core depth [m]

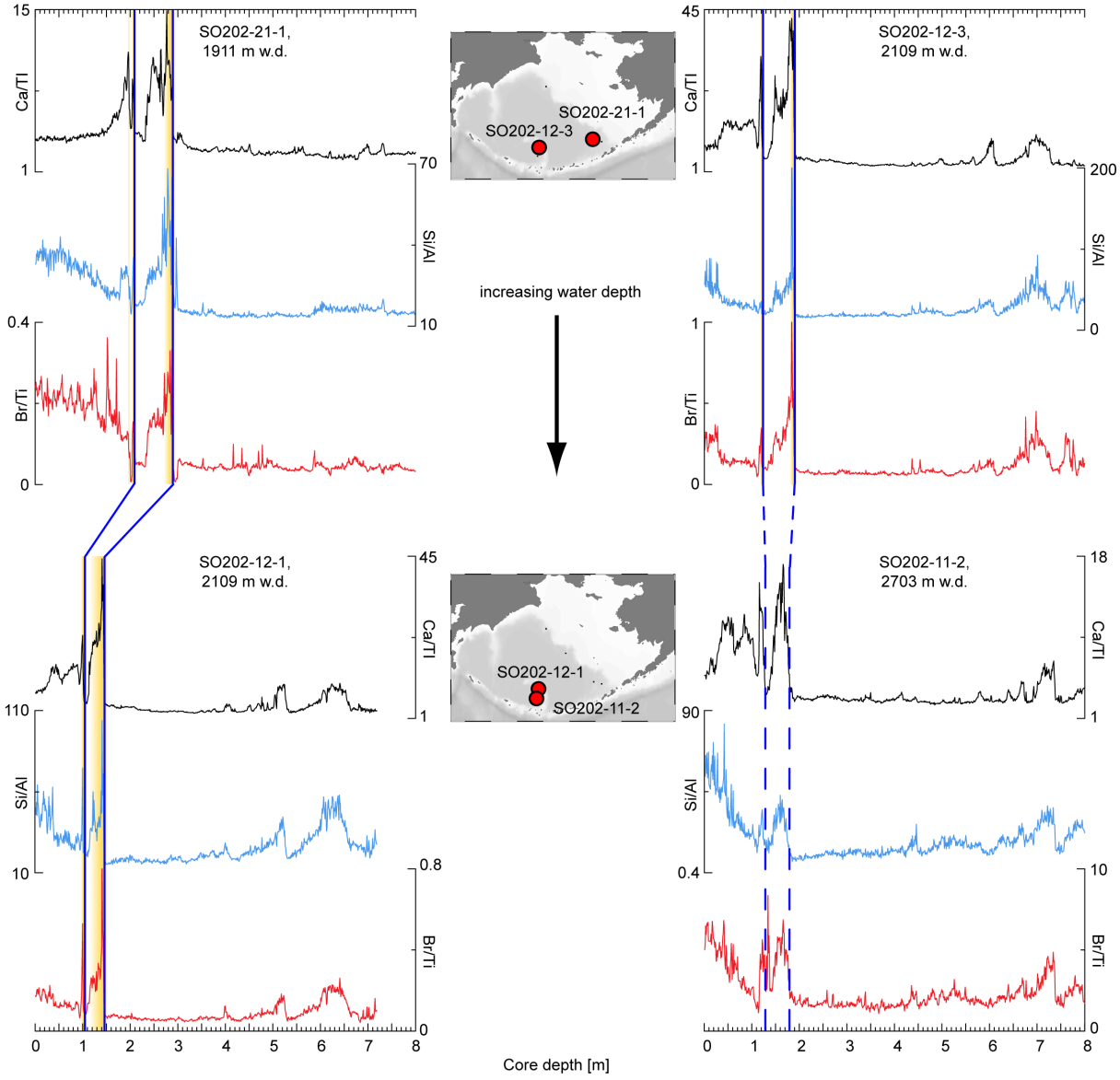

Figure 5.5: Core-core correlation between INOPEX cores with increasing water depth from 1066 m (SO202-17-1) to 2703 (SO202-11-2). Black curves show XRF-based Ca/Ti ratios, blue curves Si/Al ratios and red curves Br/Ti ratios. Yellow sections depict laminated sequences and vertical blue lines correlate onset of laminations in each core (see text for details). The onset of the Bølling lamina was not recovered in SO202-18-6. Note that correlation to deep core SO202-11-2 is based only on the XRF peaks, as no laminations are present in this core. Small maps between the plots give core locations.

5.4.3. Models for the deglacial anoxia development in the Bering Sea

The synchronous onset of anoxia at the beginning of the B/A and Holocene, and diachronous re-oxygenation and absence of anoxia on the Shirshov Ridge suggest that the oxygen drawdown is not driven by a single basin-wide factor. In principle, anoxic conditions occur via enhanced biological

productivity and the subsequent remineralization of organic matter that is transported to the sea floor, with the original oxygen concentration of the ambient bottom water masses constituting an additional important boundary condition. Our high XRF-derived elemental ratios of Ca/Ti, Si/Al and Br/Ti (5.4, Fig. 5.5) during the B/A and early Holocene indicate higher biological productivity of calcareous and siliceous plankton. The high biological productivity is also indicated by maxima biogenic opal mass accumulation rates (MARs) during the B/A and early Holocene. These results are in agreement with other mid-depth records from the Bering Sea showing the same pattern of productivity variations (Kim et al., 2011; Riethdorf et al., 2013). However, a comparable smaller increase in the biogenic opal MAR is already visible at 16.6 ka. At the same time the TOC MAR shows a sharp increase (Fig. 5.6). After 16.6 ka the TOC MAR slowly decreases and reaches lowest values occurring with the disappearance of the Holocene laminations (Fig. 5.6, Fig. S5.2). The C/N ratios start to increase at 16.6 ka and remain high until 8 ka (Fig. 5.6). Based on these results we suggest the following model for the deglacial development of the Bering Sea OMZ.

During the cold phases like the last glacial and Younger Dryas, increased sea ice cover and a possible deeper mixed layer led to light limitation and limited biological productivity (Cassie et al., 2010; Lam et al., 2012). Due to the sea-level low-stand and the dryer climate over Alaska during glacial times, less nutrients were transported via freshwater discharge into the Bering Sea from Alaska, which further hampered biological productivity (Edwards et al., 2001; Davies et al., 2012). As a result only small amounts of organic material were exported to the sea-floor and less oxygen was consumed via remineralzation. Therefore bottom water oxygen contents were >0.3 ml/l, which allowed bioturbating macrofauna (Fig. 5.7a; Behl and Kennett, 1996).

The increase in C/N ratios and TOC MARs since 16.6 ka can be interpreted as a result of the flooded continental shelf in the Bering Sea, due to the global deglacial sea level rise (Fig. 5.6; Manley, 2002; Lambeck et al., 2014). The palaeoenvironment on the shelf during that time was most likely dominated by birch-graminoid tundra with small ponds (Elias et al., 1996) and therefore was a possible source for terrestrial materíal and organic material. The ongoing shelf flooding would also explain the continuously high TOC MARs during the cold Younger Dryas (Fig. 5.6) and the decrease in C/N ratios starting at 8 ka, as most of the shelf areas were already inundated at that time. Another explanation for high C/N ratios at 16.6 ka could be terrestrial material delivered by enhanced freshwater input, e.g. via the Yukon River.

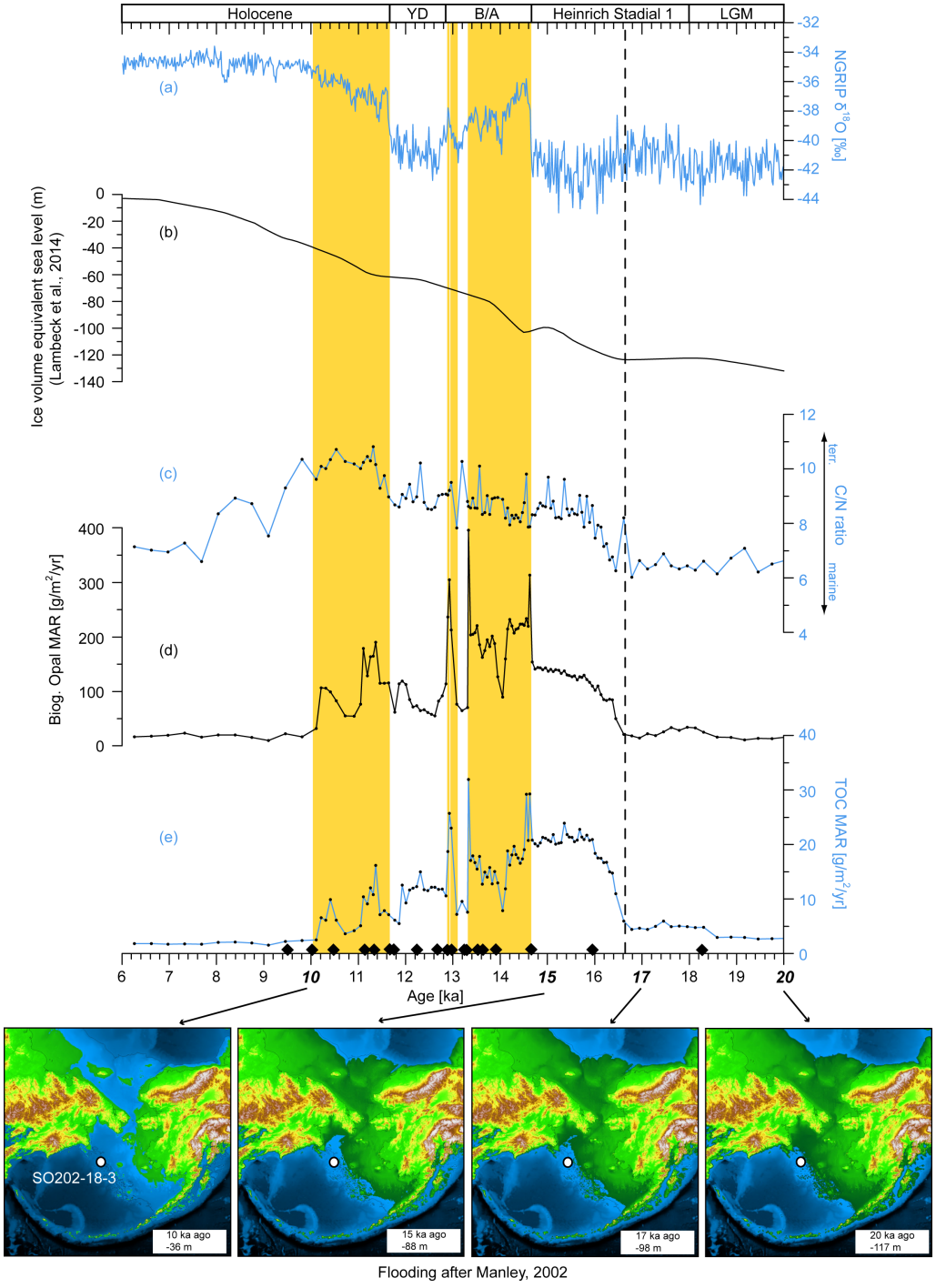

Figure 5.6: Mass accumulation rates (MAR) of TOC, biogenic opal, C/N ratios of core SO202-18-3 and global sea level change (Lambeck et al., 2014). Layered to laminated sections in SO202-18-3 are shown in orange, highlighting the close correlation to the NGRIP stable isotope record (NGRIP members, 2004). The lower panel shows the coastline development during the deglacial sea level rise (Manley, 2002 modified) and the position of core SO202-18-3. Note the synchronous onset of higher TOC and biogenic opal MAR and the higher C/N ratios with the beginning of increased sea level rise at 16.6 ka, marked by a vertical dashed line. Black squares mark planktic 14C ages of SO202-18-3 and neighbouring kasten core SO202-18-6. YD: Younger Dryas, B/A: Bølling|/Allerød, LGM: Last Glacial Maximum.

Such a scenario would be in line with a recent study that found evidence for increased glacial meltwater input into the North Pacific at 16 ka, based on diatom $d^{18}O$ and $d^{30}Si$ isotope records (Maier et al., 2015). However, with the data presented here, we are not able to distinguish between the shelf or increased meltwater as a possible source. Despite the input of nutrients and organic carbon via the shelf flooding or freshwater input, our slightly higher biogenic opal MARs between 16.6 – 14.6 ka indicate only a small increase in the productivity of siliceous plankton. A further increase in biological productivity was hampered by ongoing lower temperatures, the still high sea ice cover (Caissie et al., 2010) and the deep mixed layer (Lam et al., 2012). As a result, bottom water oxygen contents did not decreased to values that allowed lamina formation (Fig. 5.7b).

During the B/A and early Holocene the conditions were generally favorable for high export productivity (Fig. 5.7c). The sea ice conditions changed towards perennial sea ice, as revealed in diatom assemblages from the Umnak Plateau (Caissie et al., 2010) and also the SSTs increased with the onset of the B/A and early Holocene (Max et al., 2012). Especially the bottom water oxygen contents in core SO202-18-3 varied in concert with the SST changes during the B/A and the temperature difference between the cold and warm phases of the B/A and the YD was 1°C (Kuehn et al., 2014). Further, increased differences between alkenone derived SSTs and Mg/Ca-derived temperatures of planktic foraminifera showed enhanced thermal sstratification (Riethdorf et al., 2013a), which removed light limitation. As with the onset of the B/A the sea level was still 88 m lower compared to today (Manley, 2002), the continuous flooding of the shelf areas delivered nutrients and organic material. Also riverine input from the Yukon an its hinterlands was a possible source of nutrients, as with onset of the warmer B/A the climate in Alaska became wetter (Edwards et al., 2001) and the higher temperatures led to thawing of permafrost soils (Köhler et al., 2014). One important contributer to the export productivity were diatoms blooming events of mainly sea-ice-relates species, which developed during spring and summer. The increased export of diatom frustules resulted in the formation of seasonal laminae with high ammounts of biosiliceous material (Fig. 5.7c; Kuehn et al., 2014).

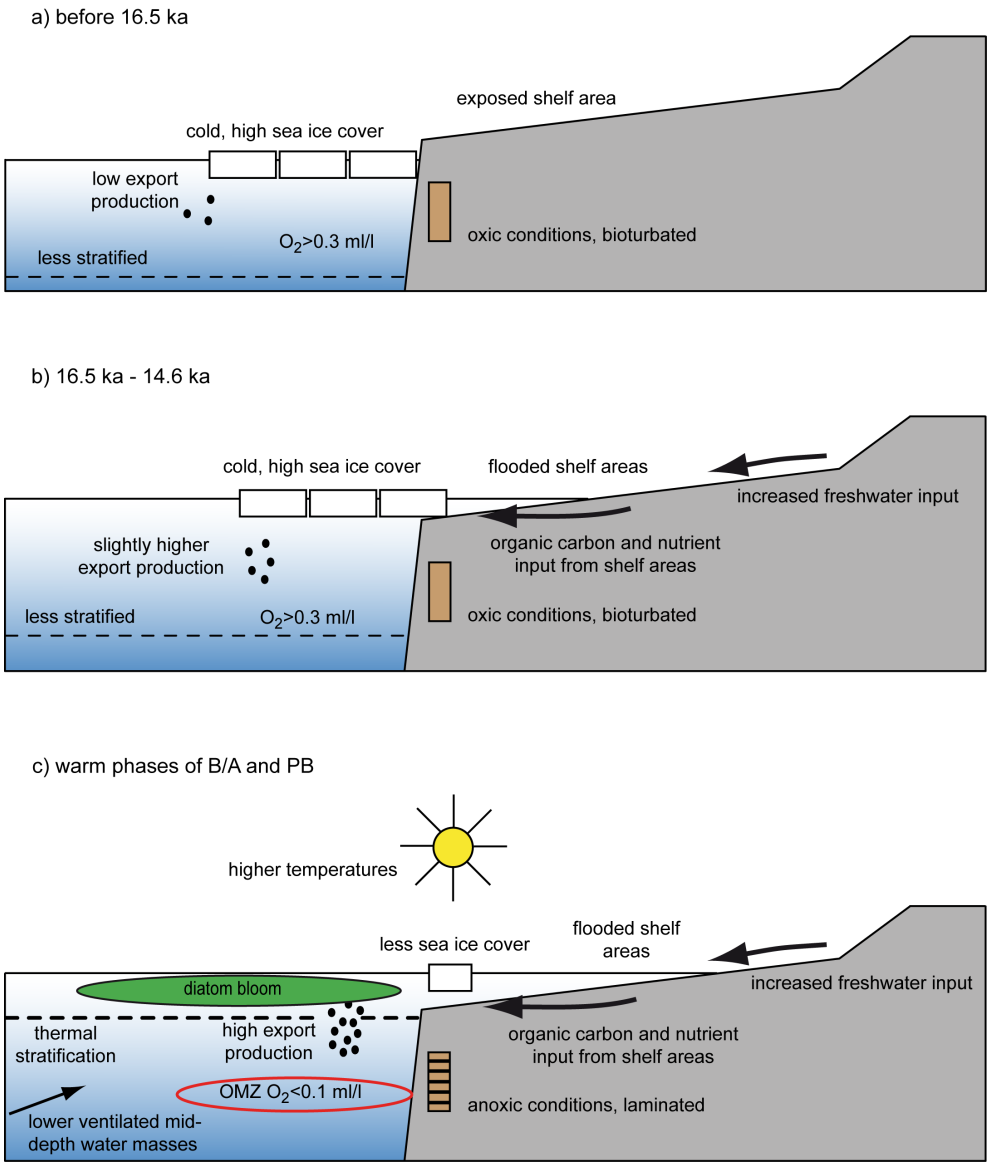

Figure 5.7: Model for the OMZ development and environmental changes in the Bering Sea based on our data for the time slices of (a) late glacial (before 16.5 ka), (b) for the time interval of 16.5 ka – 14.6 ka, (c) for the warmer B/A and early Holocene.

However, the increased export productivity and export of organic material to the sea-floor, was not sufficient to drive down bottom water oxygen contents to values that allow deposition of laminae. Oxygen contents of <0.1 ml/l and thus lamina formation were reached only in combination with oxygen poor, but not significantly older mid-depth water masses entering the Bering Sea (Fig. 5.7c, Kuehn et al., 2014). With water depths of over 1900 m, cores SO202-21-1 and SO202-12-1 (Fig. 5.2) lie, however, below depths influenced by the North Pacific Intermediate Water during the last deglaciation, which reached down to 1800 m (Max et al., 2014). While we cannot exclude with our

presented data the effect of upwelling from old, oxygen-poor North Pacific Deep Water masses as a driving mechanism, we speculate that this did not significantly contribute to OMZ intensification, as higher benthic $d^{13}C$ values recorded in the deglacial North Pacific do not indicate the presence of such water masses (Keigwin, 1998; Max et al., 2014).

Most of the described processes, that contribute to the development of anoxia, have basin-wide implications and therefore can not explain the differences in the duration of anoxia or their absence on the Shirshov Ridge. However, the presence of shelf areas are the most promising factors for the observed differences in the duration of anoxia or their absence on the Shirshov Ridge. As large shelf areas do not occur in the western Bering Sea (Fig. 5.1), the land masses that became flooded during the deglacial sea level rise were small compared to the eastern Bering Sea, and less nutrients were transported to the Shirshov Ridge. As a result the amount of organic material that was exported to the sea floor was comparable low, and the remineralization of organic material rate did not consumed all oxygen and allowed bioturbating macrofauna. Only in nearshore core SO201-2-114 laminated sequences occurred as it is located closer to a smaller shelf area (Fig. 5.1, Fig. 5.4b). Nutrient input from the shelf areas could have also influenced the early disappearance of laminated intervals in cores SO202-12-1 and SO202-22-4, as with ongoing sea level rise the coastline retreated to far away from the core position. This resulted in a decline of delivered nutrients and less export productivity. Another possible reason for the absence of anoxia on the Shirshov Ridge could have been better ventilated mid-depth waters due to a better connection to the eastern North Pacific vie the EKC and the wide Near Strait and Kamchatka Strait. Also the depth of the sediment core can influence the anoxia occurrence, as with increasing water depth less organic material reaches the bottom, leading to less oxygen consumption through remineralization.

5.5 Summary and conclusions

Based on a comparison high resolution, partly laminates sediment cores sediment cores (1100 m – 2700 m) we investigated the deglacial oxygenation history of the Bering Sea in a basin-wide context. By a comparison of ^{14}C dated sediment cores it was shown that the onset of anoxia and thus laminations during the B/A and early Holocene were synchronous events, starting at 14.6 ka and 11.7 ka respectively. The observed timing is in close correspondence to other locations in the North Pacific region, especially the Gulf of Alaska, making the onset of laminations reliable stratigraphic markers. These similarities suggest that the Bering Sea and subarctic North Pacific ocean-climate system were closely connected during the last deglaciation. The development of deglacia anoxia was driven through increased export productivity and corresponding high accumulation rates of organic material.

However, the disappearance of laminations was a diachronous process that could have been related to the nutrient delivery from the flooded shelf areas. Core sites that lie distal to these areas received less nutrients, resulting in lower export productivity and thus less organic material that is transported to the sea floor and incomplete nutrient consumption through remineralization.

Acknowledgements

We acknowledge the professional help of the crew and shipboard science party of R/V during SO202 cruise. This paper is a contribution to Topic 3.1 “Circumpolar climate variability and global teleconnections at seasonal to orbital time scales” of the AWI PACES II research program. The study was funded through the “Innovative North Pacific Experiment (INOPEX)” by the German Federal Ministry of Education and Research (BMBF Grant no. 03G0202A) and by funding to LLJ, OE and RT through the bilateral “Sino-German Pacific Ocean Experiment (SIGEPAX)” project (BMBF grant no. 03F0704A). Additional financial support came from AWI through the Helmholtz REKLIM Initiative and the MARUM – Center for Marine Environmental Sciences (Project OC 3).

Supporting Information

Timing and forcing mechanisms of anoxia in the Bering Sea during the last deglaciation

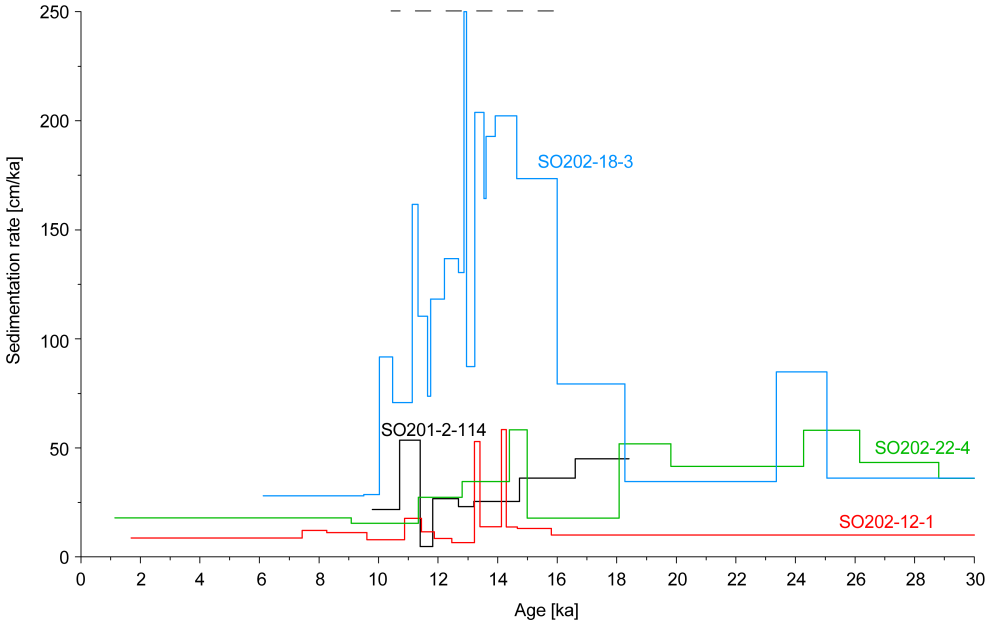

Figure S4.1: Sedimentation rates of cores SO202-12-1 (red), SO202-18-3 (blue), SO202-22-4 (green) and SO201-2-114 (black). Note the cut-off at 250 cm/ka.

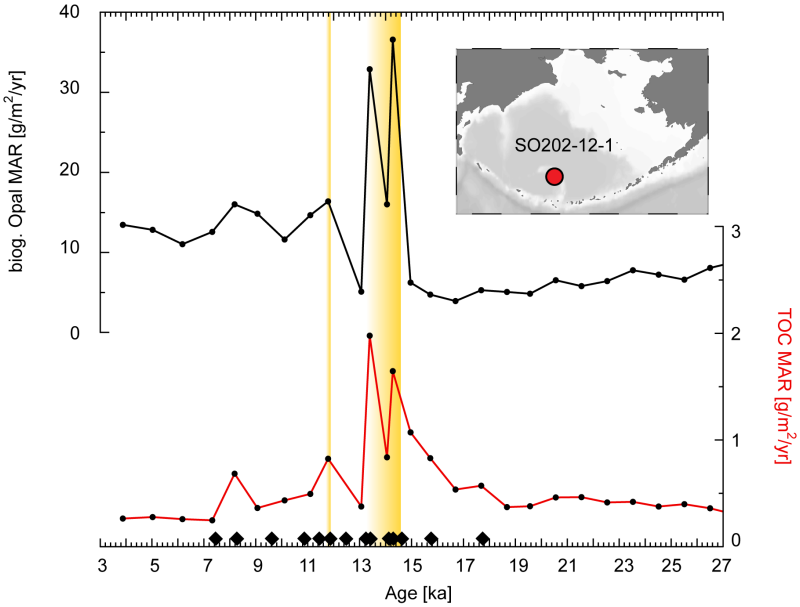

Figure S5.2: Mass accumulation rates of biogenic opal (in black) and total organic carbon (TOC) in red of core SO202-12-1. Laminated sediment sections are marked orange. The core location is depicted in the small map by a red circle.

6. Conclusions and outlook

In this thesis I studied a suite of partly laminated sediment cores, covering a depth transect of (1066 m – 2703 m) from the Bering Sea to improve our understanding of the deglacial oxygen minimum zone (OMZ) development in this region, which is one of the largest and most productive marginal seas in the world ocean. I gained new information on the characteristics and composition of discrete laminae, the lateral extension of the OMZ through time, the timing of anoxia occurrence in relation to deglacial regional and global climate changes, and the processes and forcings that led to the oxygen drawdown and lamina formation.

I showed that during the warm Bølling–Allerød (B/A) and Preboreal the Bering Sea OMZ intensified to anoxic values of <0.1 ml/l, which resulted in the formation of laminated sediments. Such oceanic oxygen depletions were widespread throughout the deglacial world ocean (Jaccard and Galbraith, 2012). In the Bering Sea laminated sediments occurred at many locations along the eastern shelf ridge, along Bowers Ridge, and at one location on the western shelf ridge. Based on the occurrence of laminated sediment sections, anoxic conditions expanded laterally to water depths of >2100 m. This is much deeper than the modern OMZ core, which is located between 900 and 1000 m. A correlation of ^{14}C-dated, laminated sediment cores revealed, that throughout the Bering Sea and the Gulf of Alaska the onset of deglacial anoxia at 14.6 ka and 11.7 ka, and thus formation of laminations was a synchronous event, making the onsets of laminated sections in sediment cores therefore reliable stratigraphic markers. The disappearance of the laminations, however, was a diachronous process and longest intervals of anoxia persisted near the eastern shelf areas. Especially during the Preboreal anoxia persisted for 1500 yr at the northern Bering Slope, compared to a rather short duration of 200 yr on the Bowers Ridge (Fig. 6.1a and 6.1b). For more detailed information on the timing and processes of OMZ variations, I used high quality sediment core SO202-18-3 from the northeastern Bering Slope as reference record (Fig. 6b). The age model of this reference core was based on laminae counting, planktic ^{14}C dates and a detailed correlation of laminated sections to the North Greenland Ice Core (NGRIP) stable isotope data, for the time interval of the B/A to Holocene. As a result of this correlation approach it became obvious that the laminae represent varves. As the age model is chronostrigraphically partly independent of radiocarbon dating, it allowed the calculation of ^{14}C surface reservoir ages for the varved intervals. Calculated mean surface reservoir ages result in values of 875 yr for the B/A, 910 yr for the Younger Dryas, and 770 yr for the Holocene. For times older than the B/A the age model was based on planktic ^{14}C dates and a correlation of the XRF-based Ca/Fe ratios to NGRIP δ^{18}O data, which showed strong similarities.

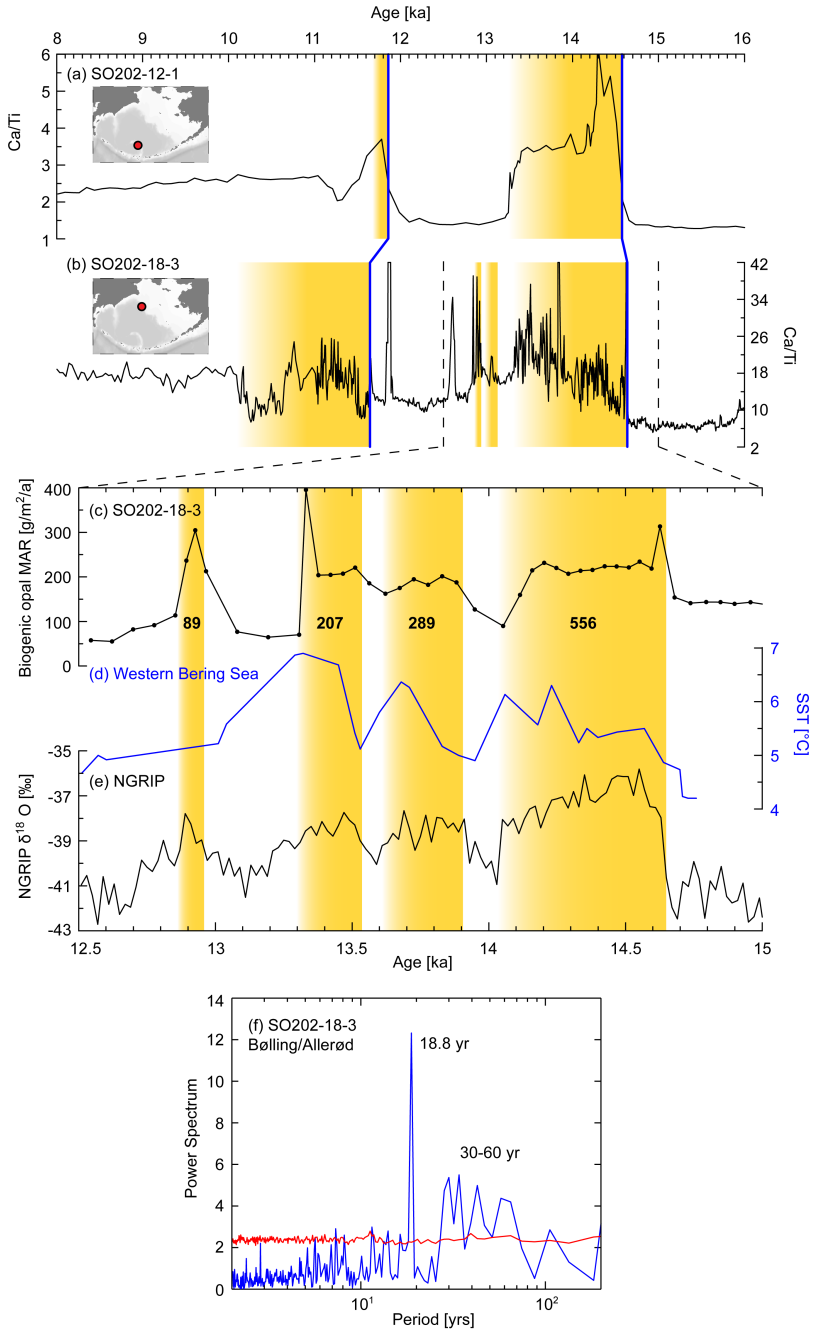

Fig. 6.1: Selected results of Bering Sea laminae analysis. XRF-based Ca/Ti ratios of (a) SO202-12-1 and reference core (b) SO202-18-3 with layered to laminated sections in each core marked in orange. Core locations are shown in the small maps. Note the synchronous onset of laminations depicted by a blue line and the diachronous lamina disappearance. (c) Biogenic opal mass accumulation rate (MAR) of core SO202-18-3. Major laminated intervals are marked in orange and numbers below the plot give results of varve counts. (d) Stacked alkenone-based sea surface temperature record from the western Bering Sea (3-pt running mean; blue plot) based on data of Max et al., 2012. (e) NGRIP $\delta^{18}O$ data (Rasmussen et al., 2006). Note the correspondence of warm intervals in NGRIP and lamination occurrence in SO202-18-3. (f) Spectral analysis of B/A laminations from core SO202-18-3 using Fast Fourier Transformation. Red line denotes the 95 % highest spectrum of 1000 AR(1) processes with the same autocorrelation.

Based on relatively constant benthic-planktic ventilation ages throughout the last deglaciation, it was shown that on millennial-scale anoxia were caused by basin-wide remineralization of organic matter in intermediate waters, while changes in the source or the formation rate of these waters were less important. Superimposed on these millennial scale changes were variations of the OMZ strength on shorter, inter-decadal timescales. Especially during the B/A, the formation of laminated sediments was tightly coupled to warm intervals within that interstadial, as recorded in Bering Sea sea surface temperature (SST) records and the NGRIP stable isotope data (Fig. 6.1c – 6e). To estimate the temperature changes, I established a stacked SST record, based on published Bering Sea alkenone SST data and showed that SSTs of about 6 °C persisted during times of lamina formation, while the SSTs were lower with values of about 5 °C during times were laminations were not common (Fig. 6.1d). The applied correlation of layer-counted, laminated sections to the NGRIP data further revealed that oceanographic changes in the Bering Sea occurred with a rapidity that is comparable to the abrupt climate changes recorded in the Greenland ice cores, corroborating the suggestion of near-synchronous, hemispheric-wide rapid transmissions of deglacial climate change (Steffensen et al., 2008). This observed close link between Bering Sea and Greenland climate implies a rapid atmospheric teleconnection, in line with previous paleoceanographic and modeling results that argued for an in-phase behavior of North Pacific and North Atlantic climate. Atmospheric transfer between the North Atlantic and North Pacific was probably influenced by decadal changes in the position and strength of the Aleutian Low, which is one of the main atmospheric "centers of action" of the Northern Hemisphere (Rodionov et al., 2007).

The Bering Sea anoxia during the B/A and Preboreal were mainly driven by higher export productivity, visible in high accumulation rates of biogenic opal, carbonate and total organic carbon (TOC), and X-ray-fluorescence (XRF)-derived elemental ratios indicative for high biological productivity like Br/Ti, Ca/Ti and Si/Ti (Fig. 6.1a – 6c). The higher temperatures during the Preboreal and B/A fostered biogenic export production as they led to a shift from perennial sea ice, which most likely persisted during the cold Younger Dryas and Heinrich Stadial I (Meheust, 2014), to seasonal sea ice. As a result, a sea-ice-related diatom bloom event developed which may have occurred during spring/summer, followed by times of low productivity during autumn and winter. These seasonal productivity variations are reflected as an alternation between diatom-rich laminae, which have low densities in radiographies and high XRF-based Cl- and Si/Ti values, and laminae that represent the terrigenous background sedimentation. The latter laminae have higher densities and lower Cl values and Si/Ti ratios. The export productivity during the Preboreal and B/A was additionally increased by thermal stratification, visible in higher temperature gradients in Mg/Ca and alkenone-based SSTs and higher freshwater input delivering nutrients, which was probably related to the melting of hinterland

permafrost soils. The still closed Bering Strait could have facilitated productivity through enhanced trapping and nutrient recirculation. Other major sources for nutrients and organic carbon were the proximal shelf areas, which became flooded due to the deglacial sea level rise. As the largest shelf areas in the Bering Sea are located in the northeastern part, cores near this area received more nutrients and organic carbon compared to cores further west. This gradient in lateral material supply was important for the diachronous OMZ weakening (Fig. 6.1a and Fig. 6.1b). Higher C/N ratios and total organic carbon mass accumulation rates suggested that the shelf flooding, and possibly also freshwater input, started within the cold Heinrich Stadial I at 16.6 ka.

The annual resolution of the laminations from reference record SO202-18-3 and the clear differences of the single laminae in the geochemical and physical properties provided the opportunity to perform spectral analysis of the laminated sediment sections. Therefore, the XRF-based Cl values of single laminae were used as a indicator for biosiliceous primary productivity, as they depend on the pore water content and thus sediment density, which is a function of the diatom concentration. Especially for the B/A, the Fast Fourier Transformation-based spectral analysis revealed a sharp peak of 18.8 yr cyclicity and a broader peak in the range of 30 – 60 yr (Fig. 6.1f). The first spectral peak is related to the 18.6 yr nodal tidal cycle, which fostered the diatom-driven productivity through enhanced nutrient supply to the surface during times of strong tidal mixing. The latter spectral peak may be related to the Pacific Decadal Oscillation (PDO), which could have influenced the primary productivity through SST variations and mixed layer dynamics. Both processes are known to influence the modern Bering Sea and North Pacific. With these results I showed that internal variability, originating from coupled ocean-atmosphere dynamics, and external forcing through the sharply expressed nodal cycle have been persistent features of the inter-decadal ocean-climate system in the subarctic North Pacific since the last glacial and are not limited to modern observations.

For future research, additional focus should be spend on the investigation of single laminae, as it was shown in this thesis that these varve-like laminae have an annual resolution in our reference record. First analyses revealed that it is possible to separate laminae and apply geochemical measurements on this material (Fig. 6.2). This provides the unique opportunity to study deglacial SSTs, sea surface salinity, mixed layer dynamics and primary productivity variations with seasonal resolution.

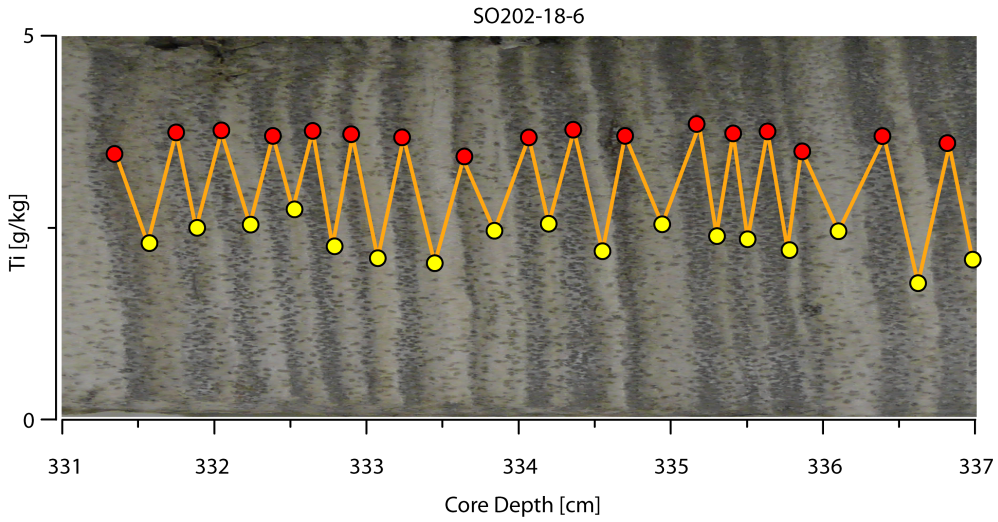

Fig. 6.2: Overlay of Ti-contents based on ICP measurements of single Holocene laminae from core SO202-18-6 and a photo of the sampled laminations. The diatom-rich laminae are shown in white and terrigenous laminae in dark color. In the plot results diatomaceous laminae are shown in yellow circles and results of terrigenous laminae in red circles.

New benthic-planktic ventilation ages for times older than the B/A might help to understand if the Bering Sea was a source of intermediate- or deep water masses during stadials. This is still a matter of discussion, with no detailed ventilation records on longer timescales beyond the Last Galcial Maximum being published so far. Therefore it would be necessary to refine the age model, which could be accomplished by the ^{14}C plateau-tuning technique (Sarnthein et al., 2007). This method also provides planktic reservoir ages, which give insights into changes in ocean currents. Furthermore, there are no detailed sea ice records available for the eastern Bering Sea, covering the last 20 ka. Here, the sediment cores from the INOPEX cruise provide the opportunity to map the IP_{25}-based sea ice distribution along a transect of the eastern shelf ridge. This information might give new insights into the effect of sea ice on ocean ventilation and long-term sea ice dynamics.

Data handling

All data presented in this thesis will be stored electronically and will be available online in the PANGAEA database (http://www.pangaea.de).

References

Addison, J. A., Finney, B. P., Dean, W. E., Davies, M. H., Mix, A. C., Stoner, J. S., and Jaeger, J. M.: Productivity and sedimentary δ15N variability for the last 17,000 years along the northern Gulf of Alaska continental slope, Paleoceanography, 27, doi:10.1029/2011PA002161, 2012.

Ahagon, N., Ohkushi, K., Uchida, M., and Mishima, T.: Mid-depth circulation in the northwest Pacific during the last deglaciation: Evidence from foraminiferal radiocarbon ages, Geophysical Research Letters, 30, 2097, doi:10.1029/2003GL018287, 2003.

Andersen, K. K., Svensson, A., Johnsen, S. J., Rasmussen, S. O., Bigler, M., Röthlisberger, R., Ruth, U., Siggaard-Andersen, M.-L., Steffensen, J. P., Dahl-Jensen, D., Vinther, B. M., and Clausen, H. B.: The Greenland Ice Core Chronology 2005, 15-42 ka. Part 1: constructing the time scale, Quaternary Science Reviews, 25, 3246-3257, doi:10.1016/j.quascirev.2006.08.002, 2006.

Bauch, D., Erlenkeuser, H., Winckler, G., Pavlova, G., and Thiede, J.: Carbon isotopes and habitat of polar planktic foraminifera in the Okhotsk Sea: the 'carbonate ion effect' under natural conditions, Marine Micropaleontology, 45, 83-99, doi:10.1016/S0377-8398(02)00038-5, 2002.

Behl, R. J., and Kennett, J. P.: Brief interstadial events in the Santa Barbara basin, NE Pacific, during the past 60 kyr, Nature, 379, 243-246, doi:10.1038/379243a0, 1996.

Blackman, R.B., and Tukey, J.W.: The measurement of power spectra from the point of view of communication engineering. Dover Publications, New York. 190 pp., 1958.

Blockley, S. P. E., Lane, C. S., Hardiman, M., Rasmussen, S. O., Seierstad, I. K., Steffensen, J. P., Svensson, A., Lotter, A. F., Turney, C. S., and Bronk Ramsey, C.: Synchronisation of palaeoenvironmental records over the last 60,000 years, and an extended INTIMATE event stratigraphy to 48,000 b2k, Quaternary Science Reviews, 36, 2-10, doi:10.1016/j.quascirev.2011.09.017, 2011.

Bond, G. C., Broecker, W. S., Johnsen, S., McManus, J., Labeyrie, L., Jouzel, J., and Bonani, G.: Correlations between climate records from North Atlantic sediments and Greenland ice, Nature, 365, 143–147, doi:10.1038/365143a0, 1993.

Brauer, A., Haug, G. H., Dulski, P., Sigman, D. M., and Negendank, J. F. W.: An abrupt wind shift in western Europe at the onset of the Younger Dryas cold period, Nature Geoscience, 1, 520-523, doi:10.1038/ngeo263, 2008.

Bronk Ramsey, C., Staff, R. A., Bryant, C. L., Brock, F., Kitagawa, H., van der Plicht, J., Schlolaut, G., Marshall, M. H., Brauer, A., Lamb, H. F., Payne, R. L., Tarasov, P. E., Haraguchi, T., Gotanda, K., Yonenobu, H., Yokoyama, Y., Tada, R., and Nakagawa, T.: A complete terrestrial radiocarbon record for 11.2 to 52.8 kyr B.P, Science (New York, NY), 338, 370-374, doi:10.1126/science.1226660, 2012.

Brown, Z. W., and Arrigo, K. R.: Contrasting trends in sea ice and primary production in the Bering Sea and Arctic Ocean, ICES Journal of Marine Science, 69, 1180-1193, doi:10.1093/icesjms/fss113, 2012.

Brunelle, B. G., Sigman, D. M., Jaccard, S. L., Keigwin, L. D., Plessen, B., Schettler, G., Cook, M. S., and Haug, G. H.: Glacial/interglacial changes in nutrient supply and stratification in the western

subarctic North Pacific since the penultimate glacial maximum, Quaternary Science Reviews, 29, 2579-2590, doi:10.1016/j.quascirev.2010.03.010, 2010.

Bubenshchikova, N., Nuernberg, D., Lembke-Jene, L., and Pavlova, G.: Living benthic foraminifera of the Okhotsk Sea: Faunal composition, standing stocks and microhabitats, Marine Micropaleontology, 69, 314-333, doi:10.1016/j.marmicro.2008.09.002, 2008.

Caissie, B. E., Brigham-Grette, J., Lawrence, K. T., Herbert, T. D., and Cook, M. S.: Last Glacial Maximum to Holocene sea surface conditions at Umnak Plateau, Bering Sea, as inferred from diatom, alkenone, and stable isotope records, Paleoceanography, 25, PA1206, doi:10.1029/2008PA001671, 2010.

Carlson, A. E., and Clarke, P. U.: Ice sheet sources of sea level rise and freshwater discharge during the last deglaciation, Reviews of Geophysics 50 (4), doi:10.1029/2011RG000371, 2012.

Clarke, P. U., Shakun, J. D., Baker, P. A., Bartlein, P. J., Brewer, S., Brook, E., Carlson, A. E., Cheng, H., Kaufman, D. S., Liu, Z., Marchitto, T. M., Mix, A. C., Morrill, C., Otto-Bliesner, B. L., Pahnke, K., Russell, J. M., Whitlock, C., Adkins, J. F., Blois, J. L., Clark, J., Colman, S. M., Curry, W. B., Flower, B. P., He, F., Johnson, T. C., Lynch-Stieglitz, J., Markgraf, V., McManus, J., Mitrovica, J. X., Moreno, P. I., and Williams, J. W.: Global climate evolution during the last deglaciation, PNAS, 109, E1134-E1142, doi:10.1073/pnas.1116619109, 2012.

Cerveny, R. S., and Shaffer, J. A.: The moon and El Niño, Geophysical Research Letters, 28, 25-28, doi:10.1029/2000GL012117, 2001.

Chavez, F. P., Ryan, J., Lluch-Cota, S. E., Niquen C., M.: From anchovies to sardines and back: Multidecadal change in the Pacific ocean, Science, 299, 217-221, doi:10.1126/science.1075880, 2003.

Cook, M. S., Keigwin, L. D., and Sancetta, C. A.: The deglacial history of surface and intermediate water of the Bering Sea, Deep Sea Research Part II: Topical Studies in Oceanography, 52, 2163-2173, doi:10.1016/j.dsr2.2005.07.004, 2005.

Croudace, I. W., Rindby, A., and Rothwell, R. G.: ITRAX: description and evaluation of a new multi-function X-ray core scanner, in: New Techniques in Sediment Core Analysis, edited by: Rothwell, R. G., Special Publications, The Geological Society, London, 51-63, 2006.

Crusius, J., Pedersen, T., Kienast, S., Keigwin, L., and Labeyrie, L.: Influence of northwest Pacific productivity on North Pacific Intermediate Water oxygen concentrations during the Boiling-Allerod interval (14.7-12.9 ka), Geology, 32, 633-636, doi:10.1130/G20508.1, 2004.

D'Arrigo, R., Villalba, R., Wiles, G.: Tree-ring estimates of Pacific decadal climate variability, Climate Dynamics, 18, 219-224, doi:10.1007/s003820100177, 2001.

Danielson, S., Curchitser, E., Hedstrom, K., Weingartner, T., and Stabeno, P.: On ocean and sea ice modes of variability in the Bering Sea, Journal of Geophysical Research: Oceans, 116, C12034, doi:10.1029/2011JC007389, 2011.

Davies, M. H., Mix, A. C., Stoner, J. S., Addison, J. A., Jaeger, J., Finney, B., and Wiest, J.: The deglacial transition on the southeastern Alaska Margin: Meltwater input, sea level rise, marine productivity, and sedimentary anoxia, Paleoceanography, 26, PA2223, doi:10.1029/2010PA002051, 2011.

Duplessy, J.-C., Arnold, M., Bard, E., Juillet-Leclerc, A., Kallel, N., and Labeyrie, L.: AMS C-14 Study of Transient Events and of the Ventilation Rate of the Pacific Intermediate Water During the Last Deglaciation, Radiocarbon, 31, 493-502, 1989.

Elias, S. A., Short, S. K., Nelson, C. H., and Birks, H. H.: Life and times of the Bering land bridge, Nature, 382, 60-63, doi:10.1038/382060a0, 1996.

EPICA community members, Eight glacial cycles from an Antarctic ice core, Nature, 429, 623-628, doi:10.1038/nature02599, 2004.

Foreman, M. G. G., Cummins, P. F., Cherniawsky, J. Y., and Stabeno, P.: Tidal energy in the Bering Sea, Journal of Marine Research, 64, 797-818, doi:10.1357/002224006779698341, 2006.

Galbraith, E. D., Jaccard, S. L., Pedersen, T. F., Sigman, D. M., Haug, G. H., Cook, M., Southon, J. R., and Francois, R.: Carbon dioxide release from the North Pacific abyss during the last deglaciation, Nature, 449, 890-893, doi:10.1038/nature06227, 2007.

Garcia, H. E., Locarnini, R. A., Boyer, T. P., Antonov, J. I., Baranova, O. K., Zweng, M. M., and Johnson, D. R.: World Ocean Atlas 2009, Volume 3: Dissolved Oxygen, Apparent Oxygen Utilization, and Oxygen Saturation, NOAA Atlas NESDIS 70, edited by: Levitus, S., U.S. Government Printing Office, Washington, D.C., 344 pp., 2010.

Gebhardt, H., Sarnthein, M., Grootes, P. M., Kiefer, T., Kühn, H., Schmieder, F., and Röhl, U.: Paleonutrient and productivity records from the subarctic North Pacific for Pleistocene glacial terminations I to V, Paleoceanography, 23, PA4212, doi:10.1029/2007PA001513, 2008.

Gersonde, R.: The Expedition of the Research Vessel ‘‘Sonne’’ to the Subpolar North Pacific and the Bering Sea in 2009 (SO202-INOPEX), in: Reports on Polar and Marine Research, Alfred Wegener Institute, Bremerhaven, 323, 2012.

Gorbarenko, S. A., Basov, I. A., Chekhovskaya, M. P., Southon, J., Khusid, T. A., and Artemova, A. V.: Orbital and millennium scale environmental changes in the southern Bering Sea during the last glacial-Holocene: Geochemical and paleontological evidence, Deep Sea Research Part II: Topical Studies in Oceanography, 52, 2174-2185, doi:10.1016/j.dsr2.2005.08.005, 2005.

Grantham, B. A., Chan, F., Nielsen, K. J., Fox, D. S., Barth, A., Lubchenco, J., and Menge, B. A.: Upwelling-driven nearshore hypoxia signals ecosystem and oceanographic changes in the northeast Pacific, Nature, 429, 749–754, doi:10.1038/nature02605, 2004.

Grebmeier, J. M.: A Major Ecosystem Shift in the Northern Bering Sea, Science (New York, NY), 311, 1461-1464, doi:10.1126/science.1121365, 2006.

Grebmeier, J. M., Cooper, L. W., Feder, H. M., Sirenko, B. I.: Ecosystem dynamics of the Pacific-influenced Northern Bering and Chukchi Seas in the Amerasian Arctic, Progress in Oceanography, 71, 331-361, doi:10.1016/j.pocean.2006.10.001, 2006.

Haigh, I. D., M. Eliot, and C. Pattiaratchi.: Global influences of the 18.61 year nodal cycle and 8.85 year cycle of lunar perigee on high tidal levels, Journal Geophysical Research - Oceans, 116, C06025, doi:10.1029/2010JC006645, 2011.

Hamilton, E. L.: Sound velocity and related properties of marine sediments, North Pacific, Journal of Geophysical Research, 75, 4423-4446, doi:10.1029/JB075i023p04423, 1970.

Haykin, S.: Nonlinear methods of spectral analysis, 2nd ed., Springer, Berlin, 1983.

Hendy, I. L., Kennett, J. P., Roark, E. B., and Ingram, B. L.: Apparent synchroneity of submillennial scale climate events between Greenland and Santa Barbara Basin, California from 30-10 ka, Quaternary Science Reviews, 21, 1167-1184, doi:10.1016/S0277-3791(01)00138-X, 2002.

Hendy, I. L., and Pedersen, T. F.: Oxygen minimum zone expansion in the eastern tropical North Pacific during deglaciation, Geophysical Research Letters, 33, L20602, doi:10.1029/2006GL025975, 2006.

Hofmann, A. F., Peltzer, E. T., Walz, P. M., Brewer, P. G.: Hypoxia by degrees: Establishing definitions for a changing ocean, Deep Sea Research Part I: Oceanographic research papers, 58, 1212-1226, doi:10.1016/j.dsr.2011.09.004, 2011.

Hood, D.W.: The Bering Sea, in: Ketchum, B.H. (Ed.), 1983. Estuaries and enclosed seas. Ecosystems of the World 26, 337-373, 1983.

Hu, A. X., Meehl, G. A., Otto-Bliesner, B. L., Waelbroeck, C., Han, W. Q., Loutre, M. F., Lambeck, K., Mitrovica, J. X., and Rosenbloom, N.: Influence of Bering Strait flow and North Atlantic circulation on glacial sea-level changes, Nature Geoscience, 3, 118-121, doi:10.1038/ngeo729, 2010.

Hughen, K. A., Overpeck, J. T., Peterson, L. C., Trumbore, S.: Rapid climate changes in the tropical Atlantic region during the last deglaciation, Nature, 380, 51-54, doi:10.1038/380051a0, 1996.

Hughen, K. A., Southon, J. R., Lehman, S. J., and Overpeck, J. T.: Synchronous radiocarbon and climate shifts during the last deglaciation, Science (New York, NY), 290, 1951-1954, doi:10.1126/science.1088470, 2000.

Ikehara, K., Ohkushi, K. a. i., Shibahara, A., and Hoshiba, M.: Change of bottom water conditions at intermediate depths of the Oyashio region, NW Pacific over the past 20,000 yrs, Global And Planetary Change, 53, 78-91, doi:10.1016/j.gloplacha.2006.01.011, 2006.

Itaki, T., Uchida, M., Kim, S., Shin, H.-S., Tada, R., and Khim, B.-K.: Late Pleistocene stratigraphy and palaeoceanographic implications in northern Bering Sea slope sediments: evidence from the radiolarian species Cycladophora davisiana, Journal of Quaternary Science, 24, 856-865, doi:10.1002/jqs.1356, 2009.

Itaki, T., Kim, S., Rella, S. F., Uchida, M., Tada, R., Khim, B-K.: Millennial-scale variations of late Pleistocene radiolarian assemblages in the Bering Sea related to environments in shallow and deep waters, Deep Sea Research Part II: Topical Studies in Oceanography, 61-64, 127-144, doi:10.1016/j.dsr2.2011.03.002, 2012.

Jenkins, R., and de Vries, J. L.: Practical X-ray spectrometry, MacMillan, London, 1970.

Jaccard, S. L., and Galbraith, E. D.: Large climate-driven changes of oceanic oxygen concentrations during the last deglaciation, Nature Geoscience, 5, 151-156, doi:10.1038/ngeo1352, 2012.

Jaccard, S. L., Galbraith, E. D., Fröhlicher, T. L., and Gruber, N.: Ocean (de)oxygenation across the last deglaciation, Oceanography, 27, 26-35, doi:10.5670/oceanog.2014.05, 2014.

Jansen, J. H. F., Van der Gaast, S. J., Koster, B., and Vaars, A. J.: CORTEX, a shipboard XRF-scanner for element analyses in split sediment cores. Marine Geology 151, 143-153, doi:10.1016/S0025-3227(98)00074-7, 1998.

Katsuki, K., Itaki, T., Khim, B-K., Uchida, M., and Tada, R.: Response of the Bering Sea to 11-year solar irradiance cycles during the Bølling-Allerød, Geophysical Research Letters, 41, 2892-2898, doi:10.1002/2014GL059509, 2014.

Keeling, R. F., Körtzinger, A., and Gruber, N.: Ocean deoxygenation in a warming world, Annu. Rev. Mar. Sci., 2, 199–229, doi:10.1146/annurev.marine.010908.163855, 2010.

Keigwin, L. D. and Jones, G. A.: Deglacial climatic oscillations in the Gulf of California, Paleoceanography, 5, 1009-1023, doi:10.1029/PA005i006p01009, 1990.

Keigwin, L., Jones, G., and Froelich, P.: A 15,000 year paleoenvironmental record from Meiji Seamount, far Northwestern Pacific, Earth And Planetary Science Letters, 111, 425-440, doi:10.1016/0012-821X(92)90194-Z, 1992.

Keigwin, L. D.: Glacial-age hydrography of the far northwest Pacific Ocean, Paleoceanography, 13, 323-339, doi:10.1029/98PA00874, 1998.

Keigwin, L. D., Donnelly, J. P., Cook, M. S., Driscoll, N. W., Brigham-Grette, J.: Rapid sea-level rise and Holocene climate in the Chukchi Sea, Geology, 34, 861-864, doi:10.1130/G22712.1, 2006.

Kennett, J., and Ingram, B.: A 20,000-year record of ocean circulation and climate change from the Santa Barbara basin, Nature, 377, 510-514, doi:10.1038/377510a0, 1995.

Khim, B.-K., Kim, S., Uchida, M., and Itaki, T.: High organic carbon deposition in the northern margin of the Aleutian Basin (Bering Sea) before the last deglaciation, Ocean Science Journal, 45, 203-211, doi:10.1007/s12601-010-0019-y, 2010.

Kim, S., Khim, B. K., Uchida, M., Itaki, T., and Tada, R.: Millennial-scale paleoceanographic events and implication for the intermediate-water ventilation in the northern slope area of the Bering Sea duriing the last 71 kyrs, Global And Planetary Change, 79, 89-98, doi:10.1016/j.gloplacha.2011.08.004, 2011.

Köhler, P., Knorr, G., Bard, E.: Permafrost thawing as a possible source of abrupt carbon release at the onset of the Bølling/Allerød, Nature communications 5, doi:10.1038/ncomms6520, 2014.

Kohfeld, K. E., and Chase, Z.: Controls on deglacial changes in biogenic fluxes in the North Pacific Ocean, Quaternary Science Reviews, 30, 3350-3363, doi:10.1016/j.quascirev.2011.08.0 07, 2011.

Kossler, A., Tarasov, P., Schlolaut, G., Nakagawa, T., Marshall, M., Brauer, A., Staff, R., Ramsey, C. B., Bryant, C., Lamb, H., Demske, D., Gotanda, K., Haraguchi, T., Yokoyama, Y., Yonenobu, H., and Tada, R.: Onset and termination of the late-glacial climate reversal in the high-resolution diatom and sedimentary records from the annually laminated SG06 core from Lake Suigetsu, Japan, Palaeogeography Palaeoclimatology Palaeoecology, 306, 103-115, doi:10.1016/j.palaeo.2011.04.004, 2011.

Kuehn, H., Lembke-Jene, L., Gersonde, R., Esper, O., Lamy, F., Arz, H., G. Kuhn, and Tiedemann, R.: Laminated sediments in the Bering Sea reveal atmospheric teleconnections to Greenland

climate on millennial to decadal timescales during the last deglaciation, Clim Past, 10, 2215-2236, doi:10.5194/cp-10-2215-2014, 2014.

Kuhn, G.: Don't forget the salty soup: Calculations for bulk marine geochemistry and radionuclide geochronology, Mineralogical Magazine, 77, 1516, doi:10.1180/minmag.2013.077.5.11, 2013.

Kuroyanagi, A., Kawahata, H., Nishi, H., and Honda, M. C.: Seasonal changes in planktonic foraminifera in the northwestern North Pacific Ocean: sediment trap experiments from subarctic and subtropical gyres, Deep Sea Research Part II: Topical Studies in Oceanography, 49, 5627-5645, doi:10.1016/S0967-0645(02)00202-3, 2002.

Ladd, C., Stabeno, P., Cokelet, E. D.: A note on cross-shelf exchange in the northern Gulf of Alaska, Deep Sea Research Part II: Topical Studies in Oceanography, 52, 667-679, doi:10.1016/j.dsr2.2004.12.022, 2005.

Lam, P. J., Robinson, L. F., Blusztajn, J., Li, C., Cook, M. S., McManus, J. F., and Keigwin, L. D.: Transient stratification as the cause of the North Pacific productivity spike during deglaciation, Nature Geoscience, 6, 622-626, doi:10.1038/ngeo1873, 2013.

Lambeck, K., Rouby, H., Purcell, A., Sun, Y., and Sambridge, M.: Sea level and global ice volumes from the Last Glacial Maximum to the Holocene, PNAS, 111, 15296-15303, doi:10.1073/pnas.141176211, 2014.

Latif, M.: On North Pacific multidecadal climate variability, Journal of Climate, 19, 2906-2915, doi:10.1175/JCLI3719.1, 2006.

Levitus, S., and Boyer, T. P.: World Ocean Atlas 1994, Volume 4: Temperature, in: NOAA Atlas NESDIS 4, US Government Printing Office, Washington, DC, 117, 1994.

Loder, J. W., and Garrett, C.: The 18.6-year cycle of sea surface temperatures in shallow seas due to variations in tidal mixing, Journal of Geophysical Research: Oceans, 83, 1967-1970, doi:10.1029/JC083iC04p01967, 1978.

Luchin, V. A., Menovshchikov, V. A., Lavrentiev, V. M., and Reed, R. K.: Thermohaline Structure and Water Masses in the Bering Sea, in: Dynamics of the Bering Sea, edited by: Loughlin, T. R., and Ohtani, K., North Pacific MArine Science Organization (PICES) and Alaska Sea Grant College Program, Fairbanks, AL, 29-60, 1999.

Lund, D. C., Mix, A. C., and Southon, J.: Increased ventilation age of the deep northeast Pacific Ocean during the last deglaciation, Nature Geoscience, 4, 771-774, doi:10.1038/ngeo1272, 2011.

Maier, E., Meheust, M., Abelmann, A., Gersonde, R., Chapligin, B., Ren, J., Meyer, H., and Tiedemann, R.: Deglacial subarctic Pacific surface water hydrography and nutrient dynamics and links to North Atlantic climate variability and atmospheric CO2, Paleoceanography, 30, 949-968, doi:10.1002/2014PA002763, 2015.

Mangerud, J., Andersen, S. T., Berglund, B. E., and Donner, J. J.: Quaternary stratigraphy of Norden, a proposal for terminology and classification, Boreas, 3, 109-126, doi:10.1111/j.1502-3885.1974.tb00669.x, 1974.

Manley, W.F.: Postglacial Flooding of the Bering Land Bridge: A Geospatial Animation: INSTAAR, University of Colorado, v1, http://instaar.colorado.edu/QGISL/bering_land_bridge, 2002.

Mantua, N. J., Hare, S. R., Zhang, Y., Wallace, J. M., and Francis, R. C.: A Pacific interdecadal climate oscillation with impacts on salmon production, Bull. Amer. Meteor. Soc., 78, 1069–1079, doi:10.1175/1520-0477(1997)078<1069:APICOW>2.0.CO;2, 1997.

Mantua, N. J., and Hare, S. R.: The Pacific Decadal Oscillation, Journal of Oceanography, 58, 35-44, doi:10.1023/A:1015820616384, 2002.

Matsumoto, K., Hashioka, T., and Yamanaka, Y.: Effect of temperature-dependent organic carbon decay on atmospheric pCO2, Journal of Geophysical Research: Atmospheres, 112, G02007, doi:10.1029/2006JG000187, 2007.

Max, L., Riethdorf, J.-R., Tiedemann, R., Smirnova, M., Lembke-Jene, L., Fahl, K., Nürnberg, D., Matul, A., and Mollenhauer, G.: Sea surface temperature variability and sea-ice extent in the subarctic northwest Pacific during the past 15,000 years, Paleoceanography, 27, PA3213, doi:10.1029/2012PA002292, 2012.

Max, L., Lembke-Jene, L., Riethdorf, J. R., Tiedemann, R., Nürnberg, D., Kühn, H., and Mackensen, A.: Pulses of enhanced North Pacific Intermediate Water ventilation from the Okhotsk Sea and Bering Sea during the last deglaciation, Clim Past, 10, 591-605, doi:10.5194/cp-10-591-2014, 2014.

McKay, J. L., Pedersen, T. F., and Southon, J.: Intensification of the oxygen minimum zone in the northeast Pacific off Vancouver Island during the last deglaciation: Ventilation and/or export production?, Paleoceanography, 20, PA4002, doi:10.1029/2003PA000979, 2005.

McManus, J. F., Francois, R., Gherardi, J.-M., Keigwin, L. D., and Brown-Leger, S.: Collapse and rapid resumption of Atlantic meridional circulation linked to deglacial climate changes, Nature, 428, 834-837, doi:10.1038/nature02494, 2004.

Meheust, M.: Late Quaternary variability of sea-ice cover, surfacewater temperature and terrigenous input in the subarctic North Pacific and the Bering Sea: A biomarker approach, Dissertation Universität Bremen, 108 pp, 2014.

Mikolajewicz, U., Crowley, T. J., Schiller, A., and Voss, R.: Modelling teleconnections between the North Atlantic and North Pacific during the Younger Dryas, Nature, 387, 384-387, doi:10.1038/387384a0, 1997.

Minobe, S.: A 50-70 year climatic oscillation over the North Pacific and North America, Geophysical Research Letters, 24, 683-686, doi:10.1029/97GL00504, 1997.

Mix, A., Lund, D., Pisias, N., Boden, P., Bornmalm, L., Lyle, M., and Pike, J.: Rapid climate oscillations in the northeast Pacific during the last deglaciation reflect Northern and Southern Hemisphere sources, in: Mechanisms of Global Climate Change at Millennial Time Scales, edited by: Clark, P. U., Webb, R. S., and Keigwin, L. D., Geophysical Monograph Series, American Geophysical Union, Washington, D.C., 127–148, 1999.

Moffitt, S. E., Moffitt, R. A., Sauthoff, W., Davis, C. V., Hewett, K., Hill, T. M.: Paleoceanographic insights on recent oxygen minimum zone expansion: Lessons for modern oceanography. PLoS ONE 10(1): e115246, doi:10.1371/journal.pone.0115246, 2015.

Monin, E., Indermühle, A., Dällenbach, A., Flückiger, J., Stauffer, B., Stocker, T. F., Raynaud, D., Barnola, J-M.: Atmospheric CO2 concentrations over the Last Glacial Termination, Science, 291, 112-114, doi:10.1126/science.291.5501.112, 2001.

Müller, P. J. and Schneider, R.: An automated leaching method for the determination of opal in sediments and particulate matter, Deep Sea Research I, 40, 425-444, doi:10.1016/0967(93)90140-X, 1993.

Nakagawa, T., Gotanda, K., Haraguchi, T., Danhara, T., Yonenobu, H., Brauer, A., Yokoyama, Y., Tada, R., Takemura, K., Staff, R. A., Payne, R., Bronk Ramsey, C., Bryant, C., Brock, F., Schlolaut, G., Marshall, M., Tarasov, P., and Lamb, H.: SG06, a fully continuous and varved sediment core from Lake Suigetsu, Japan: stratigraphy and potential for improving the radiocarbon calibration model and understanding of late Quaternary climate changes, Quaternary Science Reviews, 36, 164-176, doi:10.1016/j.quascirev.2010.12.013, 2012.

Nakamura, T., Awaji, T., Hatayama, T., Akitomo, K., Takizawa, T., Kono, T., Kawasaki, Y., and Fukasawa, M.: The generation of large-amplitude unsteady lee waves by subinertial K1 tidal flow: A possible vertical mixing mechanism in the Kuril Straits, Journal of Physical Oceanography, 30, 1601-1621, doi:10.1175/1520-0485(2000)030<1601:TGOLAU>2.0.CO;2, 2000.

Nakatsuka, T., Watanabe, K., Handa, N., Matsumoto, E., and Wada, E.: Glacial to Interglacial Surface Nutrient Variations of Bering Deep Basins Recorded by d13C and d15N of Sedimentary Organic-Matter, Paleoceanography, 10, 1047-1061, doi:10.1029/95PA02644, 1995.

Nederbragt, A. J., and Thurow, J. W.: A 6000yr varve record of Holocene climate in Saanich Inlet, British Columbia, from digital sediment colour analysis of ODP Leg 169S cores, Marine Geology, 174, 95-110, doi:10.1016/S0025-3227(00)00144-4, 2001.

Nederbragt, A. J., and Thurow, J. W.: Amplitude of ENSO cycles in the Santa Barbara Basin, off California, during the past 15 000 years, Journal of Quaternary Science, 20, 447-456, doi:10.1002/jqs.946, 2005.

NGRIP-Members, Andersen, K. K., Azuma, N., Barnola, J. M., Bigler, M., Biscaye, P., Caillon, N., Chappellaz, J., Clausen, H. B., DahlJensen, D., Fischer, H., Flückiger, J., Fritzsche, D., Fujii, Y., Goto-Azuma, K., Gronvold, K., Gundestrup, N. S., Hansson, M., Huber, C., Hvidberg, C. S., Johnsen, S. J., Jonsell, U., Jouzel, J., Kipfstuhl, S., Landais, A., Leuenberger, M., Lorrain, R., Masson-Delmotte, V., Miller, H., Motoyama, H., Narita, H., Popp, T., Rasmussen, S. O., Raynaud, D., Röthlisberger, R., Ruth, U., Samyn, D., Schwander, J., Shoji, H., Siggard-Andersen, M. L., Steffensen, J. P., Stocker, T., Sveinbjornsdottir, A. E., Svensson, A., Takata, M., Tison, J. L., Thorsteinsson, T., Watanabe, O., Wilhelms, F., and White, J. W. C.: High-resolution record of Northern Hemisphere climate extending into the last interglacial period, Nature, 431, 147-151, doi:10.1038/nature02805, 2004.

Niebauer, H. J.: Sea ice and temperature variability in the eastern Bering Sea and the relation to atmospheric fluctuations, Journal of Geophysical Research: Oceans, 85, 7507-7515, doi:10.1029/JC085iC12p07507, 1980.

Niebauer, H. J.: Multiyear sea ice variability in the eastern Bering Sea: An update, Journal of Geophysical Research: Oceans, 88, 2733-2742, doi:10.1029/JC088iC05p02733, 1983.

Niebauer, H. J., and Alexander, V.: Oceanographic frontal structure and biological production at an ice edge, Cont Shelf Res, 4, 367-388, doi:10.1016/0278-4343(85)90001-9, 1985.

Niebauer, H. J., Alexander, V., and Henrichs, S. M.: A time-series study of the spring bloom at the Bering Sea ice edge I. Physical processes, chlorophyll and nutrient chemistry, Cont Shelf Res, 15, 1859-1877, doi:10.1016/0278-4343(94)00097-7, 1995.

Nishioka, J., Ono, T., Saito, H., Nakatsuka, T., Takeda, S., Yoshimura, T., Suzuki, K., Kuma, K., Nakabayashi, S., Tsumune, D., Mitsudera, H., Keith Johnson, W., and Tsuda, A.: Iron supply to the western subarctic Pacific: Importance of iron export from the Sea of Okhotsh, Journal of Geophysical Research: Oceans, 112, C10012, doi:10.1029/2006JC004055, 2007.

Nuernberg, D., Tiedemann, R.: Environmental change in the Sea of Okhotsk during the last 1.1 million years, Paleoceanography, doi:10.1029/2004PA001023, 2004.

Ohkushi, K., Itaki, T., Nemoto, N.: Last Glacial–Holocene change in intermediate-water ventilation in the Northwestern Pacific, Quaternary Sciene Reviews, 22, 1477-1484, doi:10.1016/S0277-3791(03)00082-9, 2003.

Okada, M., Takagi, M., Narita, H., Takahashi, K.: Chronostratigraphy of sediment cores from the Bering Sea and the subarctic Pacific based on paleomagnetic and oxygen isotopic analysis, Deep Sea Research Part II: Topical Studies in Oceanography, 52, 2092-2109, doi:10.1016/j.dsr2.2005.08.004, 2005.

Okazaki, Y., Takahashi, K., Asahi, H., Katsuki, K., Hori, J., Yasuda, H., Sagawa, Y., and Tokuyama, H.: Productivity changes in the Bering Sea during the late Quaternary, Deep Sea Research Part II: Topical Studies in Oceanography, 52, 2150-2162, doi:10.1016/j.dsr2.2005.07.003, 2005.

Okazaki, Y., Timmermann, A., Menviel, L., Harada, N., Abe-Ouchi, A., Chikamoto, M. O., Mouchet, A., and Asahi, H.: Deepwater formation in the North Pacific during the Last Glacial Termination, Science, 329, 200-204, doi:10.1126/Science.1190612, 2010.

Okumura, Y. M., Deser, C., Hu, A., Timmermann, A., and Xie, S.-P.: North Pacific Climate Response to Freshwater Forcing in the Subarctic North Atlantic: Oceanic and Atmospheric Pathways, Journal Of Climate, 22, 1424-1445, doi:10.1175/2008JCLI2511.1, 2009.

Ortiz, J. D., O'Connell, S. B., Delviscio, J., Dean, W., Carriquiry, J. D., Marchitto, T., Zheng, Y., and Van Geen, A.: Enhanced marine productivity off western North America during warm climate intervals of the past 52 ky, Geology, 32, 521-524, doi:10.1130/G20234.1, 2004.

Osafune, S., and Yasuda, I.: Bidecadal variability in the intermediate waters of the northwestern subarctic Pacific and the Okhotsk Sea in relation to 18.6-year period nodal tidal cycle, Journal of Geophysical Research: Oceans, 111, doi:10.1029/2005JC003277, 2006.

Osafune, S., and Yasuda, I.: Bidecadal variability in the Bering Sea and the relation with 18.6 year period nodal tidal cycle, Journal of Geophysical Research: Oceans, 115, doi:10.1029/2008JC005110, 2010.

Overland, J. E., Adams, J. M., and Bond, N. A.: Decadal variability of the Aleutian low and its relation to high-latitude circulation, Journal Of Climate, 12, 1542-1548, doi:10.1175/1520-0442(1999)012<1542:DVOTAL>2.0.CO;2, 1999.

Overland, J. E., Wang, M., Wood, K. R., Percival, D. B., Bond, N. A.: Recent Bering Sea warm and cold events in a 95-year context, Deep Sea Research Part II: Topical Studies in Oceanography, 65-70, 6-13, doi:10.1016/j.dsr2.2012.013, 2012.

Paillard, D., Labeyrie, L., Yiou, P.: Macintosh program performs time-series analysis, EOS Trans. AGU, 77, doi:10.1029/96EO00259, 1996.

Paulmier, A., and Ruiz-Pino, D.: Oxygen minimum zones (OMZs) in the modern ocean, Prog Oceanogr, 80, 113-128, doi:10.1016/j.pocean.2008.08.001, 2009.

Praetorius, S. K., and Mix, A. C.: Synchronization of North Pacific and Greenland climates preceeded abrupt deglacial warming, Science, 345, 444-448, doi:10.1126/science.125200, 2014.

Rasmussen, S., Andersen, K., Svensson, A., Steffensen, J., Vinther, B., Clausen, H., Siggaard-Andersen, M., Johnsen, S., Larsen, L., Dahl-Jensen, D., Bigler, M., Rothlisberger, R., Fischer, H., Goto-Azuma, K., Hansson, M., and Ruth, U.: A new Greenland ice core chronology for the last glacial termination, Journal of Geophysical Research: Atmospheres, 111, D06102, doi:10.1029/2005JD006079, 2006.

Rasmussen, S. O., Vinther, B. M., Clausen, H. B., and Andersen, K. K.: Early Holocene climate oscillations recorded in three Greenland ice cores, Quaternary Science Reviews, 26, 1907-1914, doi:10.1016/j.quascirev.2007.06.015, 2007.

Reimer, P. J., Bard, E., Bayliss, A., Beck, J. W., Blackwell, P. G., Bronk Ramsey, C., Buck, C. E., Cheng, H., Edwards, R. L., Friedrich, M., Grootes, P. M., Thomas, P. G., Haflidason, H., Hajdas, I., Hatte, C., Heaton, T. J., Hoffmann, D. L., Hogg, A. G., Hughen, K. A., Kaiser, K. F., Kromer, B., Manning, S. W., Niu, M., Reimer, R. W., Richards, D. A., Scott, E. M., Southon, J. R., Staff, R. A., Turney, C. S. M., and van der Plicht, J.: INTCAL13 and MARINE13 Radiocarbon Age Calibration Curves 0-50,000 Years cal. BP, Radiocarbon, 55, 1869-1887, doi:10.2458/azu_js_rc.55.16947, 2013.

Rella, S. F., Tada, R., Nagashima, K., Ikehara, M., Itaki, T., Ohkushi, K. i., Sakamoto, T., Harada, N., and Uchida, M.: Abrupt changes of intermediate water properties on the northeastern slope of the Bering Sea during the last glacial and deglacial period, Paleoceanography, 27, PA3203, doi:10.1029/2011PA002205, 2012.

Ren, J., Gersonde, R., Esper, O., and Sancetta, C.: Diatom distributions in northern North Pacific surface sediments and their relationship to modern environmental variables, Palaeogeography, Palaeoclimatology, Palaeoecology, doi:10.1016/j.palaeo.2014.03.008, 2014.

Reynolds, R. W., Rayner, N. A., Smith, T. M., Stokes, D. C., Wang, W.: An improved in situ and satellite SST analysis for climate, Journal of climate, 15, 1609-1625, doi:10.1175/1520-0442(2002)015<1609:AIISAS>2.0.CO;2, 2002.

Richter, T. O., van der Gaast, S., Koster, B., Vaars, A., Gieles, R., de Stigter, H. C., De Haas, H., van Weering, T. C. E.: The Avaatech XRF core scanner: technical description and application to NE Atlantic sediments, Geological Society, London, Special Publications, 267, 39-50, doi:11.1144/GSL.SP.2006.267.01.03, 2006.

Riethdorf, J.-R., Max, L., Nürnberg, D., Lembke-Jene, L., and Tiedemann, R.: Deglacial history of (sub) sea surface temperatures and salinity in the subarctic NW Pacific: Implications for upper-ocean stratification, Paleoceanography, 28, 91-104, doi:10.1002/palo.20014, 2013a.

Riethdorf, J. R., Nürnberg, D., Max, L., Tiedemann, R., Gorbarenko, S. A., and Malakhov, M. I.: Millennial-scale variability of marine productivity and terrigenous matter supply in the western Bering Sea over the past 180 kyr, Clim Past, 9, 1345-1373, doi:10.5194/cp-9-1345-2013, 2013.

Roden, G. I.: Aleutian Basin of the Bering Sea: Thermohaline , oxygen, nutrient and current structure in July 1993, Journal of Geophysical Research: Oceans, 100, 13539-13554, doi:10.1029/95JC01291, 1995.

Roark, E. B., Ingram, B. L., Southon, J., and Kennett, J. P.: Holocene foraminiferal radiocarbon record of paleocirculation in the Santa Barbara Basin, Geology, 31, 379-382, doi:10.1130/0091-7613(2003)031<0379:HFRROP>2.0.CO;2, 2003.

Rodionov, S. N., Bond, N. A., and Overland, J. E.: The Aleutian Low, storm tracks, and winter climate variability in the Bering Sea, Deep-Sea Research Part II: Topical Studies in Oceanography, 54, 2560-2577, doi:10.1016/j.dsr2.2007.08.002, 2007.

Royer, T. C.: High-latitude oceanic variability associated with the 18.6-year nodal tide, Journal of Geophysical Research: Oceans, 98, 4639-4644, doi:10.1029/92JC02750, 1993.

Ruth, U., Bigler, M., Röthlisberger, R., Siggaard-Andersen, M.-L., Kipfstuhl, S., Goto-Azuma, K., Hansson, M. E., Johnsen, S. J., Lu, H., and Steffensen, J. P.: Ice core evidence for a very tight link between North Atlantic and east Asian glacial climate, Geophysical Research Letters, 34, L03706, doi:10.1029/2006GL027876, 2007.

Saenko, O. A., Schmittner, A., and Weaver, A. J.: The Atlantik-Pacific seasaw, Journal of climate, 17, 2033-2038, doi:10.1175/1520-0442(2004)017<2033:TAS>2.0CO;2, 2004.

Sancetta, C., Heusser, L., Labeyrie, L., Naidu, A. S., and Robinson, S. W.: Wisconsin Holocene Paleoenvironment of the Bering Sea - Evidence from Diatoms, Pollen, Oxygen Isotopes and Clay-Minerals, Marine Geology, 62, 55-68, doi:10.1016/0025-3227(84)90054-9, 1984.

Sarnthein, M., Winn, K., Jung, S. J. A., Duplessy, J-C., Labeyrie, L., Erlenkeuser, H., Ganssen, G.: Changes in east Atlantic deepwater circulation over the last 30,000 years: Eight time slice reconstructions, Paleoceanography, 9, 209-267, doi:10.1029/93PA03301, 1994.

Sarnthein, M., Stattegger, K., Dreger, D., Erlenkeuser, H., Grootes, P., Haupt, B. J., Jung, S., Kiefer, T., Kuhnt, W., Pflaumann, U., Schäfer-Neth, C., Schulz, H., Schulz, M., Seidov, D., Simstich, J., van Kreveld, S., Vogelsang, E., Völker, A and Weinelt, M.: Fundamental modes and abrupt changes in North Atlantic circulation and climate over the last 60 ky – Concepts, reconstruction and numerical modeling, In: The North Atlantic: A changing environment. Edited by P. Schäfer, W. Ritzrau, M. Schlüter and J. Thiede, pp. 365-410, Springer, Berlin, 2000.

Sarnthein, M., Grootes, P. M., Kennett, J. P., and Nadeau, M.: 14C Reservoir Ages Show Deglacial Changes in Ocean Currents and Carbon Cycle, in: Ocean Circulation: Mechanisms and Impacts, 1st ed., edited by: Schmittner, A., Chiang, J., and Hemming, S., Geophysical Monograph Series, 173, American Geophysical Union, Washington, 175-196, 2007.

Sarnthein, M., Schneider, B., and Grootes, P. M.: Peak glacial ^{14}C ventilation ages suggest major draw-down of carbon into the abyssal ocean, Clim Past, 9, 2595-2614, doi:10.5194/cp-9-2595-2013, 2013.

Sarnthein, M., Balmer, S.,. Grootes, P. M., Mudelsee, M.: Planktic and benthic ^{14}C reservoir ages for three ocean basins, calibrated by a suite of ^{14}C plateaus in the glacial-to-deglacial Suigetsu atmospheric ^{14}C record, Radiocarbon, 57, 1-23,doi:10.2458/azu_rc.57.17916, 2015.

Schlitzer, R.: Interactive analysis and visualization of geoscience data with Ocean Data View, Computers & Geosciences, 28, 1211-1218, doi:10.1016/S0098-3004(02)00040-7, 2002.y

Schlung, S. A., Christina Ravelo, A., Aiello, I. W., Andreasen, D. H., Cook, M. S., Drake, M., Dyez, K. A., Guilderson, T. P., Lariviere, J. P., Stroynowski, Z., and Takahashi, K.: Millennial-scale climate change and intermediate water circulation in the Bering Sea from 90 ka: A high-resolution record from IODP Site U1340, Paleoceanography, 28, doi:10.1029/2012PA002365, 2013.

Schmittner, A., Oschlies, A., Matthews, H. D., and Galbraith, E.D.: Future changes in climate, ocean circulation, ecosystems, and biogeochemical cycling simulated for a business-as-usual CO2 emission scenario until year 4000 AD, Global Biogeochem. Cycles, 22, GB1013, doi:10.1029/2007GB002953, 2008.

Shaffer, G., Olsen, S. M., and Pedersen, J. O., P.: Long-term ocean oxygen depletion in response to carbon dioxide emissions from fossil fuels, Nat. Geosci., 2, 105–109, doi:10.1038/ngeo420, 2009.

Shibahara, A., Ohkushi, K., Kennett, J. P., and Ikehara, K.: Late Quaternary changes in intermediate water oxygenation and oxygen minimum zone, northern Japan: A benthic foraminiferal perspective, Paleoceanography, 22, PA3213, doi:10.1029/2005PA001234, 2007.

Sigman, D. M., Hain, M. P., and Haug, G. H.: The polar ocean and glacial cycles in atmospheric CO2 concentration, Nature, 466, 47-55, doi:10.1038/nature09149, 2010.

Southon, J., and Fedje, D.: A post-glacial record of 14C reservoir ages for the British Columbia coast, Canadian Journal of Archaeology, 27, 95-111, 2003.

Springer, A. M., McRoy, C. P., and Flint, M. V.: The Bering Sea Green Belt: shelf-edge processes and ecosystem production, Fisheries Oceanography, 5, 205-223, do:10.1111/j.1365-2419.1996.tb00118.x, 1996.

Stabeno, P.J., Schumacher, J.D. and Ohtani, K.: Physical oceanography of the Bering Sea, in Loughlin, T.R. & Ohtani, K., eds, The Bering Sea: a Summary of physical, chemical and biological characteristics and a synopsis of research: Alaska Sea Grant Press, 1–28, 1999.

Stabeno, P. J., Bond, N. A., Kachel, N. B., Salo, S. A., and Schumacher, J. D.: On the temporal variability of the physical environment over the south-eastern Bering Sea, Fisheries Oceanography, 10, 81-98, doi:10.1046/j.1365-2419.2001.00157.x, 2001.

Stabeno, P. J., Kachel, D. G., Kachel, N. B., and Sullivan, M. E.: Observation from moorings in the Aleutian Passes: temperature, salinity and transport, Fisheries Oceanography, 14, 39-54, doi:10.1111/j.1365-2419.2005.00362.x, 2005.

Staff, R. A., Nakagawa, T., Schlolaut, G., Marshall, M. H., Brauer, A., Lamb, H. F., Bronk Ramsey, C., Bryant, C. L., Brock, F., Kitagawa, H., van der Plicht, J., Payne, R. L., Smith, V. C., Mark, D. F., MacLeod, A., Blockley, S. P. E., Schwenninger, J.-L., Tarasov, P. E., Haraguchi, T., Gotanda K., Yonenobu, H., Yokoyama, Y. and Suigetsu 2006 Project Members.: The multiple chronological techniques applied to the Lake Suigetsu SG06 sediment core, Japan, Boreas, 42(2), 259-266, doi:10.1111/j.1502-3885.2012.00278.x, 2012.

Steffensen, J. P., Andersen, K. K., Bigler, M., Clausen, H. B., Dahl-Jensen, D., Fischer, H., Goto-Azuma, K., Hansson, M., Johnsen, S. J., Jouzel, J., Masson-Delmotte, V., Popp, T., Rasmussen, S. O., Rothlisberger, R., Ruth, U., Stauffer, B., Siggaard-Andersen, M. L., Sveinbjornsdottir, A. E., Svensson, A., and White, J. W. C.: High-Resolution Greenland Ice Core Data Show Abrupt Climate Change Happens in Few Years, Science (New York, NY), 321, 680-684, doi:10.1126/science.1157707, 2008.

Stramma, L., Schmidtko, S., Levin, L. A., Johnson, G. C.: Ocean oxygen minima expansions and their biological impacts. Deep Sea Research I, 57, 587-595, doi:10.1016/j.dsr.2010.01.005, 2010.

Stuiver, M., and Polach, H.: Discussion: Reporting of 14C Data, Radiocarbon, 19, 355-363, 1977.

Stuiver, M., and Reimer, P. J.: Extended 14C database and revised CALIB radiocarbon calibration program, Radiocarbon, 35, 215-230, 1993.

Tadokoro, K., Ono, T., Yasuda, I., Osafune, S., Shiomoto, A., and Sugisaki, H.: Possible mechanisms of decadal-scale variation in PO4 concentration in the western North Pacific, Geophysical Research Letters, 36, L08606, doi:10.1029/2009GL037327, 2009.

Takahashi, K.: The Bering Sea and paleoceanography, Deep Sea Research Part II: Topical Studies in Oceanography, 52, 2080-2091, doi:10.1016/j.dsr2.2005.08.003, 2005.

Takahashi, K., Fujitani, N., Yanada, M.: Long term monitoring of particle fluxes in the Bering Sea and the central subarctic Pacific Ocean, 1990-2000, Progress in Oceanography, 55, 95-112, doi:10.1016/S0079-6611(02)00072, 2002.

Takahashi, K., Ravelo, A. C., Alvarez Zarikian, C., and Expedition323Scientists: Bering Sea Paleoceanography Expedition 323 of the riserless drilling platform. Victoria, British Columbia (Canada), to Yokohama, Japan; Sites U1339–U1345; 5 July–4 September 2009, in: Proceedings of the Integrated Ocean Drilling Program, Volume 323, Integrated Ocean Drilling Program Management International, Inc., Tokyo, 2011.

Tanaka, S., and Takahashi, K.: Late Quaternary paleoceanographic changes in the Bering Sea and the western subarctic Pacific based on radiolarian assemblages, Deep Sea Research Part II: Topical Studies in Oceanography, 52, 2131-2149, doi:10.1016/j.dsr2.2005.07.002, 2005.

Taylor, K. C., Mayewski, P. A., Alley, R. B., Brook, E. J., Gow, A. J., Grootes, P. M., Meese, D. A., Saltzman, E. S., Severinghaus, J. P., Twickler, M. S., White, J. W. C., Whitlow, S., and Zielinski, G. A.: The Holocene-Younger Dryas Transition Recorded at Summit, Greenland, Science (New York, NY), 278, 825-827, doi:10.1126/science.278.5339.825, 1997.

Telford, R. J., Heegaard, E., and Birks, H. J. B.: The intercept is a poor estimate of a calibrated radiocarbon age, The Holocene, 14, 296-298, doi:10.1191/0959683604hl707fa, 2004.

Tjallingii, R.: Application and quality of X-Ray Fluorescence core scanning in reconstructing late Pleistocene NW African continental margin sedimentation patterns and paleoclimate variations. Dissertation Universität Bremen, 114 pp, 2006.

Tjallingii, R., Rohl, U., Kolling, M., and Bickert, T.: Influence of the water content on X-ray fluorescence core-scanning measurements in soft marine sediments, Geochem Geophy Geosy, 8, Q02004, doi:10.1029/2006GC001393, 2007.

Tsunogai, S., Kusakabe, M., Iizumi, H., Koike, I., and Hattori, A.: Hydrographic features of the deep water of the Bering Sea — The Sea of Silica, Deep Sea Research Part A. Oceanographic Research Papers, 26, 641-659, doi:10.1016/0198-0149(79)90038-4, 1979.

van der Plicht, J., van Geel, B., Bohncke, S. J. P., Bos, J. A. A., Blaauw, M., Speranza, A. O. M., Muscheler, R., and Bjorck, S.: The Preboreal climate reversal and a subsequent solar-forced climate shift, Journal of Quaternary Science, 19, 263-269, doi:10.1002/jqs.835, 2004.

van Geen, A., Zheng, Y., Bernhard, J. M., Cannariato, K. G., Carriquiry, J., Dean, W. E., Eakins, B. W., Ortiz, J. D., and Pike, J.: On the preservation of laminated sediments along the western margin of North America, Paleoceanography, 18, doi:10.1029/2003/PA000911, 2003.

van Loon, H., Meehl, G. A., and Shea, D.J.: Coupled air-sea response to solar forcing in the Pacific region during northern winter, Journal of Geophysical Research: Atmospheres, 112, D02108, doi:10.1029/2006JD007378, 2007.

Vellinga, M., and Wood, R. A.: Global climatic impacts of a collapse of the Atlantic thermohaline circulation, Climatic Change, 54, 251-267, doi:10.1023/A:1016168827653, 2002.

Watanabe, S., Tada, R., Ikehara, K., Fujine, K., and Kido, Y.: Sediment fabrics, oxygenation history, and circulation modes of Japan Sea during the Late Quaternary, Palaeogeography Palaeoclimatology Palaeoecology, 247, 50-64, doi:10.1016/j.palaeo.2006.11.021, 2007.

Whitney, F. A., Freeland, H. J., Robert, M.: Persistently declining oxygen levels in the interior waters of the eastern subarctic Pacific, Progress in Oceanography 75, 179-199, doi:10.1016/j.pocean.2007.08.0007, 2007.

Wilhelms-Dick, D., Westerhold, T., Röhl, U., Wilhelms, F., Vogt, C., Hanebuth, T. J. J., Römmermann, H., Kriews, M., and Kasten, S.: A comparison of mm scale resolution techniques for element analysis in sediment cores, Journal of Analytical Atomic Spectrometry, 27, 1574-1584, doi:10.1039/c2ja30148b, 2012.

Wilson, R., Wiles, G., D'Arrigo, R., Zweck, C.: Cycles and shifts: 1,300 years of multi-decadal temperature variability in the Gulf of Alaska, Climate Dynamics, 28, 425-440, doi:10.1007/s00382-006-0194-9, 2007.

Woodgate, R. A., Weingartner, T., and Lindsay, R.: The 2007 Bering Strait oceanic heat flux and anomalous Arctic sea-ice retreat, Geophysical Research Letters, 37, L01602, doi:10.1029/2009GL041621, 2010.

Yasuda, I., Osafune, S., Tatebe, H.: Possible explanation linking 18.6-year nodal tidal cycle with bi-decadal variations of ocean and climate in the North Pacific, Geophysical Research Letters, 33, L08606, doi: 10.1029/2005GL025237, 2006.

Yasuda, I.: The 18.6-year period moon-tidal cycle in Pacific Decadal Oscillation reconstructed from tree-rings in western North America, Geophysical Research Letters, 36, L05605, doi:10.1029/2008GL036880, 2009.

Zheng, Y., Van Geen, A., Anderson, R. F., Gardner, J. V., and Dean, W. E.: Intensification of the northeast Pacific oxygen minimum zone during the Bolling-Allerod warm period, Paleoceanography, 15, 528-536, doi:10.1029/1999PA000473, 2000.

Ziegler, M., Jilbert, T., de Lange, G. J., Lourens, L. J., and Reichart G-J.: Bromine counts from XRF scanning as an estimate of the marine organic carbon content of sediment cores, Geochemistry Geophysics Geosystems, 9, doi:10.1029/2007GC001932, 2008.

Appendix 1

Pulses of enhanced North Pacific Intermediate Water ventilation from the Okhotsk Sea and Bering Sea during the last deglaciation

Lars Max[1], Lester Lembke-Jene[1], Jan-Rainer Riethdorf[2], Ralf Tiedemann[1], Dirk Nürnberg[2], **Hartmut Kühn**[1], and Andreas Mackensen[1]

[1] Alfred-Wegener-Institut Helmholtz-Zentrum für Polar- und Meeresforschung, Bremerhaven, Germany

[2] GEOMAR, Helmholtz-Zentrum für Ozeanforschung Kiel, Wischhofstr. 1–3, 24148 Kiel, Germany

Published in Climate of the Past (2014), doi:10.5194/cp-10-591-2014

Abstract

Under modern conditions only North Pacific IntermediateWater is formed in the northwest Pacific Ocean. This situation might have changed in the past. Recent studies with general circulation models indicate a switch to deep-water formation in the northwest Pacific during Heinrich Stadial 1 (17.5 – 15.0 ka) of the last glacial termination. Reconstructions of past ventilation changes based on paleoceanographic proxy records are still insufficient to test whether a deglacial mode of deep-water formation in the North Pacific Ocean existed. Here we present deglacial ventilation records based on radiocarbon-derived ventilation ages in combination with epibenthic stable carbon isotopes from the northwest Pacific including the Okhotsk Sea and Bering Sea, the two potential source regions for past North Pacific ventilation changes. Evidence for most rigorous ventilation of the intermediate-depth North Pacific occurred during Heinrich Stadial 1 and the Younger Dryas, simultaneous to significant reductions in Atlantic Meridional Overturning Circulation. Concurrent changes in $d^{13}C$ and ventilation ages point to the Okhotsk Sea as driver of millennial-scale changes in North Pacific Intermediate Water ventilation during the last deglaciation. Our records additionally indicate that changes in the $d^{13}C$ intermediate-water (700 – 1750 m water depth) signature and radiocarbon-derived ventilation ages are in antiphase to those of the deep North Pacific Ocean (>2100m water depth) during the last glacial termination. Thus, intermediate- and deep-water masses of the northwest Pacific have a differing ventilation history during the last deglaciation.

Appendix 2

IP_{25} proxy records of sea-ice variability in the subarctic North Pacific and adjacent Bering Sea during the past 25,000 years

Marie Méheust[1], Edith Maier1, **Hartmut Kühn**[1], Ruediger Stein[1], Kirsten Fahl[1], Rainer Gersonde[1]

[1] Alfred-Wegener-Institut Helmholtz-Zentrum für Polar- und Meeresforschung, Bremerhaven, Germany

To be submitted to Quaternary Science Reviews

Abstract

Here we reconstructed changes in sea-surface conditions in the eastern and western subarctic Pacific and the northern Bering Sea throughout the last glacial-deglacial- Holocene time interval by mean of specific biomarkers. New insights about the spatial and temporal variations of sea-surface temperature and sea-ice coverage are provided by the analyses of alkenones and sea-ice proxy (IP25) respectively. For a better assessment of sea-ice coverage, IP_{25} was combined to phytoplankton biomarkers data to calculate the marker-IP_{25} index (PIP_{25}).

The results show that an extensive sea-ice cover prevailed over large parts of the subarctic Pacific and the Bering Sea during the LGM. The deglaciation is characterized by a rapid sea-ice advance and retreat. During cold periods (Heinrich Stadial 1 and Younger Dryas) seasonal sea-ice cover generally coincides with low alkenone SSTs and low primary productivity. Conversely, during warmer intervals (Bølling–Allerød) predominance of reduced sea ice or ice-free conditions are associated with increase in alkenone SSTs and primary productivity. During the Holocene, ice-free conditions dominated in the subarctic Pacific and the southern Bering Sea. In the northern Bering Sea continental shelf ice-free conditions, associated with high alkenone SSTs and primary productivity, prevailed during the Holocene Thermal Maximum, but shifted to marginal sea-ice conditions at late early-Holocene. The variability can be explained by a combination of local factors (e.g. solar insolation), as well as global climate anomalies and sea-level changes controlling the oceanographic circulation between the subarctic Pacific and the Bering Sea.